TAMIRES KAWAHARA OISHI

MULTIPHYSICS MODELING OF ELECTRO-TECHNOLOGIES IN FOOD PROCESSING: CONTINUOUS FLOW MICROWAVE THERMAL PROCESSING AND ELECTROHYDRODYNAMIC DRYING

SÃO PAULO

2023

TAMIRES KAWAHARA OISHI

MULTIPHYSICS MODELING OF ELECTRO-TECHNOLOGIES IN FOOD PROCESSING: CONTINUOUS FLOW MICROWAVE THERMAL PROCESSING AND ELECTROHYDRODYNAMIC DRYING

REVISED VERSION

Ph.D. thesis presented to the Graduate Program in Chemical Engineering at the Escola Politécnica, University of São Paulo, to obtain the degree of Doctor of Science.

Concentration area: Chemical Engineering

Advisor: Prof. Dr. Jorge Andrey Wilhelms Gut
Co-advisor: Prof. Dr. Eduardo Victor dos Santos Pouzada

SÃO PAULO
2023

Este exemplar foi revisado e corrigido em relação à versão original, sob responsabilidade única do autor e com a anuência de seu orientador.

São Paulo, 13 de dezembro de 2023

Assinatura do autor: gov.br Documento assinado digitalmente TAMIRES KAWAHARA OISHI Data: 13/12/2023 15:13:14-0300 Verifique em https://validar.iti.gov.br

Assinatura do orientador: gov.br Documento assinado digitalmente JORGE ANDREY WILHELMS GUT Data: 13/12/2023 15:18:59-0300 Verifique em https://validar.iti.gov.br

Catalogação-na-publicação

Oishi, Tamires Kawahara
MULTIPHYSICS MODELING OF ELECTRO-TECHNOLOGIES IN FOOD PROCESSING: CONTINUOUS FLOW MICROWAVE THERMAL PROCESSING AND ELECTROHYDRODYNAMIC DRYING / T. K. Oishi -- versão corr. -- São Paulo, 2023.
111 p.

Tese (Doutorado) - Escola Politécnica da Universidade de São Paulo. Departamento de Engenharia Química.

1.Pasteurization 2.Apple juice 3.Coconut water 4.Corona discharge 5.COMSOL multiphysics I.Universidade de São Paulo. Escola Politécnica. Departamento de Engenharia Química II.t.

ACKNOWLEDGEMENTS

I sincerely thank Prof. Jorge A. W. Gut, my academic advisor, for all his kind, trust, friendship and patience. Jorge was always present and gave me all the support and solutions to help me to face the problems and to reach my goals. Thanks for letting me experience different areas of modeling and food processing.

I would like to thank my co-advisor Prof. Eduardo V. S. Pouzada. His unending enthusiasm and knowledge of multiphysics modeling and electromagnetism made me cross the line between Food and Electrical Engineering.

In the last year of my PhD, I got a scholarship to do research at McGill University in Prof. Vijaya Raghavan's group. His encouragement with so much enthusiasm made me experience the electrohydrodynamic drying area. Thanks for letting me watch your post-harvest classes and encouraging me to talk about my Brazilian background during the seminars.

During my Master's and PhD, Prof. Carmem C. Tadini was always present for valuable debates, suggestions and teachings for my personal and academic growth.

To Érica Siguemoto and Marcella Cassares to make the experimental data available to validate the COMSOL models.

To Food Research Center (FoRC) and *Laboratório de Engenharia de Alimentos* (LEA) for infrastructure and financing. To the Graduate Program in Chemical Engineering at the *Escola Politécnica*, University of São Paulo (USP), especially the professors and fellows for their friendship and all the help they provided.

To my friends at LEA (Bianca, Eduardo, Érica, Giulliana, Guilherme, Kaiky, Marcella, Nilo and Tiago) and the friends I made during the 6 years at USP (Alexandre, Carol, Dielle, Fernanda, Juliana, Leticia, Mariana, Priscila, Samanta and Thamiris) for making my academic life more enjoyable.

To Rafael for finding me at USP and showing me that we can share our dreams and passion for science. To my parents and brother, to Neusa, Fernando and Túlio, for their unconditional love, motivation and support.

I would like to thank the *Coordenação de Aperfeiçoamento de Pessoal de Nível Superior* – CAPES (Finance Code 001) for the PhD scholarship, the *Conselho Nacional de Desenvolvimento Científico e Tecnológico* – CNPq (grants 200394/2022-3 and 316388/2021-1) for helping to finance the microwave project and my visiting research period at McGill University and the *Fundação de Amparo à Pesquisa do Estado de São Paulo* – FAPESP (grant 2013/07914-8).

RESUMO

OISHI, TK. **Modelagem multifísica de electro-tecnologias no processamento de alimentos: processamento térmico por micro-ondas de fluxo contínuo e secagem eletrohidrodinâmica.** Tese (Doutorado) – Escola Politécnica, Universidade de São Paulo, São Paulo, 2023.

O aumento da utilização de energias renováveis e o desenvolvimento de electro-tecnologias inovadoras no processamento de alimentos têm o potencial de reduzir as emissões e o consumo de recursos naturais e aumentar a eficiência energética. Tratamentos assistidos por campo elétrico (micro-ondas e eletrohidrodinâmica (EHD)) têm sido utilizados como alternativa aos processos de aquecimento e secagem de alimentos devido ao menor tempo de processamento e melhor preservação da qualidade dos alimentos. A interação entre o campo elétrico, escoamento de fluidos e temperatura é complicada de avaliar apenas através de ensaios experimentais. Um modelo multifísico é uma ferramenta útil para melhor avaliar ou otimizar um processamento de alimentos. Este trabalho tem como objetivo a modelagem multifísica do processamento térmico assistido por micro-ondas em fluxo contínuo e de um sistema de secagem por eletrohidrodinâmica na configuração fio-placa com fluxo de ar cruzado. Uma cavidade de micro-ondas e um tubo de retenção projetados para processamento térmico de fluxo contínuo de alimentos líquidos foram avaliados para o tratamento de suco de maçã fresco e água de coco. Foi construído um modelo tridimensional baseado em uma unidade de processamento térmico assistida por micro-ondas (MicroThermics, 2,45 GHz, 6 kW). As simulações foram implementadas usando o Método de Elementos Finitos no COMSOL Multiphysics (v.6.1). As físicas de ondas eletromagnéticas, escoamento laminar e transferência de calor foram combinadas iterativamente para resolver e predizer a intensidade do campo elétrico, o perfil de velocidade e a distribuição de temperatura dentro do domínio do fluido. A inativação térmica das enzimas polifenol oxidase (PPO) e peroxidase (POD) foi predita adicionando a física de transporte de espécies diluídas ao modelo. Para validação do modelo, o suco de maçã não clarificado foi anteriormente processado na unidade com vazões de 0,4 e 0,8 L/min e temperaturas de pasteurização de 70, 80 e 90 °C. Os resultados da distribuição de temperatura foram úteis para determinar regiões quentes e frias dentro do tubo e mostraram um gradiente de temperatura da seção transversal na saída do tubo. A água de coco fresca foi processada em diferentes vazões (0,5, 0,7, 0,9 e 1,1 L/min) e temperaturas (80, 90, 100 e 110 °C). A comparação entre os resultados numéricos e experimentais mostraram que o modelo tem uma

boa capacidade de predição da temperatura de saída do aquecedor, com erro absoluto médio de 3,3 °C. Também foram fornecidas predições confiáveis para as atividades residuais de PPO e POD após o tubo de retenção, com a maioria dos desvios abaixo de 10%. A secagem convectiva EHD é uma tecnologia não térmica para preservar alimentos por desidratação de materiais sensíveis ao calor. Um sistema EHD (fio-placa) foi modelado usando COMSOL Multiphysics (v.6.1). As físicas de eletrostática, escoamento turbulento, transferência de calor em fluidos e transporte de umidade e energia foram totalmente acopladas para prever a intensidade do campo elétrico, escoamento do ar, coeficiente convectivo de transferência de calor e remoção de umidade. Foi possível simular o fluxo de ar induzido por EHD do fio para a placa combinado com um fluxo de ar cruzado. O coeficiente convectivo de transferência de calor resultante, a velocidade do ar na superfície do alimento, o teor de umidade e o tempo crítico de secagem foram apresentados para cada uma das 11 condições de secagem. A combinação do potencial elétrico (0, 10, 15 e 20 kV) com a velocidade de fluxo de ar cruzado (0, 1 e 2 m/s) impactou o coeficiente convectivo de transferência de calor e a remoção de umidade; entretanto, o aumento individual de potencial elétrico e/ou velocidade do ar pouco reduziu o tempo crítico de secagem. Os principais resultados mostram que o modelo proposto pode simular adequadamente os fenômenos de fluxo de ar EHD e o processo de secagem e pode ser utilizado para melhoria da qualidade do produto, análise de eficiência energética e estudos de otimização.

Palavras-chave: maçã, água de coco, enzima, pasteurização, COMSOL, descarga corona.

ABSTRACT

OISHI, TK. **Multiphysics modeling of electro-technologies in food processing: continuous flow microwave thermal processing and electrohydrodynamic drying.** Thesis (Doctoral), Escola Politécnica, University of São Paulo, São Paulo, 2023.

The increase in renewable energy utilization and the development of innovative electro-technologies in food processing have the potential to reduce emissions and consumption of natural resources and increase energy efficiency. Electric field assisted treatments (e.g., microwave and electrohydrodynamic (EHD)) have been used as an alternative heating and drying food processes due to shorter processing time and better preservation of food quality. The interaction involving electric field, fluid flow and temperature is complicated to evaluate only through experimental assays. A multiphysics model is a useful tool to better evaluate or optimize a food process. This work aimed to multiphysics model the continuous flow microwave thermal processing and the electrohydrodynamic wire-to-plate with air crossflow drying system. A microwave cavity and holding tube designed for continuous flow thermal processing of liquid foods was evaluated for the treatment of fresh apple juice and coconut water. A three-dimensional model was built based on the assembly of the microwave-assisted thermal processing unit (MicroThermics, 2.45 GHz, 6 kW). Simulations were implemented using the Finite Element Method in COMSOL Multiphysics (v.6.1). The physics for electromagnetic waves, laminar flow and heat transfer were combined iteratively to solve and predict the electric field intensity, the velocity profile and the temperature distribution within the fluid domain. Polyphenol oxidase (PPO) and peroxidase (POD) enzymatic thermal inactivation could be predicted by adding the physics of transport of diluted species to the model. To validate the model, cloudy apple juice was previously processed in the unit with flow rates of 0.4 and 0.8 L/min and pasteurization temperatures of 70, 80 and 90 °C. Temperature distribution results were useful for determining hot and cold spots within the tube and showed an important temperature gradient at the outlet cross section of the tube. Fresh coconut water was processed at different flow rates (0.5, 0.7, 0.9 and 1.1 L/min) and target temperatures (80, 90, 100 and 110 °C). Comparison between numerical and experimental results showed that the model is reliable for predicting outlet temperature of the heater, with a mean absolute error of 3.3 °C. Reliable predictions for residual activities of PPO and POD after the holding tube were also provided, with most deviations under 10%. EHD convective drying is a non-thermal technology to preserve foods by dehydration of heat-sensitive materials. An EHD (wire-to-

plate) system was modeled using COMSOL Multiphysics (v.6.1). Electrostatics, turbulent flow, heat transfer in fluids and moisture and energy transport physics were fully-coupled to predict the electric field strength, airflow, convective heat transfer coefficient and moisture removal. The COMSOL Multiphysics software could well represent the EHD-driven airflow from wire to ground combined with air crossflow. The resulting convective heat transfer coefficient, air velocity on the food surface, moisture content and drying time were presented for each of the 11 drying conditions. Combining high voltage (0, 10, 15 and 20 kV) and air crossflow velocity (0, 1 and 2 m/s) was found to have a significant effect on the convective heat transfer coefficient and moisture removal; however, the increase in one of the drying factors had a low effect on drying time. The main results show that the proposed model can adequately simulate the EHD airflow phenomena and the drying process and can be used for product quality improvement, energy efficiency analysis and optimization studies.

Keywords: apple, coconut water, enzyme, pasteurization, COMSOL, corona discharge.

LIST OF FIGURES

LIST OF TABLES

LIST OF ACRONYMS AND ABBREVIATIONS

CFD	Computational Fluid Dynamics
CMC	Carboxymethyl Cellulose
DC	Direct Current
DW	Distilled Water
EHD	Electrohydrodynamic
FEM	Finite Element Method
FVM	Finite Volume Method
HDPE	High-Density Polyethylene
ISM	Industrial, Scientific and Medical
MD	Molecular dynamics
MEQ	Mesh Element Quality
PDE	Partial Differential Equation
PEC	Perfect Electric Conductor
POD	Peroxidase
PPO	Polyphenol Oxidase
PTFE	Polytetrafluoroethylene
RF	Radio Frequency
SDG	Suitable Development Goals
TE	Transverse Electric
TM	Transverse Magnetic
TSS	Total Soluble Solids
TT	Temperature Transmitter
UN	United Nations

LIST OF SYMBOLS

CHAPTER 1 – GENERAL INTRODUCTION

A	Residual activity of a thermal process biological target (-)
A_0	Initial activity of a thermal process biological target (-)
D	Decimal reduction time (s)
D_{Tref}	Decimal reduction time known at a reference temperature (s)
E	Electric field vector (V/m)
f	Frequency (Hz)
H	Magnetic field vector (A/m)
k	First-order inactivation rate constant (1/s)
t	Time (s)
T	Temperature (K)
T_{ref}	Reference temperature (K)
V	Voltage (V)
z	Increase in temperature necessary to cause a 90% reduction in D (K)

Greek letters

ε_0	Permittivity of the free space (F/m)
ε_r'	Relative dielectric permittivity (-)
ε_r''	Relative dielectric loss factor (-)
ε_c	Complex permittivity of the material (-)
σ	Electrical conductivity (S/m)
μ_0	Permeability of free space (H/m)
μ_r	Relative permeability (-)
ω	Angular frequency (rad/s)

CHAPTER 2 – EXPERIMENTAL VALIDATION OF A MULTIPHYSICS MODEL FOR THE MICROWAVE-ASSISTED PASTEURIZATION OF APPLE JUICE

C_P	Specific heat capacity (J/(kg.K))
E	Electric field vector (V/m)
f	Frequency (Hz)
H	Magnetic field vector (A/m)
H_c	Microwave cavity high (m)
k	Thermal conductivity (W/(m.K))
p	Hydrodynamic pressure (Pa)
P_{abs}	Absorbed microwave power (W)
P_{sup}	Supplied microwave power (W)
q	Absorbed power (W)
Q	Volumetric power generation (W/m^3)
$\dot{Q}$	Volumetric flow rate (m^3/s)
r	Radial direction (m)
R	Inner radius of the tube (m)
T	Temperature (K)
$\overline{T}$	Mixing cup average temperature (K)
u	Velocity vector (m/s)
u	Axial velocity profile (m/s)
$\overline{u}$	Average velocity (m/s)

Greek letters

ε_0	Permittivity of the free space (F/m)
ε_r'	Relative dielectric permittivity (-)
ε_r''	Relative dielectric loss factor (-)
ε_c	Complex permittivity of the material (-)
σ	Electrical conductivity (S/m)
ρ	Average liquid food density (kg/m^3)
μ	Dynamic viscosity (Pa.s)
μ_0	Permeability of free space (H/m)
μ_r	Relative permeability (-)
ω	Angular frequency (rad/s)

CHAPTER 3 – MULTIPHYSICS MODELING OF POLYPHENOL OXIDASE AND PEROXIDASE INACTIVATION IN CONTINUOUS-FLOW MICROWAVE THERMAL PROCESSING OF COCONUT WATER

A	Enzymatic activity (U)
A_0	Initial enzymatic activity (U)
c	First-order inactivation rate constant (1/s)
C_P	Specific heat capacity (J/(kg.K))
D_{Tref}	Decimal reduction time at a reference temperature (s)
E	Electric field vector (V/m)
E_D	Enzyme diffusivity (m^2/s)
f	Frequency (Hz)
k	Thermal conductivity (W/(m.K))
p	Hydrodynamic pressure (Pa)
P_{abs}	Absorbed microwave power (W)
P_{gen}	Volumetric power generation (W)
Q	Volumetric flow rate (m^3/s)
r	Radial direction (m)
R	Inner radius of the tube (m)
t	Time (s)
T	Temperature (K)
T_{ref}	Reference temperature (K)
$\overline{T}$	Mixing cup average temperature (K)
u	Velocity vector (m/s)
u	Axial velocity profile (m/s)
$\overline{u}$	Average velocity (m/s)
z	Increase in temperature necessary to cause a 90% reduction in D value (K)

Greek letters

ε_0	Permittivity of the free space (F/m)
ε_r'	Relative dielectric permittivity (-)
ε_r''	Relative dielectric loss factor (-)
σ	Electrical conductivity (S/m)
ρ	Average liquid food density (kg/m^3)

μ Dynamic viscosity (Pa.s)

μ_0 Permeability of free space (H/m)

μ_r Relative permeability (-)

ω Angular frequency (rad/s)

CHAPTER 4 – MULTIPHYSICS MODELING OF WIRE-TO-PLATE ELECTROHYDRODYNAMIC WITH AIR CROSSFLOW

a_w Water activity (-)

AF Analogy factor (-)

b Ion mobility ($m^2/(V.s)$)

C_m Moisture capacity (s^2/m^2)

C_{Pair} Air specific heat capacity (J/(kg.K))

C_{Pl} Specific heat capacity of liquid water (J/(kg.K))

C_{Ps} Specific heat capacity of dry matter (J/(kg.K))

C_{Pv} Specific heat capacity of water vapor (J/(kg.K))

D_m Moisture diffusivity (m^2/s)

$\mathbf{E}$ Electric field vector (V/m)

$\mathbf{f_E}$ Electric force (N/m^3)

h_l Liquid Water enthalpy (J/kg)

h_M Convective mass transfer coefficient (s/m^2)

h_T Convective heat transfer coefficient ($W/(m^2.K)$)

h_v Water vapor enthalpy (J/kg)

$\mathbf{J}$ Current density (A/m^2).

k_{air} Air thermal conductivity (W/(m.K))

k_{food} Food thermal conductivity (W/(m.K))

K_m Moisture permeability of food (s)

p Air pressure (Pa)

$p_{v,sat}$ Saturated vapor pressure (Pa)

p_{vw} Air-food interface vapor pressure (Pa)

q Space charge density (C/m^3)

RH_{air} Reference relative humidity of ambient air (%)

R_v Specific gas constant for water vapor (J/(kg.K))

t Time (s)

T_{air} Air temperature (K)

T_{food} Food temperature (K)

$\mathbf{u}$ Air velocity (m/s)

u_{cross} Air crossflow velocity (m/s)

u_{fs} Average air velocity of food surface (m/s)

V Electric potential (V)

V_w Wire potential (V)

w_m Moisture content of food (kg/m^3)

w_s Dry matter density (kg/m^3)

w_{safe} Safe moisture content (kg/m^3)

Greek letters

ε_0 Permittivity of the free space (F/m)

ε_r Relative dielectric permittivity (-)

σ Electrical conductivity (S/m)

ρ_{air} Air density (kg/m^3)

ρ_l Density of liquid water (kg/m^3)

δ Water vapor diffusion coefficient (m^2/s)

μ_{air} Air viscosity (kg/(m.s))

ψ Water potential (Pa)

CONTENTS

1 GENERAL INTRODUCTION

In 2015, the United Nations (UN) approved the 17 "Suitable Development Goals" (SDG) to eradicate poverty and hunger worldwide and protect the environment by 2030. Halfway to the deadline of the 2030 SDG agenda, the goals of "Affordable and Clean Energy" (G7), "Industrial, Innovation and Infrastructure" (G9) and "Responsible Consumption and Production" (G12) are the goals with the best progress in 2023 SDG report (UN, 2023). Since 2015, the worldwide use of renewable energy has grown from 16.7% to 30.0% of the total energy consumption (UN, 2023). However, the heating industry's progress on renewable energy has been the most limited sector over the years (UN, 2023). Decarbonization through electrification and improving the energy efficiency of heating processes can contribute to the SDGs by 2030 (Zuberi et al., 2022). In 2022, the overall global transition of manufacturing industries to medium-high and high-technology industries demonstrated robust growing rating, with the potential to contribute to "green growth" (less emissions, energy and water consumption) (UN, 2023). From G12 goal, 13.2% of the "world's food production" was wasted after harvest in 2021, and this goal aims to reduce this food post-harvest losses by investing in innovative food processing technologies, infrastructure and education (UN, 2023).

These efforts on clean energy usage, innovative technologies development and responsible food production are an ideal opportunity to develop electro-technologies for the food thermal and non-thermal processing. The electro-technologies used for food industrial processes are infrared, laser, microwave, ohmic heating, radio waves, plasma, electrical resistance, ultraviolet, pulsed electric fields, electrohydrodynamic, electric fan and freeze-drying. Microwave and electrohydrodynamic technologies are used in food processing as an alternative to conventional heating and drying processes. These electro-technologies can present shorter processing time, better preservation of food quality and greater energy efficiency.

The continuous flow thermal processing of liquid foods aims for the inactivation of enzymes and microorganisms of concern for food safety and shelf-life with minimal quality degradation. This thermal continuous treatment typically consists in the food stream being subjected to a temperature increase followed by a holding period in a tube and then following to the cooling step (Singh and Heldman, 2009). In the use of conventional heat exchangers (tubular or plates), thermal exchange occurs only by convection, which makes heating slow and non-uniform when in laminar flow (Tajchakavit et al., 1998).

Microwave-assisted processing of liquid foods is of interest to the food industry due to the rapid volumetric heating without overheated surfaces. Microwave radiation penetrates directly into the food resulting in high heat transfer rates and high energy efficiency (Zhu, Kunestov and Sandeep, 2007). This benefit can result in a better-quality food product due to the reduced degradation of thermosensitive components responsible for flavor and nutrition aspects (vitamins, phenolic components and antioxidant capacity) (Siguemoto et al., 2019; Sierra et al., 1999).

Food drying is an essential post-harvest way to prevent food losses by increasing the shelf-life of perishable goods, inhibiting microorganism growth and/or enzymatic activity (Bonazzi and Dumoulin, 2014). Airflow and/or temperature increase can be induced in drying processes (hot air ovens, microwaves and electrohydrodynamic) to increase convective heat and mass transfer coefficients, increasing the drying rate (Aregawi et al., 2013). However, applying high drying temperatures can adversely affect the quality properties of food products (appearance, taste, texture and nutrients) (Raghavan et al., 2005).

Electrohydrodynamic (EHD) is a non-thermal food processing technology of inducing ionic wind by applying high voltage to an electrode over the food surface (Singh et al., 2012). In general, EHD drying helps to retain color and nutritional qualities of heat-sensitive foods better than conventional drying (Dalvi-Isfahan et al., 2023; Mirzaei-Baktash et al., 2022; Ni et al., 2020). However, the corona discharge from EHD can generate ozone and free radicals with potential to reduce the effective capacity of antioxidant and phenolic compounds in quince (Elmizadeh et al., 2017).

The design, application and optimization of these electro-technologies require further knowledge of the interaction of multiphysics phenomena (Knoezer et al., 2015). The interaction between electric field, fluid flow and temperature is complicated to evaluate only through experimental assays. A multiphysics model is a useful tool to better evaluate or optimize a food process. The evaluation of heat transfer and flow is essential to predict velocity and temperature distributions and effects on chemical and microbiological components in the food (Teixeira et al., 1969 Erdogdu et al., 2018).

1.1 GENERAL OBJECTIVES

The purpose of this work is to develop and evaluate multiphysics models for the continuous flow microwave thermal processing and for the electrohydrodynamic (EHD) wire-to-plate with air crossflow drying system.

This study was divided into three main parts:

1) Multiphysics model and simulation of the continuous flow microwave heater in COMSOL Multiphysics (v.6.1). Model validation using experimental data from apple juice processing for microwave processing temperature.
2) Model the microwave heater with a holding tube. Model validation using experimental results from green coconut water processing, verification of process temperature, power absorbed and polyphenol oxidase (PPO) and peroxidase (POD) enzyme residual activities.
3) Multiphysics model of the EHD wire-to-plate with air crossflow system. Model the EHD system effect in the convective heat transfer coefficient over a portion of solid food and the drying kinetics.

1.2 LITERATURE REVIEW

1.2.1 Electromagnetic governing equations for microwave heating

Microwaves are nonionizing, time-varying electromagnetic waves of radiant energy that comprise a magnetic and electric field oriented perpendicularly to each other (Datta, Sumnu and Raghavan, 2005). Plane wave is useful to visualize practical field configurations (Meredith, 1998). Figure 1.1 shows a schematic configuration of plane wave, it consists of the electric field vector (**E**, V/m) and the complementary magnetic field vector (**H**, A/m), orthogonal to each other, and the direction of propagation (Coleman, 2020).

Figure 1.1. Schematic representation of electromagnetic plane wave.

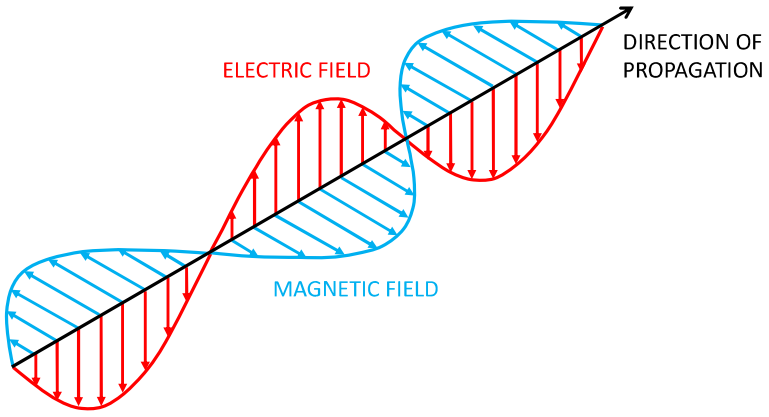

Source: Adapted from Coleman (2020).

In microwave processing, electromagnetic waves of a certain frequency are used to heat food products. The Industrial, Scientific and Medical (ISM) frequencies used in microwave equipment for food processing are mainly 915 and 2,450 MHz. The two mechanisms of heat generation by microwave radiation in food materials are ionic conduction and dielectric (Tewari, 2007). Ionic conduction is due to the oscillatory movement of free ions in the food under the influence of the oscillating electric field, this kinetic energy can be converted into heat (Tewari, 2007). Dielectric heating occurs when the polar molecules (e.g., water) line up continuously according to the electric field polarity (Tewari, 2007). The dielectric properties of foods are the relative dielectric permittivity (ε_r') and loss factor (ε_r''), both properties are dimensionless. The dielectric permittivity represents the amount of incident power absorbed or reflected while the dielectric loss factor measures the amount of absorbed energy dissipated or transmitted within the food sample (Tewari, 2007). The temperature distribution of a food

material is determined by the dielectric and thermal properties of the food and the distribution of absorbed microwave energy (determined by the propagation of electromagnetic radiation through the microwave cavity and food) (Dibben, 2001).

The general solution of Maxwell's equations is a good mathematical description for this phenomenon; however, the analytical solution for arbitrary geometry is not trivial if not impossible. The four Maxwell's field equations can relate the time-varying electric field with the corresponding time-varying magnetic field (Sadiku, 2012). Eqs. (1.1)-(1.4) are first-order differential equations presented in vector form for time-varying fields with an angular frequency of $\omega = 2\,\pi\,f$ without any source of electric charge or magnetic dipoles (Meredith, 1998):

$$\nabla \times \mathbf{H} = j\,\omega\,\varepsilon_0\,\varepsilon_c\,\mathbf{E} \qquad \text{Ampere's law} \qquad (1.1)$$

$$\nabla \times \mathbf{E} = -\,j\,\omega\,\mu_0\,\mu_r\,\mathbf{H} \qquad \text{Faraday's law} \qquad (1.2)$$

$$\nabla \cdot \mu_0\,\mu_r\,\mathbf{H} = 0 \qquad \text{Gauss' law} \qquad (1.3)$$

$$\nabla \cdot \varepsilon_0\,\varepsilon_c\,\mathbf{E} = 0 \qquad \text{Gauss' law} \qquad (1.4)$$

where $\varepsilon_0 = 8.854 \times 10^{-12}$ is the permittivity of the free space (F/m), $\varepsilon_c = \varepsilon_r' - j\,\varepsilon_r''$ is the complex permittivity of the material (characterizes the interaction between the **E** field and the food material) given by a real (ε_r') and imaginary part (ε_r''), j is the imaginary number $\sqrt{-1}$, $\mu_0 = 4\,\pi\,\times 10^{-7}$ is the magnetic permeability of free space (H/m) and μ_r is the relative permeability of the surrounding medium (for air $\mu_r = 1$).

1.2.2 Inactivation kinetics in thermal processing

In the food industry, thermal processing is the most important method to guarantee food safety and preservation by the inactivation of microorganisms (Kubo et al., 2023). Bacteria are the main concern of a thermal processing; however, for acidic foods (e.g., fruit juices), endogenous enzymes showed higher resistance to heat than microorganisms (Tribess and Tadini, 2006). The efficiency of a thermal process can be measured by the inactivation of undesired microorganisms and/or enzymes present in the food when submitted to high temperatures. These biological indicators of thermal processing are naturally present in many biological raw materials (e.g., fruits and vegetables) and can affect the functional properties of foods in many ways (Van Loey et al., 2003). Some of them are positively used in food processing for improving sensorial aspects, such as flavor and texture. Otherwise, some biological indicators can also have detrimental effects in a food product, e.g., enzymatic

browning (Van Loey et al., 2003). Enzymatic browning can alter sensory aspects (appearance, taste and texture) of the food, and it can be inactivated through the thermal processing of foods (Mayer, 2006).

The kinetic for the inactivation of a biological target can describe the inactivation progress in function of time. In general, thermal inactivation of a biological target can often be described as a first-order reaction at a given temperature (Van Loey et al., 2003; Gut and Tadini, 2018):

$$\frac{dA}{dt} = -k\,A \tag{1.5}$$

where A is the residual activity of a biological target during thermal processing as a constant lethal temperature (number of surviving microorganisms or activity of enzyme), t is time (s) and k is the first-order inactivation rate constant (1/s).

The integral form of Eq. (1.5) is based on the logarithmic expression, where for initial condition $t = 0$ s and $A = A_0$:

$$\ln\left(\frac{A}{A_0}\right) = \ln(10)\,\log\left(\frac{A}{A_0}\right) = -k\,t \tag{1.6}$$

where A_0 is the initial activity of a thermal process biological target.

In food process, the first order kinetic parameters D and z are commonly used to describe the inactivation of a biological target as a semi-logarithmic decay under isothermal conditions (Bigelow, 1921). The decimal reduction time (D, s) is the time needed for a 90% reduction of the initial activity (A_0) at a given temperature (Toledo, 1999):

$$\log\left(\frac{0.1\,A_0}{A_0}\right) = \frac{-\,k}{\ln\,(10)}\,D \tag{1.7}$$

From Eq. (1.7), D can be expressed in function of the kinetic first-order constant (k):

$$k = \frac{\ln\,(10)}{D} \tag{1.8}$$

Substitution of Eq. (1.6) in Eq. (1.8) yields:

$$\log\left(\frac{A}{A_0}\right) = -\frac{t}{D} \tag{1.9}$$

For a first-order reaction, the z parameter is defined as the increase in temperature necessary to cause a 90% reduction in D value (Gut and Tadini, 2018):

$$\log\left(\frac{D}{D_{Tref}}\right) = -\frac{(T - T_{ref})}{z} \tag{1.10}$$

where D_{Tref} is the decimal reduction time known at a reference temperature (T_{ref}, °C).

1.2.3 Modeling of continuous flow microwave heating

Food materials have a complex heterogeneous composition that can present different rheological and thermophysical properties and biological composition that varies during thermal processing (Sevda, Garlapati and Singh, 2020). The majority of the food engineering problems, e.g., heat and mass transfer operations, are variable. A mathematical model approach based on transport phenomena can manage these food engineering problems by providing a real understanding of the food process (Sevda, Garlapati and Singh, 2020). Mathematical models are critical tools for optimization, design and scale-up of food processes (Topcam and Erdogdu, 2021).

For a continuous flow microwave thermal treatment of liquid foods, partial differential equations related to fluid flow, electric field and heat transfer can be solved using a numerical method that can be based on finite differences, finite elements or finite volumes. When a problem involves heat transfer and fluid flow, it is known as a Computational Fluid Dynamics (CFD) problem. In CFD models, most software are based on the Finite Element Method (FEM) (COMSOL Multiphysics, COMSOL AB, Stockholm, Sweden) or the Finite Volume Method (FVM) (ANSYS Multiphysics, ANSYS Inc., Canonsburg, USA) due to the flexibility to be applied over irregular or moving domains (Dutta, Erdogdu and Sarghini, 2020).

Salvi et al. (2011) made a critical comparison between continuous flow microwave heating models using COMSOL and ANSYS. Both mathematical methods (FEM and FVM) presented similar results for power absorption and temperature profile and cross-sectional distribution at the fluid outlet with a predicted temperature difference lower than 13%. According to the authors, the main differences between software were that in COMSOL is possible to couple electromagnetism, fluid dynamics and heat transfer modules in the same mesh and in a simplified way, resulting in a lower processing time of 15 minutes against 2.5 hours with ANSYS.

These CFD software are useful tools for analyzing single or multiphase flow with complex heat transfer and/or chemical reactions in several industrial applications. However, these complex applications demand high computational resources (cost and time) to run large-scale models and have numerical limitations (e.g., discretization or interpolation errors) (Dutta et al., 2010). Nowadays, the cost of computational hardware is lower and the CFD software have a user-friendly interface, so the number of uses and studies applying CFD for food engineering processes are increasing (Dutta, Erdogdu and Sarghini, 2020).

A CFD model of a continuous flow microwave heater typically consists of an applicator tube (made of a material transparent to the microwave energy) housed inside of a cavity or chamber connected to a waveguide and a magnetron (source of the electromagnetic energy) (Figure 1.2). To model this system of microwave cavity, a computational study coupling electromagnetic waves, fluid flow and heat transfer in a multiphysics software is required.

Figure 1.2. Schematic representation of a microwave system for continuous flow heating.

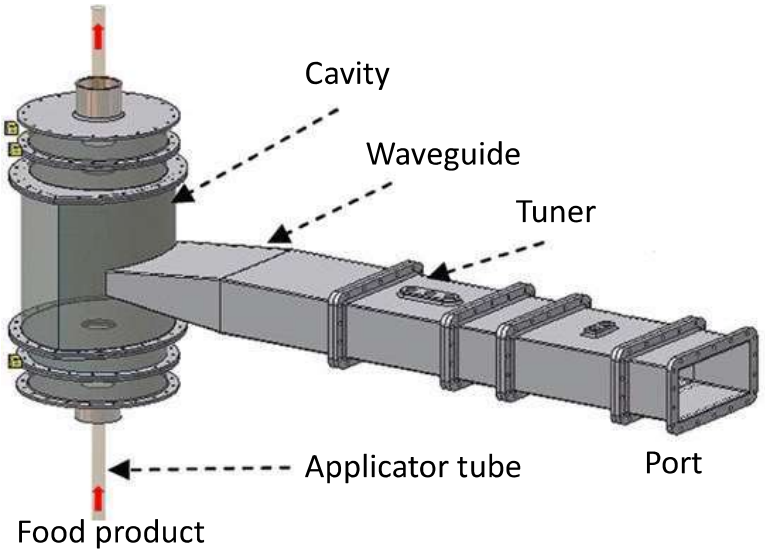

Source: Adapted from Salvi et al. (2008).

Many researchers have modeled different continuous-flow microwave cavity geometries with straight (Yang et al., 2021; Topcam and Erdogdu, 2021; Cuccurullo, Giordano, Viccione, 2016; Puangsuwan, Tongurai and Chongcheawchamnan, 2015; Muley and Boldor, 2012; Salvi et al., 2011), helical (Zhang et al., 2021; Tuta and Palazoğlu, 2017) or curved (Topcam and Erdogdu, 2021; Damilos et al., 2019) applicator tubes in COMSOL Multiphysics to obtain predictions of temperature distribution in Newtonian (water, salt water solutions and fruit juices) and non-Newtonian (CMC solutions, whole liquid egg and surimi paste) pumpable fluids.

Topcam and Erdogdu (2021) developed an optimization study for a cylindrical microwave cavity. The authors tested different numbers of applicator tubes (1 to 5 tubes) and several layouts (Figure 1.3). The process variable observed to determine the best system was the outlet temperature of the liquid food in the applicator tubes. As a result, the higher numbers of applicator tubes (3 to 5 tubes) housed in the cylindrical cavity, the lower were the outlet temperature and its uniformity among the tubes. Therefore, the number of tubes and their

orientation can directly affect the process efficiency (changing the electromagnetic field and the temperature distribution); these are significant parameters in an optimization study.

Figure 1.3. Electric field within the 915 MHz microwave cavity and temperature distribution within pipes orientation: a) 1-pipe, b) 2-pipe, c) 3-pipe, d) 4-pipe, e) 5-pipe (layout 1) and f) 5-pipe (layout 2).

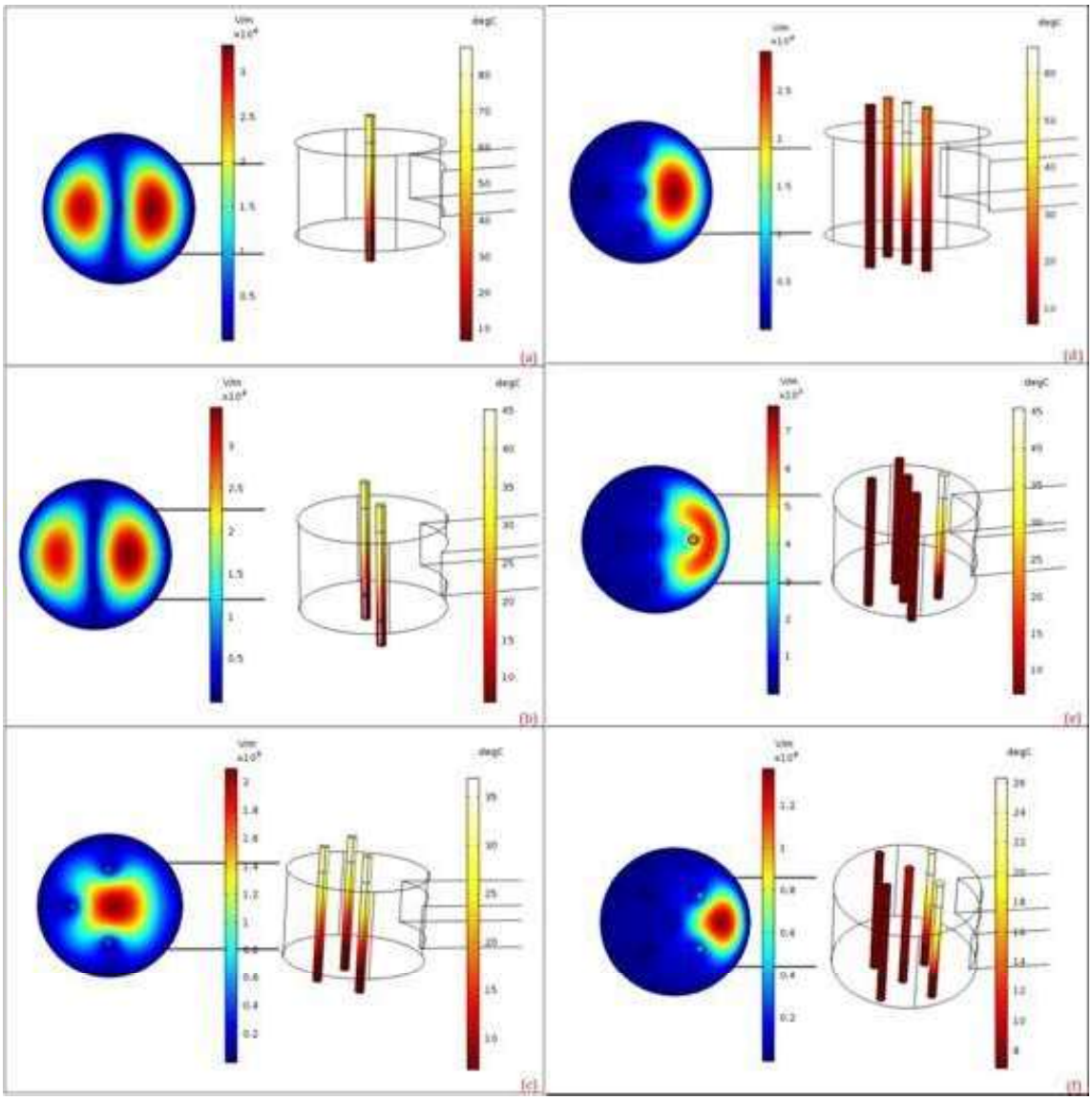

Source: Topcam and Erdogdu (2021).

Tuta and Palazoğlu (2017) modeled a continuous flow microwave heater with a helical pipe housed inside of a cylindrical cavity (Figure 1.4). Helical coils have benefits because they can increase the holding time for microwave heating and the curves can enhance mixing effects by the presence of secondary flow in the radial direction, increasing temperature uniformity.

The authors tested Carboxymethyl Cellulose (CMC) solutions (0.5 and 1.0%) and Distilled Water (DW) at 1, 2 and 3 L/min flow rate under 4 kW microwave power. DW results presented better temperature uniformity since the low viscosity of the liquid increases the flow mixing effects. However, CMC 1% presented a larger temperature increase due to the CMC dielectric properties facilitating the conversion of electromagnetic energy into heat, the CMC 1% high viscosity decreases the flow mixing effects resulting in non-uniform temperatures.

Figure 1.4. Electric field distribution in microwave system (top), electric field distribution (left) and heat generation (right) along the helical tube: a) distillated water, b) 0.5% and c) 1.0% CMC solution.

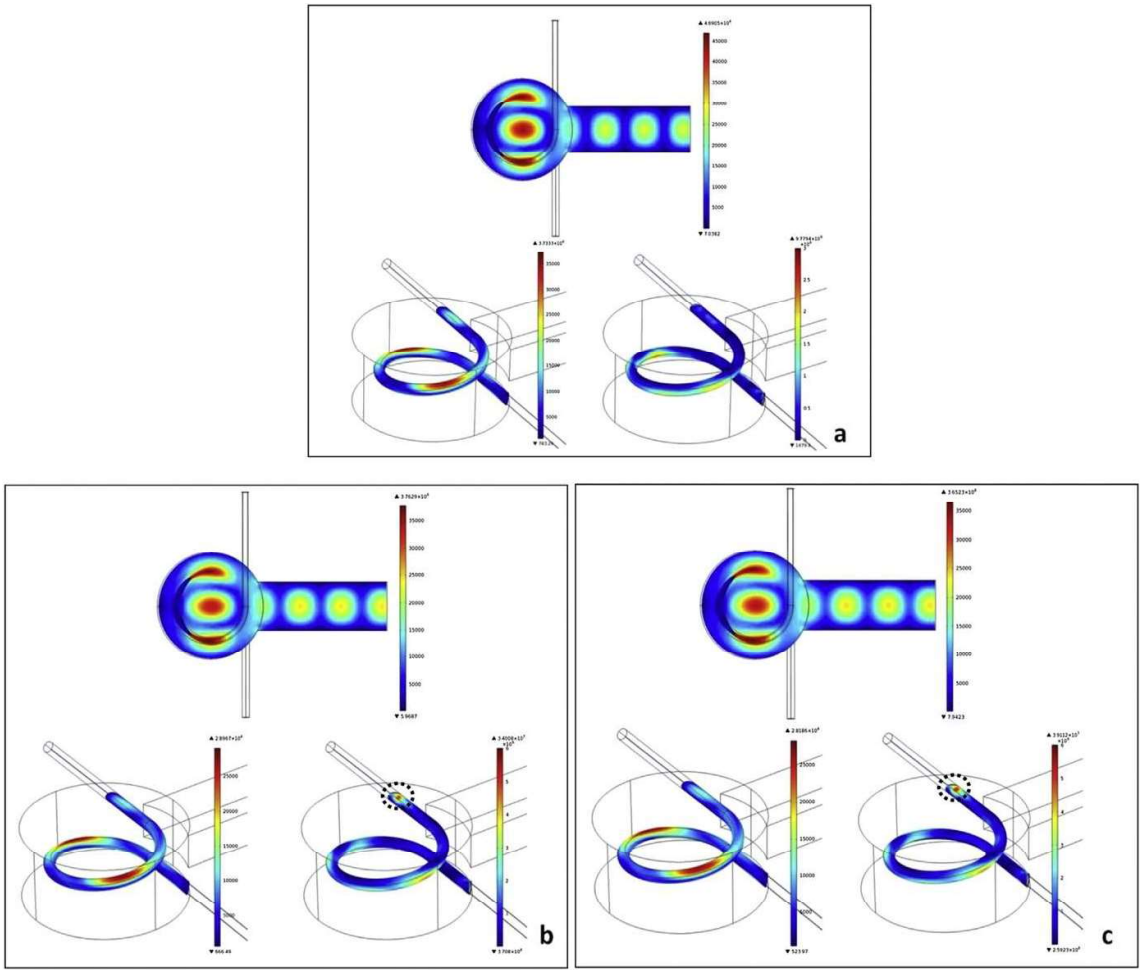

Source: Tuta and Palazoğlu *(2017).*

Raaholt, Hamberg and Isaksson (2016) designed and evaluated a pilot-scale unit for continuous flow microwave processing of viscous particulate liquid foods (Figure 1.5). The food was pre-heated to 60 °C and pumped into the microwave applicator tube where the target

temperatures were set to 100-130 °C. The microwave heating unit consists of one Transverse Magnetic (TM) TM_{020} cavity and two TM_{120} cavities. The combination of these two types of cavities can allow more uniform heating since TM_{020} heats primarily the tube center and TM_{120} heats the tube periphery first.

Figure 1.5. Schematic view of the microwave-assisted HTST unit including the microwave heating with 3 TM applicators.

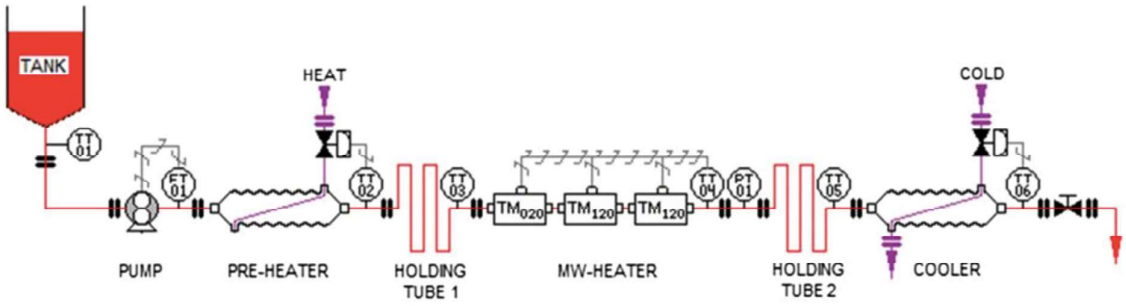

Source: Raaholt, Hamberg and Isaksson (2016).

1.2.4 Apple juice treatment

Apple juice is a source of monosaccharides, minerals, fibers, vitamin C and phenolic compounds (Podsędek et al., 2000). These organoleptic components determine the juice quality (flavor, bitterness, astringency and color) and depend on the fruit variety and maturity (Wu et al., 2007). The phenolic compounds act as antioxidants and their concentration can contribute to the apple juice discoloration and haze formation (Podsędek et al., 2000). The apple juice browning happens during juice extraction due to oxidation. The exposure to air allows the action of the oxidative enzymes (e.g., polyphenol oxidase (PPO)) on different groups of reactive phenolic compounds (catechins, chlorogenic acids and caffeic acids) (Lea, 1992).

The apple juice production comprises several food processing steps (washing, crushing and pressing). The most common apple juice is the clarified one (obtained after the clarification and filtration processes); however, the cloudy juice is a healthier alternative due to the presence of native macromolecules (pectins and proteins), insoluble solids and some phenolic compounds (Oszmianski et al., 2007). To prevent juice discoloration, ascorbic acidic can be added during juice extraction and a thermal processing can inactivate the enzymes responsible for the enzymatic browning (Massini, Rico and Martin-Diana, 2018).

Siguemoto et al. (2019) compared flavor and nutritional quality of apple juice before and after microwave-assisted pasteurization. Phenolic contents, total organic acids, total soluble sugars and volatile profile of apple juice were not significantly different between the fresh and microwave processed samples, as opposed to conventional processing with heat exchangers. Therefore, that study indicated the potential of microwave processing technology to allow the retention of fresh-like qualities of apple juice after thermal processing. Quality improvement was attributed to the fast heating and to the lack of overheated heat exchange surfaces, which reduced the product exposure to high temperatures.

1.2.5 Coconut water treatment

Green coconut water is a tropical refreshing natural drink, low in calories and fat, rich in minerals and vitamins (Naik et al., 2020). This water is the clear liquid inside of the endosperm of young green coconuts (*Cocos nucifera L.*) that counts for nearly 25% of weight of the whole nut. Coconuts have a spherical outer fibrous husk, inner hard shell and endosperm or pulp filled with sweet and nutritious water. Coconut oil, water and milk are the main products of this fruit for the food and beauty industry (Naik et al., 2020).

The physicochemical composition of 8-9 months old green coconut water is presented in Table 1.1. The composition of the coconut water may vary with the age of the fruit. Also, the maturation of the coconut can increase the pH and the concentration of sodium and iron ions.

The industrialization of coconut water is necessary due to the large volume of coconut shells, reducing transportation costs. However, after the extraction of coconut water, the fruit exposure to air occurs, allowing the action of enzymes (that alter color and flavor) and contaminant microorganisms (Campos et al., 1996). Polyphenol oxidase (PPO) and peroxidase (POD) are enzymes responsible for enzymatic browning and alteration of sensorial aspects of the coconut (Veitch, 2004; Mayer, 2006).

Currently, coconut water processing taking into account electric and dielectric emerging technologies that can substitute conventional heat exchangers has been used in previous works for pasteurization or sterilization processing, such as microwave heating (Cavalcante, Funcia and Gut, 2021; Pinto et al., 2021; Arteza-Ríos et al., 2020; Franco et al., 2015; Matsui et al., 2008; Matsui et al., 2006) and ohmic heating (Kanjanapongkul and Baibua, 2021; Delfiya and Thangavel, 2016). These technologies offer the potential for high quality products, short processing time and low usage of plant space (Tang, 2015).

Table 1.1. Physicochemical composition of 8-9 months old green coconut water.

Particulars	
Protein	0.05 mg/mL
Fat	0.60 g/100 g
Calcium	0.22 g
Magnesium	24.96 mg/100 mL
Potassium	372.10 mg/100 mL
Sodium	2.59 mg/100 mL
Iron	0.20 mg/L
pH	5.17
Total soluble solids	6.00 °Brix
Turbidity	7.52
Total Phenolic Content	62.56 mg/GAE/L

Source: Adapted from Keng et al. (2017).

In experimental studies comparing conventional and microwave-assisted thermal processing, enzymes naturally present in coconut water (PPO and POD) showed lower heat resistance in microwave treatment, facilitating enzyme inactivation (Cavalcante, Funcia and Gut, 2021; Matsui et al., 2008). This increase in enzyme inactivation after high intensity electric field tests is known in the literature as a non-thermal effect, as electric field might cause additional changes in molecular structure impacting the mechanisms of enzyme inactivation. However, the non-thermal effect of electric field is still a controversial topic in the literature and needs more study (Kubo et al., 2021).

1.2.6 Electrohydrodynamic drying

Food drying is a typical post-harvest process to remove water and prevent food losses (Iranshahi et al., 2023). Moisture in a wet solid can be presented as excess liquid on the boundaries and as a solution within the solid. To remove moisture from a solid food, the energy transfer from the surrounding environment evaporates the surface moisture and the internal moisture transfer to the surface occur (Mujumdar, 2006). Airflow and/or temperature variation can be induced in drying processes (hot air ovens, microwaves and electrohydrodynamic) to increase convective heat and mass transfer, increasing the drying rate (Aregawi et al., 2013).

The electrohydrodynamic (EHD) drying mechanism involves the induction of ionic winds that can increase the airflow in the space between the emitter electrode (high-voltage wire) and the ground collector surface (metallic plate) (Figure 1.6) (Singh et al., 2012). The ionized particles around the wire are accelerated outwards by the Coulomb force, collide with neutral air particles and induce the ionic wind toward the ground (Defraeye and Martynenko, 2018; Iranshahi et al., 2020). This induced airflow increases convective heat and mass transfer coefficients at ambient temperature and pressure and, therefore, can be employed to accelerate the convective drying of heat-sensitive food products.

Figure 1.6. Schematic representation of EHD airflow generation process from a positive corona discharge (not to scale).

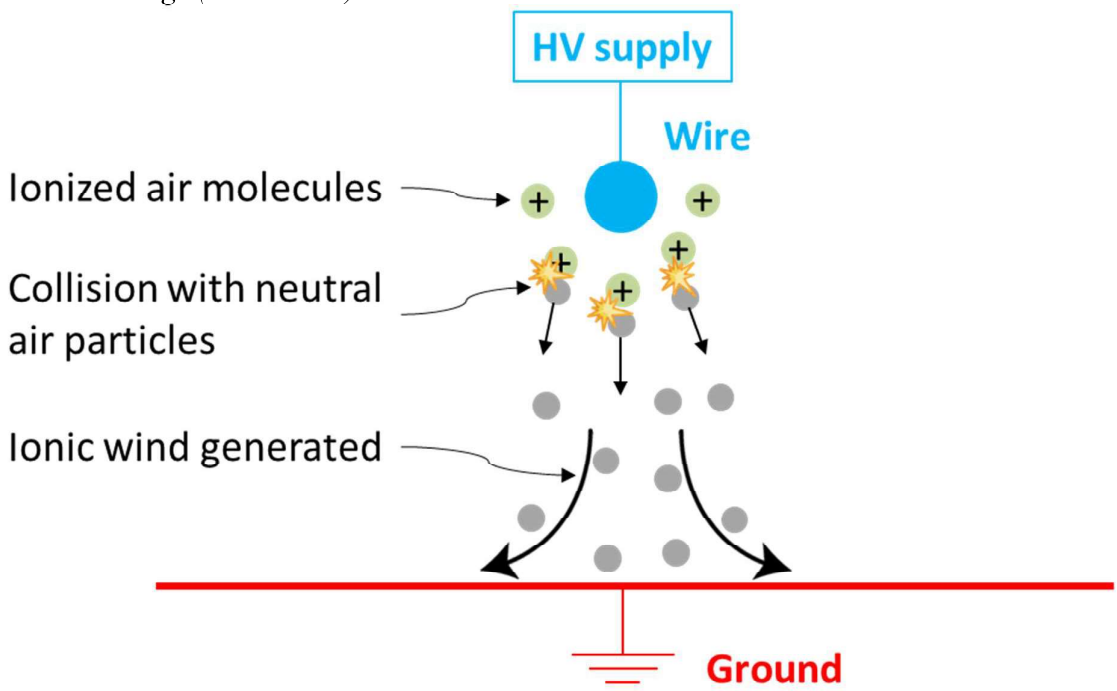

Source: The author (2023).

Defraeye and Martynenko (2018) developed an extensive multiphysics simulation study comparing different EHD wire-to-ground configurations (wire-to-plate, wire-to-mesh, mesh-to-mesh and wire-to-parallel plates) (Figure 1.7). Different geometric configurations were tested to increase the airflow over the food surface and improve drying rate and uniformity. The wire-to-mesh with a large mesh can minimize the drying time and energy consumption due to the airflow increase at the food boundary surfaces (Iranshahi et al., 2020). Onwude et al. (2021) modeled the scale-up of an EHD dryer with wire-to-mesh geometry to dry fruit slices (Figure

1.8). They verified that the EHD drying of multiple slices can be faster and consume less energy than in a conventional forced-air dryer.

Figure 1.7. Simulation results of airflow field around a fruit (5 x 10 mm) and the water activity inside the fruit (range 0-1, after 5 h of low-temperature drying) for all configurations. Maximal air speed and surface-average convective heat transfer coefficient (CHTC) are also reported.

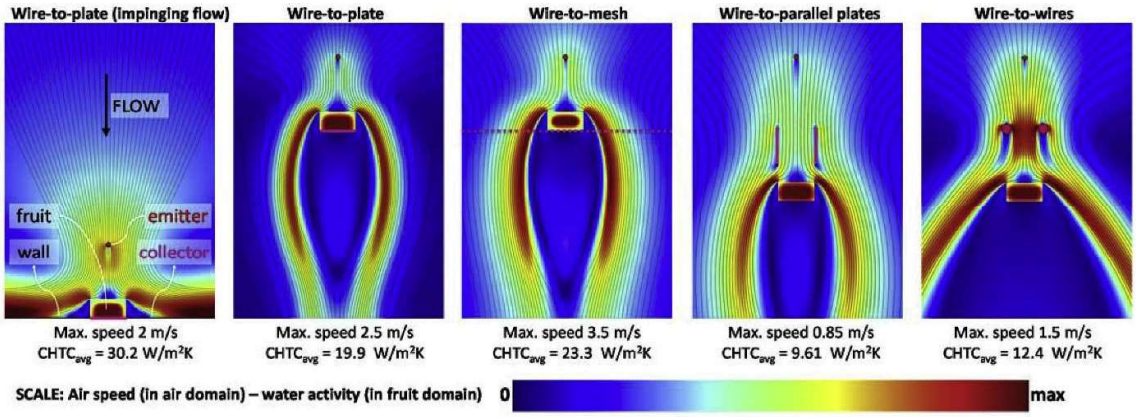

Source: Defraeye and Martynenko (2018).

Figure 1.8. Schematic of EHD wire-to-mesh dryer configuration for drying of large amounts of fruits (not to scale).

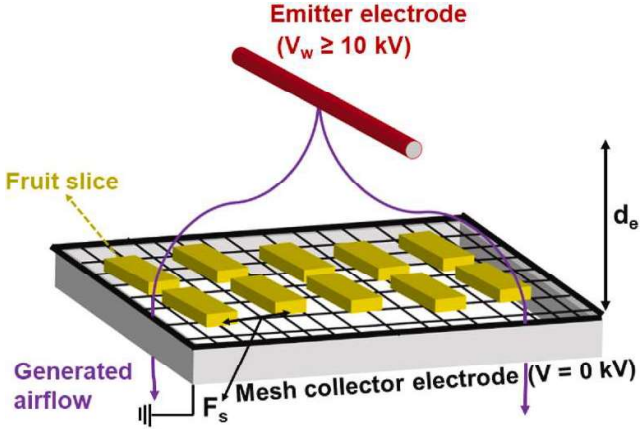

Source: Onwude et al. (2021).

Zhong et al. (2019) 3-D simulated a multi-pin (needles as the emitter electrode) EHD dryer with a crossflow air stream (Figure 1.9). The authors tested combinations of 16 and 20 kV electric potential and air crossflow velocity from 0.1 to 2.5 m/s. In Figure 1.10, the effect of different air crossflow velocities for the same electric voltage (16 kV) was studied. The velocity distribution was symmetric between two needles in the simulation without air

crossflow (a1 and b1). The increase in air crossflow velocity (from 0.10 to 0.24 m/s, a2-a3 and b2-b3), both EHD and air crossflow, seemed to contribute to the drying process, disturbing the flow field pattern. In the runs with air crossflow velocities higher than 0.69 m/s, the EHD air jet shifted from the inlet (left side) to the outlet (right side), reducing EHD flow contact with the drying material. The optimal combinations of EHD and air crossflow were 0.15 m/s and 16 kV or 0.25 m/s and 20 kV (Zhong et al., 2019).

Figure 1.9. Experimental setup: 1) drying chamber, 2) multiple-pin, 3) grounded plate, 4) digital scale and 5) air blower with flow stabilizer.

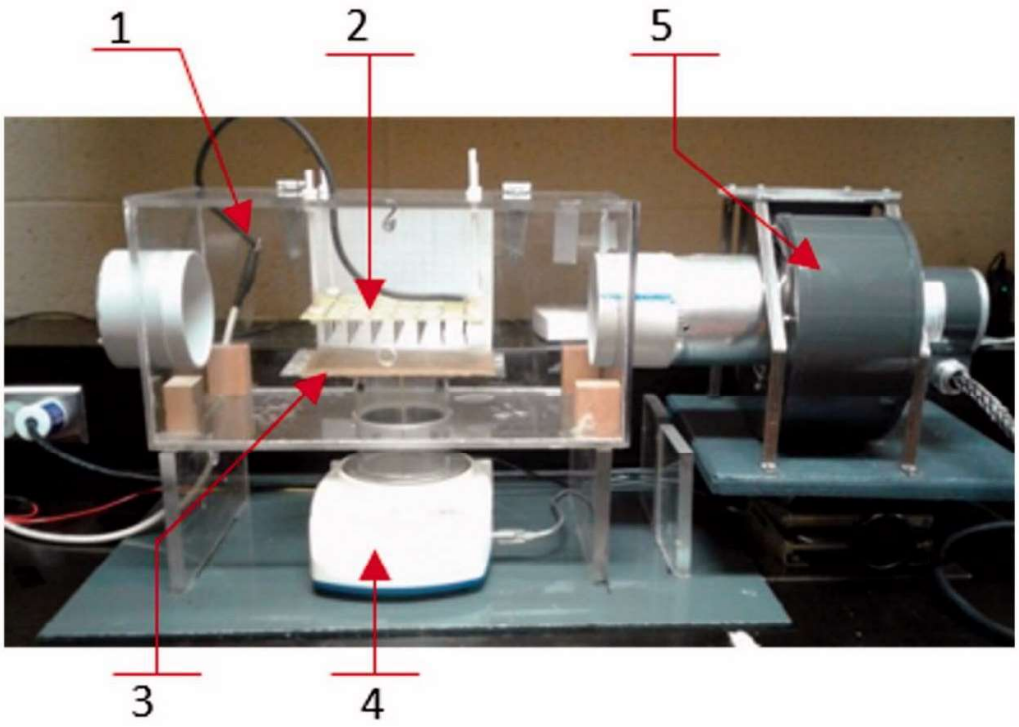

Source: Zhong et al. (2019).

Figure 1.10. Model simulation results of fluid flow with different cross-flow velocities and 16 kV electric potential: velocity distribution on a1-a4) the vertical plane and b1-b4) the horizontal plane (0.5 mm above the drying surface).

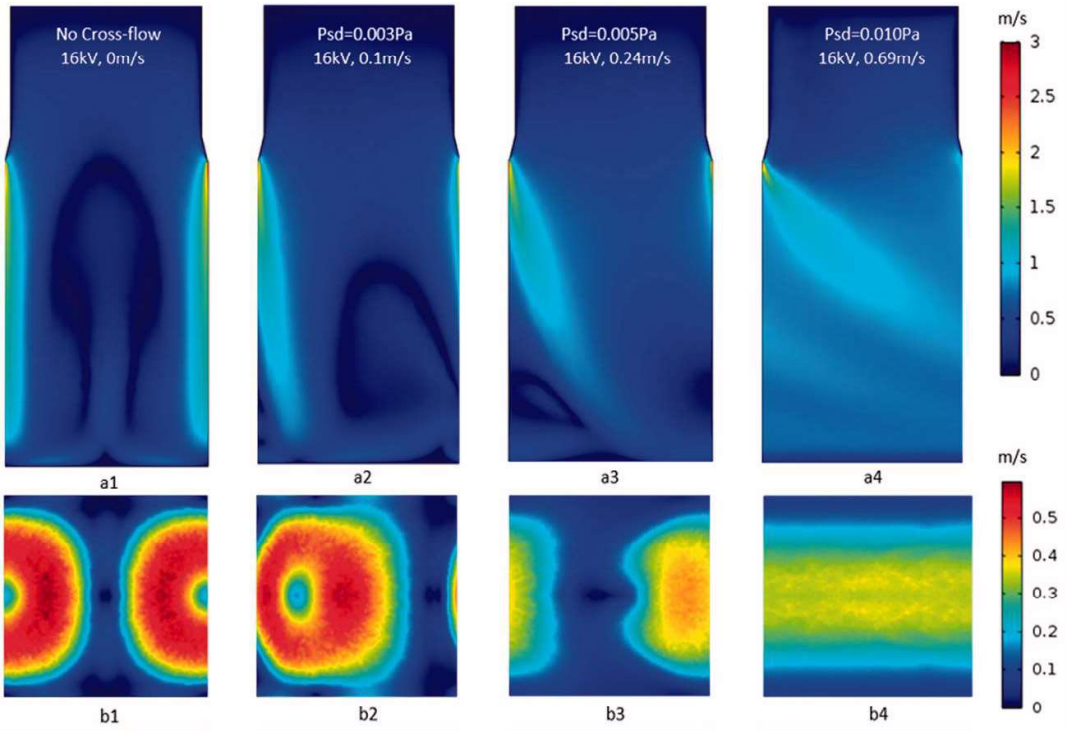

Source: Zhong et al. (2019).

1.3 REFERENCES

Aregawi W, Defraeye T, Saneinejad S, Vontobel P, Lehmann E, Carmeliet J, Derome D, Verboven P, Nicolai B. Dehydration of apple tissue: Intercomparison of neutron tomography with numerical modelling. Int J Heat Mass Transfer 2013;67:173-182. https://doi.org/10.1016/j.ijheatmasstransfer.2013.08.017

Arzeta-Ríos AJ, Guerra-Ramírez D, Reyes-Tejedo B, Ybarra-Moncada MC, Zuleta-Prada H. Microwave heating effect on total phenolics and antioxidant activity of green and mature coconut water. J. Food Eng. 2020;16:20190378. https://doi.org/10.1515/ijfe-2019-0378.

Bigelow WD. The logarithmic nature of thermal death time curves. The Journal of Infectious Diseases 1921;528-536.

Bonazzi C, Dumoulin E. Quality changes in food materials as influenced by drying processes. Modern Drying Technology 2014;3(4):1–20. https://doi.org/10.1002/9783527631728.ch14.

Campos CF, Souza PEA, Coelho JV, Glória MBA. Chemical composition, enzyme activity and effect of enzyme inactivation on flavor quality of green coconut water. J. Food Processing and Preservation 1996;20:487-500. https://doi.org/10.1111/j.1745-4549.1996.tb00761.x.

Cavalcante TABB, Funcia ES, Gut JAW. Inactivation of polyphenol oxidase by microwave and conventional heating: Investigation of thermal and non-thermal effects of focused microwaves. Food Chemistry 2021;340:127911. https://doi.org/10.1016/j.foodchem.2020.127911.

Coleman S. Key to 5G: plain talk on electromagnetic plane waves. Available in: https://www.ansys.com/fr-fr/blog/5g-plane-waves [Accessed in 7 October 2021].

Cuccurullo G, Giordano L, Viccione G. Numerical and experimental modeling for thermal developing pipe flow with microwave heating. Int. J. Mechanics 2016;10:68-74.

Dalvi-Isfahan M, Havet M, Hamdami N, Le-Bail A. Recent advances of high voltage electric field technology and its application in food processing: A review with a focus on corona discharge and static electric field. J Food Eng 2023;353:111551. https://doi.org/10.1016/j.jfoodeng.2023.111551

Damilos S, Radhakrishnan ANP, Dimitrakis G, Tang J, Gravriilidis A. Experimental and computational investigation of heat transfer in a microwave-assisted flow system. Chem. Eng. & Processing: Process Intensification 2019;142:107537. https://doi.org/10.1016/j.cep.2019.107537.

Datta AK, Sumnu G, Raghavan GSV. Dielectric properties of food. In: Rao MA, Rizvi SS, Datta AK. Engineering Properties of Foods. Boca Raton: CRC Press 2005;101-147.

Defraeye T, Martynenko A. Electrohydrodynamic drying of food: New insights from conjugate modeling. J. Cleaner Production 2018;198:269-284.

Delfiya ADS, Thangavel K. Effect of Ohmic Heating on Polyphenol Oxidase Activity, Electrical and Physicochemical Properties of Fresh Tender Coconut Water. Int. J. Food Eng 2016;12:691-700. DOI 10.1515/ijfe-2015-0329.

Dibben D. Electromagnetics: fundamental aspects and numerical modeling. In: Datta AK, Anantheswaran RC. Handbook of microwave technology for food applications. Boca Ratón: CRC Press, 2001;1-31.

Dutta A, Ekatpure R, Heynderickx G, de Broqueville A, Marin G. Rotating fluidized bed with a static geometry: Guidelines for design and operating conditions. Chem. Eng. Sci. 2010;65:1678-1693.

Dutta A, Erdogdu F, Sarghini F. Computational fluid dynamics (CFD) simulations in food processing. In: Sevda S, Singh A. Mathematical and statistical applications in food engineering. Boca Ratón: CRC Press, 2020;223-262.

Elmizadeh A, Shahedi M, Hamdami N. Comparison of electrohydrodynamic and hot-air drying of the quince slices. Innovat. Food Sci. Emerg. Technol. 2017;43:130–135. https://doi.org/10.1016/j.ifset.2017.07.030.

Erdogdu F, Karatas O, Sarghini F. A short update on heat transfer modelling for computational food processing in conventional and innovative processing. Curr Opin Food Sci 2018; 23:113–9.

Franco AP, Yamamoto LY, Tadini CC, Gut JAW. Dielectric Properties of Green Coconut Water Relevant to Microwave Processing: Effect of Temperature and Field Frequency. J. Food Eng. 2015;155:69–78. https://doi.org/10.1016/j.jfoodeng.2015.01.011.

Gut JAW, Tadini CC. Processamento térmico de alimentos. In: Tadini CC et al. Operações Unitárias na Indústria de Alimentos. Rio de Janeiro: LTC, 2018;443-488.

IMS, Industrial Microwave Systems, 6 kW Liquid Heating Microwave System, 2450 MHz, 2022. Available in: https://industrialmicrowave.com/microwave-systems-liquids-fluids-heating/6kw-microwave-system/ [Accessed in 29 Apr 2022].

Iranshahi K, Rubinetti D, Onwude DI, Psarianos M, Schlüter OK, Defraeye T. Electrohydrodynamic drying versus conventional drying methods: A comparison of key performance indicators. Energy Conversion and Management 2023;279116661. https://doi.org/10.1016/j.enconman.2023.116661.

Iranshahi K, Martynenko A, Defraeye T. Cutting-down the energy consumption of electrohydrodynamic. Energy 2020;208:118168.

Kanjanapongkul K, Baibua V. Effects of ohmic pasteurization of coconut water on polyphenol oxidase and peroxidase inactivation and pink discoloration prevention. J. Food Eng. 2021;292:110268. https://doi.org/10.1016/j.jfoodeng.2020.110268.

Keng SE, Easa AM, Muhamed AMC, Ooi CH, Chew TT. Composition and physicochemical properties of fresh and freeze-concentrated coconut (Cocos nucifera) water. J. Agrobiotech, 2017;8(1):13-24.

Knoerzer K, Buckow R, Trujillo FJ, Juliano P. Multiphysics Simulation of Innovative Food Processing Technologies. Food Eng Rev 2015;7:64-81. DOI 10.1007/s12393-014-9098-3.

Kubo MTK, Reis BHG, Sato LNI, Gut JAW. Microwave and conventional thermal processing of soymilk: Inactivation kinetics of lipoxygenase and trypsin inhibitors activity. LWT 2021;145:111275. https://doi.org/10.1016/j.lwt.2021.111275.

Kubo MTK, Baicu A, Erdogdu F, Poças MF, Silva CLM, Ricardo Simpson, Vitali AA, Augusto PED. Thermal processing of food: Challenges, innovations and opportunities. A position paper. F Reviews Int 2023;39(6):3344-3369. https://doi.org/10.1080/87559129.2021.2012789

Kumar C, Joardder MHU, Farrell TW, Millar GJ, Karim A. A porous media transport model for apple drying. Biosystems Engineering 2018;176:12-25. https://doi.org/10.1016/j.biosystemseng.2018.06.021.

Lea AGH. Flavor, Color, and Stability in Fruit Products: The Effect of Polyphenols. In: Richard W. Hemingway, Peter E. Laks. Springer New York, NY (1992) 827-847.

Martynenko A, Zheng W. Electrohydrodynamic drying of apple slices: Energy and quality aspects. J Food Eng 2016;168:215–22. https://doi.org/10.1016/j.jfoodeng.2015.07.043.

Massini L, Rico D, Martin-Dianna AB. Quality Attributes of Apple Juice: Role and Effect of Phenolic Compounds. In: Rajauria G, Tiwari BK. Fruit juices: extraction, composition, quality and analysis. Oxford: Academic Press, 45-57 (2021). https://doi.org/10.1016/B978-0-12-802230-6.00004-7.

Matsui KN, Granadob LM, de-Oliveira PV, Tadini CC. Peroxidase and Polyphenol Oxidase Thermal Inactivation by Microwaves in Green Coconut Water Simulated Solutions. LWT-Food Sci. Technol. 2007;40:852-859. https://doi.org/10.1016/j.lwt.2006.03.019.

Mayer AF. Polyphenol oxidases in plants and fungi: going places? A review. Phytochemistry 2006;67:2318-2331. https://doi.org/10.1016/j.phytochem.2006.08.006.

Meredith R. Introduction and fundamental concepts. In: Meredith R. Engineer's handbook of industrial microwave heating. Fort Collins: IET, 1998;1-18.

Mirzaei-Baktash H, Hamdami N, Torabi P, Fallah-Joshaqani S, Dalvi-Isfahan M. Impact of different pretreatments on drying kinetics and quality of button mushroom slices dried by hot-air or electrohydrodynamic drying. LWT 2022;15:112894. https://doi.org/10.1016/j.lwt.2021.112894.

Mujumdar AS. Principles, Classification, and Selection of Dryers. In: Mujumdar AS. Handbook of Industrial Drying. Boca Ratón: CRC Press 2006;4-31.

Muley PD, Boldor D. Multiphysics numerical modeling of the continuous flow microwave-assisted transesterification process. J. Microwave Power and Electromagnetic Energy 2012;46:139-162. https://doi.org/10.1080/08327823.2012.11689832.

Naik M, Sunil CK, Rawson A, Venkatachalapathy N. Tender Coconut Water: A Review on Recent Advances in Processing and Preservation. Food Reviews International, 2020. DOI: 10.1080/87559129.2020.1785489.

Ni J, Ding C, Zhang Y, Song Z. Impact of different pretreatment methods on drying characteristics and microstructure of goji berry under electrohydrodynamic (EHD) drying process. Innovat. Food Sci. Emerg. Technol. 2020;61:102318. https://doi.org/10.1016/j.ifset.2020.102318.

Oishi TK, Gut JAW. Modeling time-temperature history and sterilization value of mango puree under conventional and microwave assisted pasteurization. Int. J. Food Engineering 2021. https://doi.org/10.1515/ijfe-2020-0335.

Oszmianski J, Wolniak M, Wojdylo A, Wawer I. Comparative study of polyphenolic content and antiradical activity of cloudy and clear apple juices. J. Food Agriculture (2007) 87(4), 573-579. https://doi.org/10.1002/jsfa.2707.

Onwude Di, Iranshahi K, Rubinetti D, Martynenko A, Defraeye T. Scaling-up electrohydrodynamic drying for energy-efficient food drying via physics-based simulations. J. Cleaner Production 2021;329:129690.

Podsędek A, Wilska-Jeszka J, Anders B, Markowski J. Compositional characterization of some apple varieties. Eur Food Res Technol (2000) 210 :268–272. https://doi.org/10.1007/s002179900101.

Porto E, Filho EGA, Silva LMA, Fonteles TV, Nascimento RBR, Fernandes FAN, Brito ES, Rodrigues S. Ozone and plasma processing effect on green coconut water. Food Research International 2020;131:109000. https://doi.org/10.1016/j.foodres.2020.109000.

Prades A, Dornier N, Diop J, Pain P. Coconut water preservation and processing: a review. Fruits 2012;157-171. http://dx.doi.org/10.1051/fruits/2012009.

Puangsuwan K, Tongurai C, Chongcheawchamnan M. Design of microwave heating continuous belt system for palm fruit. Asia-Pacific Microwave Conference 2015. DOI: 10.1109/APMC.2015.7413502.

Raaholt BW, Hamberg L, Isaksson S. Continuous tubular microwave heating of particulate foods at high temperatures. Journal of Microwave Power and Electromagnetic Energy 2016;51:259-285. https://doi.org/10.1080/08327823.2016.1157318.

Raghavan, V, Rennie TJ, Sunjka PS, Orsat V, Phaphuangwittayakul W, Terdtoon P. Overview of new techniques for drying biological materials with emphasis on energy aspects. Brazilian Journal of Chemical Engineering 2005;22:195-201.

Sadiku M. Maxwell's equations. In: Sadiku M. Elements of electromagnetics. Oxford: Oxford University Press, 2012;369-409.

Salvi D, Boldor D, Sabliov CM, Rusch KA. Numerical and experimental analysis of continuous microwave heating of ballast water as preventive treatment for introduction of invasive species. J. Marine Environmental Eng. 2008;9:45-64.

Salvi D, Boldor D, Aita GM, Sabliov CM. COMSOL Multiphysics model for continuous flow microwave heating of liquids. J. Food Engineering 2011;104:422-429. https://doi.org/10.1016/j.jfoodeng.2011.01.005.

Sevda S, Garlapati VK, Singh A. Role of mathematical and statistical modeling in food engineering. In: Sevda S and Singh A. Mathematical and statistical applications in food engineering. Boca Ratón: CRC Press, 2020:1-4.

Sierra I, Vidal-Valverde C, Olano A. The effects of continuous flow microwave treatment and conventional heating on the nutritional value of milk as shown by influence on vitamin B 1 retention. European Food Research and Technology 1999;209:352–354. https://doi.org/10.1007/s002170050508.

Siguemoto ÉS, Gut JAW. Dielectric Properties of Cloudy Apple Juices Relevant to Microwave Pasteurization. Food and Bioprocess Technology, 2016;9(8):1345–1357. https://doi.org/10.1007/s11947-016-1723-0.

Siguemoto ÉS, Pires MN, Funcia ES, Gut JAW. Evaluation and modeling of a microwave-assisted unit for continuous flow pasteurization of liquid foods: Residence time distribution, time–temperature history, and integrated lethality. Journal of Food Process Engineering, v. 41(8), p.1-13, 2018. https://doi.org/10.1111/jfpe.12910.

Siguemoto ÉS, Funcia ES, Pires MN, Gut JAW. Modeling of time-temperature history and enzymatic inactivation of cloudy apple juice in continuous flow microwave assisted pasteurization. Food and bioproducts processing 2018;111:45-53. https://doi.org/10.1016/j.fbp.2018.06.004.

Siguemoto ÉS, Purgatto E, Hassimotto NMA, Gut, JAW. Comparative Evaluation of Flavour and Nutritional Quality after Conventional and Microwave-Assisted Pasteurization of Cloudy Apple Juice. LWT 2019;111:853-60. https://doi.org/10.1016/j.lwt.2019.05.111.

Singh A, Orsat V, Raghavan V. A Comprehensive Review on Electrohydrodynamic Drying and High-Voltage Electric Field in the Context of Food and Bioprocessing. Drying Tech.: An Int. J. 2012;30:1812-1820.

Singh A, Vanga SKK, Nair GR, Gariepy Y, Orsat V, Raghavan V. Electrohydrodynamic Drying of Sand. Drying Tech: An Int. J. 2016;35:312-322.

Tang J. Unlocking potentials of microwaves for food safety and quality. J Food Eng. 2015;8:E1776-E1793. https://doi.org/10.1111/1750-3841.12959.

Tajchakavit S, Ramaswamy HS. Continuous-flow microwave heating of orange juice: evidence of nonthermal effects. Journal of Microwave Power and Electromagnetic Energy 1995;30:141-148. DOI:10.1080/08327823.1995.11688270.

Teixeira AA, Dixon JR, Zahradnik JW, Zinsmeister GE. Computer optimization of nutrient retention in the thermal processing of conduction-heated foods. Food Technol 1969;23:137–42.

Tewari G. Microwave and Radio-Frequency heating. In: Tewari G, Junega V. Advances in thermal and non-thermal food preservation. Iowa: Blackwell Publishing 2007;91-98.

Toledo RT. Fundamentals of Food Process Engineering. New York: Springer, 1999.

Topcam H, Erdogdu F. Designing system cavity geometry and optimizing process variables for continuous flow microwave processing. Food and Bioproducts Processing 2021;127:295-308. https://doi.org/10.1016/j.fbp.2021.03.006.

Tribess TB, Tadini CC. Inactivation kinetics of pectin methylesterase in orange juice as a function of pH and temperature/time process conditions. J Sci F Agri 2006;86(9):1328-1335. https://doi.org/10.1002/jsfa.2512.

Tuta S, Palazoğlu TK. Finite element modeling of continuous-flow microwave heating of fluid foods and experimental validation. J. Food Engineering 2017;192:79-92. https://doi.org/10.1016/j.jfoodeng.2016.08.003.

UN, United Nation, The Sustainable Development Goals Report 2023: Special Edition, 2023. Available in: https://unstats.un.org/sdgs/report/2023/ [Accessed in 15 Oct 2023].

Van Loey A, Indrawati, Smout C, Hendrickx M. Inactivation of enzymes from experimental design to kinetic modeling. In: Whitalker JL, Voragen, AGJ, Wang DWS. Handbook of Food Enzymology. Boca Raton: CRC press 2003;49-58.

Veitch NC. Horseradish peroxidase: a modern view of a classic enzyme. Phytochemistry 2004;65:249-259. doi:10.1016/j.phytochem.2003.10.022.

Wu J, Gao H, Zhao L, Liao X, Chen F, Wang Z, Hu X. Chemical compositional characterization of some apple cultivars. Food Chem. (2007) 103(1), 88-93. https://doi.org/10.1016/j.foodchem.2006.07.030.

Yang H, Zhang Y, Gao W, Yan B, Zhao J, Zhang H, Chen W, Fan D. Steam replacement strategy using microwave resonance: A future system for continuous-flow heating applications. Applied Energy 2021;283:116300. https://doi.org/10.1016/j.apenergy.2020.116300.

Zhang Y, Yang H, Yan B, Zhu H, Gao W, Zhao J, Zhang H, Chen W, Fan D. Continuous flow microwave system with helical tubes for liquid heating. J. Food Engineering 2021;294:110409. https://doi.org/10.1016/j.jfoodeng.2020.110409.

Zhong C, Martynenko A, Wells P, Adamiak K. Numerical investigation of the multi-pin electrohydrodynamic dryer: Effect of cross-flow air stream. Drying Technology 2019;37(13):1665-1677. DOI: 10.1080/07373937.2018.1531291.

Zhu J, Kusnetsov AV, Sandeep KP. Mathematical modeling of continuous flow microwave heating of liquids (effects of dielectric properties and design parameters), Int. J. Therm. Sci. 2007;46:326-341.

Zuberi MJS, Hasanbeigi A, Morrow W. Bottom-up assessment of industrial heat pump applications in U.S. Food manufacturing. Energy Conversion Management 2022;272:116349. https://doi.org/10.1016/j.enconman.2022.116349.

2 EXPERIMENTAL VALIDATION OF A MULTIPHYSICS MODEL FOR THE MICROWAVE-ASSISTED PASTEURIZATION OF APPLE JUICE

*This chapter is based on the following paper:

Oishi TK, Pouzada EVS, Gut JAW. Experimental validation of a multiphysics model for the microwave-assisted pasteurization of apple juice. Digital Chemical Engineering 2022;5:100053. DOI: 10.1016/j.dche.2022.100053

2.1 INTRODUCTION

Apple juice is a food product of great importance in the beverage industry due to its unique aroma, color and flavor; however, these organoleptic characteristics may deteriorate during thermal treatment. The continuous flow thermal processing of liquid foods aims for the inactivation of enzymes and microorganisms with minimal quality degradation. In the use of conventional heat exchangers (tubular or plate), thermal exchange occurs only by convection, which makes heating slow and non-uniform when in laminar flow (Tajchakavit et al., 1998). Microwave-assisted processing is of interest for the food industry due to the rapid volumetric heating. Microwave radiation penetrates directly into the food resulting in high rates of heat transfer, high energy conversion efficiency and lower wall temperatures (Zhu et al., 2007).

Continuous flow microwave-assisted systems have been researched for pasteurization or sterilization of liquid foods, such as apple juice (Tajchakavit et al., 1998; Siguemoto et al., 2018), apple cider (Gentry and Roberts, 2005), milk (Sierra et al., 1999; Valero et al., 2000; Coronel et al., 2003), peanut beverages (Sabliov et al., 2008), tomato juice (Stratakos et al., 2016), pomegranate juice (Gómez-Sánchez et al., 2020), kava juice (Abdullah et al., 2013), orange juice (Tajchakavit and Ramaswamy, 1995), sweet potato puree (Coronel et al., 2005; Brinley et al., 2007; Steed et al., 2008), model soup (Raaholt et al., 2016), parsley with cheese (Kumar et al., 2007), strawberry puree (Marszałek, et al. 2015) and mango puree (Oishi and Gut, 2021). Over the years, technological advances have been improving the design and operational procedures of continuous flow microwave applicators in order to overcome shortcomings for scaling up and certification (Simunovic and Sandeep, 2021).

Siguemoto et al. (2019) compared flavor and nutritional quality of apple juice before and after microwave-assisted pasteurization. Phenolic contents, total organic acids, total soluble sugars and volatile profile of apple juice were not significantly different between the fresh and microwave processed samples, as opposed to conventional processing with heat exchangers.

Therefore, this study indicated the potential of microwave processing technology to allow the retention of fresh-like qualities of apple juice after thermal processing. Quality improvement was attributed to the fast heating and to the lack of overheated heat exchange surfaces, which reduced the product exposure to high temperatures.

To adequately evaluate or optimize a thermal process, phenomenological mathematical modeling can be used. The evaluation of heat transfer and flow is essential to predict temperature distributions and effects on chemical and microbiological components of the food (Teixeira et al., 1969 Erdogdu et al., 2018). Researchers have modeled different continuous-flow microwave cavity geometries with straight (Yang et al., 2021; Topcam and Erdogdu, 2021; Cuccurullo et al., 2016; Puangsuwan et al., 2015; Muley and Boldor, 2012; Salvi et al., 2011), helical (Zhang et al., 2021; Tuta and Palazoğlu, 2017) or curved (Topcam and Erdogdu, 2021; Damilos et al., 2019) applicator tubes using multiphysics software to obtain predictions of temperature distribution in Newtonian (water, sodium chloride solutions and fruit juices) and non-Newtonian (CMC solutions, whole liquid egg and surimi paste) pumpable food and model foods. Due to the complexity of coupling electromagnetic wave propagation with flow and heat transfer, multiphysics modeling has been an important tool for the design of applicators.

This work aims to model and simulate the continuous flow microwave cavity used to pasteurization of apple juice. The model of the microwave cavity includes electromagnetism, heat transfer and fluid flow in the finite element software package COMSOL Multiphysics (v.6.0). To validate the multiphysics model, experimental runs were carried out in a MicroThermics pasteurization unit (2.45 GHz and 6 kW) and the processing temperature after the microwave heater was measured and compared with the temperature predicted by the model.

2.2 METHODOLOGY

In continuous flow thermal treatments, the food stream is subjected to a temperature increase followed by a holding period in a tube and, then, the food is subjected to a cooling step (Singh and Heldman, 2009). A continuous flow pasteurization unit Lab25-UHT/HTST EHVH (MicroThermics, Raleigh, USA) was used to validate the proposed mathematical model. As can be seen in Figure 2.1, the liquid flows through conventional pre-heater, the microwave heater, the holding tube and the cooler.

Pre-heater and cooler sections consist of helical coil heat exchangers connected to a 18.0 kW hot water and a 3.5 kW cold water closed circuits, respectively. The microwave heater consists of a Polytetrafluoroethylene (PTFE) tube with a ceramic pressure sleeve housed inside

of a single-mode cavity connected to a 6 kW magnetron at 2450 MHz (Industrial Microwave Systems, 2022). The magnetron is equipped with a reflected power sensor and linked to a Microwave Power Meter software. The 3-stub tuner in Figure 2.1 was used to minimize the reflected power. Manual adjustment of the stubs must be carried out in order to obtain the reflected power under 20 W (Siguemoto et al., 2018).

Figure 2.1. Diagram of apple juice thermal processing in the pasteurization unit Lab25-UHT/HTST EHVH (MicroThermics, Raleigh, EUA).

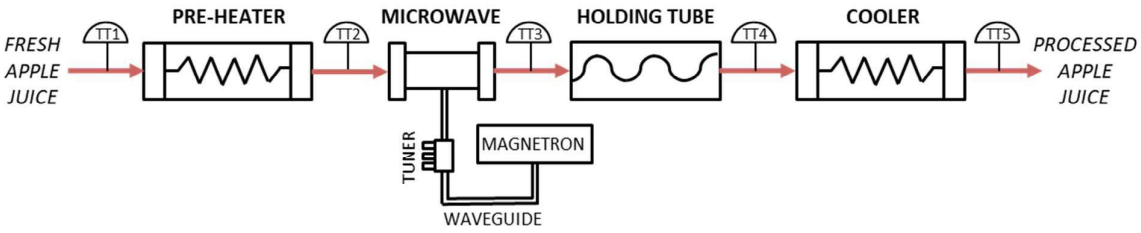

Source: Oishi, Pouzada and Gut (2022).

2.2.1 Multiphysics modeling

The mathematical model of the microwave cavity was developed as follows. Continuous flow microwave thermal processing requires coupling the physics of electromagnetic wave propagation, laminar flow and heat transfer in fluids. This was accomplished using the finite element software COMSOL Multiphysics (v.6.0). The main assumptions of the model were:

1) Apple juice: incompressible Newtonian fluid with temperature dependent viscosity, thermal conductivity and dielectric properties, and average values for density and specific heat.
2) The flow was assumed in laminar regime ($2856 \leq Re \leq 8781$).
3) Steady-state operation.
4) The applicator tube was considered to be electromagnetic lossless (transparent to the microwave energy).
5) The air inside of the cavity and the waveguide were assumed as lossless media.
6) Negligible power and heat losses at the waveguide and cavity walls.

2.2.2 Model geometry

The 3-D geometry was developed using the geometry node in COMSOL Multiphysics (v. 6.0, Stockholm, Sweden). The microwave cavity geometry (IMS, Gorhan, USA) was based on the assembly as in the unit Lab25-UHT/HTST EHVH (MicroThermics, Raleigh, USA) (Figure 2.2a). The microwave cavity has an octagonal prism and is stimulated by a magnetron, responsible for the generation of microwaves at a nominal frequency of 2.45 GHz and a maximum power of 6 kW (Figure 2.2b). Inside the cavity, there is a vertical tube (inside diameter of 6.60 mm and 0.33 m of tube length) in which the apple juice flows.

Figure 2.2. a) Picture and b) Schematic representation of the microwave cavity.

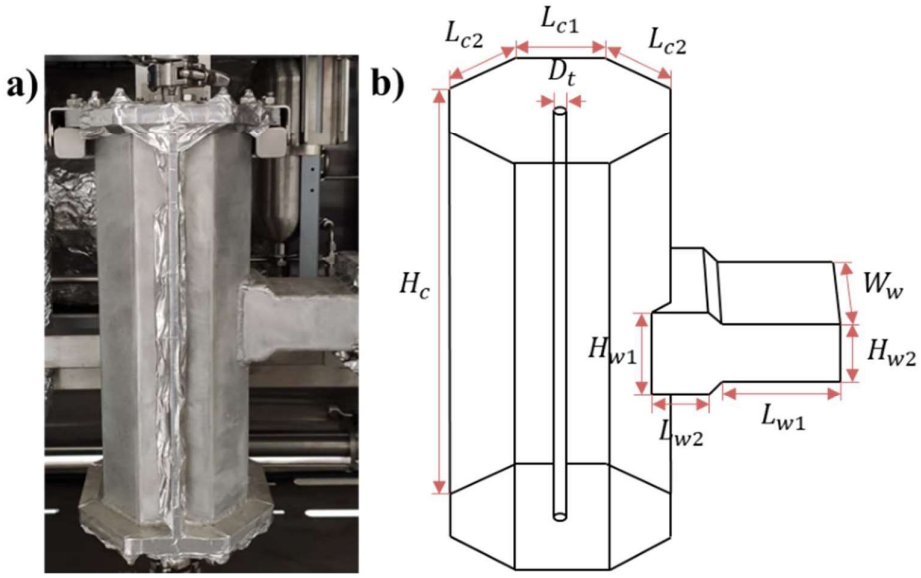

Source: Oishi, Pouzada and Gut (2022).

2.2.3 Governing equations

ELECTROMAGNETIC MODEL:

For the microwave cavity, the model includes the Radio Frequency (RF) module and Electromagnetic Waves, Frequency-Stationary as the physics-based model interface in the software. The electromagnetic heating is a function of the intensity of the local electric field, which depends on the system geometry, electromagnetic coupling and liquid food properties. Maxwell's equations were solved to obtain the electric field distribution (Dibben, 2001):

$$\nabla \times \frac{1}{\mu_0 \, \mu_r} \nabla \times \mathbf{E} - \omega^2 \, \varepsilon_0 \, \varepsilon_c \, \mathbf{E} = 0 \tag{2.1}$$

where $\mu_0 = 4\,\pi \times 10^{-7}$ is the permeability of free space (H/m), μ_r is the relative permeability, $\mathbf{E}$ is the local electric field intensity (V/m), $\omega = 2\,\pi\,f$ is the angular wave frequency (rad/s), $\varepsilon_0 = 8.854 \times 10^{-2}$ is the free space permittivity (F/m), and $\varepsilon_c = \varepsilon_r' - i\,\varepsilon_r''$ is the relative complex permittivity given by real (ε_r', dielectric permittivity) and imaginary (ε_r'', dielectric loss factor) parts (Zhang and Datta 2003; Geedipali et al. 2007). The ε_r' represents the amount of stored due to polarization while the ε_r'' measures the amount of energy dissipated as heat within the material (Tewari, 2007).

From the electric field distribution and the medium complex permittivity, the volumetric power generation (Q, W/m^3) is defined as the power absorbed by the dielectric liquid food due to the incident microwave energy and it was determined as follows (Geedipali et al. 2007):

$$Q = \frac{1}{2} \omega \, \varepsilon_0 \, \varepsilon_r'' \, |\mathbf{E}|^2 \tag{2.2}$$

HEAT TRANSFER IN FLUIDS MODEL:

Heat transfer was solved within the fluid stream using the Heat Transfer in fluids module of the software. The temperature distribution in fluid interface is given by the energy equation with the volumetric power generation from Eq. (2.2) as the source term:

$$\rho \, C_p \, \mathbf{u} \cdot \nabla \, T = \nabla \cdot (k \, \nabla \, T) + Q \tag{2.3}$$

where ρ is the density (kg/m^3), C_P is the specific heat (J/(kg.K)), $\mathbf{u}$ is the velocity vector (m/s), T is the temperature (K) and k is the thermal conductivity (W/(m.K)).

The mixing cup average temperature ($\bar{T}$, K) of the fluid was calculated as follows:

$$\bar{T} = \frac{\int u \, T \, 2\,\pi \, r \, dr}{\bar{u}} \tag{2.4}$$

where u is the axial velocity profile, $\bar{u}$ is the average velocity (m/s) and r is the radial direction in the tube (m).

LAMINAR FLOW MODEL:

The fluid flow was modeled considering laminar flow behavior of a Newtonian incompressible fluid using CFD module and Laminar Flow interface of the software. The velocity profile of the fluid domain was described by the momentum conservation equation in steady-state condition:

$$\rho \, \mathbf{u} \cdot \nabla \mathbf{u} = -\nabla p + \mu \nabla^2 \mathbf{u} \tag{2.5}$$

where p is the hydrodynamic pressure (Pa).

To model the flow of apple juice entering the tube, the velocity profile of a fully-developed laminar flow in a cylindrical tube is presented by Bird, Stewart and Lightfoot (2002):

$$u = 2\,\bar{u}\left(1 - \left(\frac{r}{R}\right)^2\right) \tag{2.6}$$

$$\bar{u} = \frac{\dot{Q}}{\pi R^2} \tag{2.7}$$

where $\dot{Q}$ is the volumetric flow rate (m^3/s) and R is the inner radius of the applicator tube (m).

2.2.4 Boundary conditions

For the physics of electromagnetic waves, the perfect electric conductor boundary condition ($\mathbf{n} \times \mathbf{E} = 0$) was applied to the cavity and waveguide metallic walls. The TE_{10} (Transverse Electric) mode was applied as the RF source. The frequency and supplied power values used as port boundary conditions were 2.45 GHz and 1.4 kW, respectively, but, later, for validation purposes, the supplied power was based on the experimental results. In the physics for laminar flow and heat transfer in fluids, the apple juice temperature at the applicator tube inlet was set to 30 °C. The no-slip condition was applied over the tube. For the volumetric flow rates 0.4 and 0.8 L/min, the average inlet velocities ($\bar{u}$) were 0.19 and 0.39 m/s.

2.2.5 Mesh and solvers

For reliable numerical results, good meshing is an important issue to be defined. To solve the electromagnetic equations, a large number of iterations is required to obtain the electric field at each time step (Pitchai et al., 2012). Free tetrahedral meshing was used for the model domains (air, PTFE tube and apple juice). Zhou et al. (2019) considered a reliable Mesh Element Quality (MEQ) < 0.2. MEQ represents the regularity of elements morphology, and coarse mesh resolution can lead to inaccurate results or even “no result” (COMSOL, 2022).

The selected number of finite elements in the microwave cavity model was 809,462 tetrahedral elements, resulting in a total of 5,678,364 equations. Figure 2.3 shows the final mesh for the microwave cavity model with a zoom view applied in the applicator tube radial outlet surface mesh.

Figure 2.3. Numerical mesh for the model solution: waveguide, cavity and applicator tube.

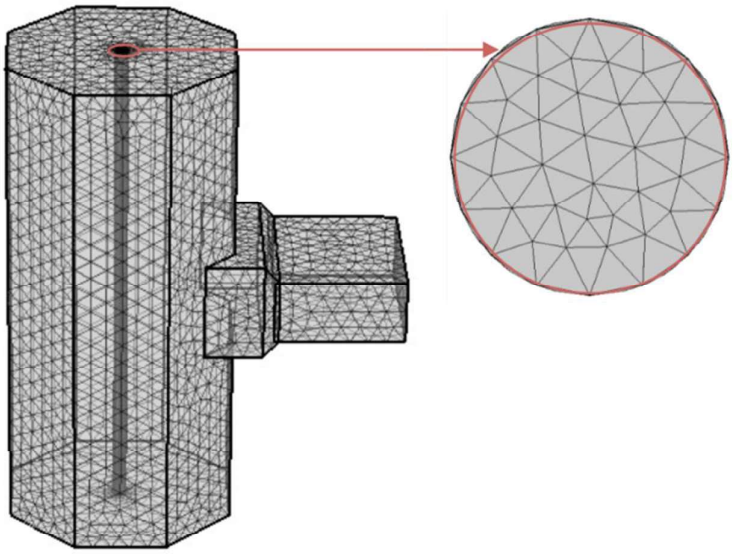

Source: Oishi, Pouzada and Gut (2022).

The numerical model was solved using a Finite Element Method (FEM) in COMSOL Multiphysics (v.6.0, Stockholm, Sweden). A Frequency-Stationary study was used to compute the heat transfer and the electromagnetic field distribution with the physics interfaces for electromagnetic waves, laminar flow and heat transfer (COMSOL, 2022). These physics were combined iteratively to solve and predict the electric field, velocity profile and temperature distribution through the fluid domain. The simulations were performed on an Intel Xeon 2403 @ 1.8 GHz workstation with 64 GB RAM and the simulation time was around 1 hour and 42 minutes.

The simulation procedure flow chart is summarized in Figure 2.4. The Frequency-Stationary study was divided into two domains: stationary (laminar flow) and frequency (electromagnetic and heat transfer). First, in the stationary domain, the fluid velocity distribution was calculated. Then, in the frequency domain, the electric and magnetic fields, the volumetric power generated in the liquid food and the temperature distribution were determined.

Figure 2.4. Simulation procedure flow chart for the microwave cavity model.

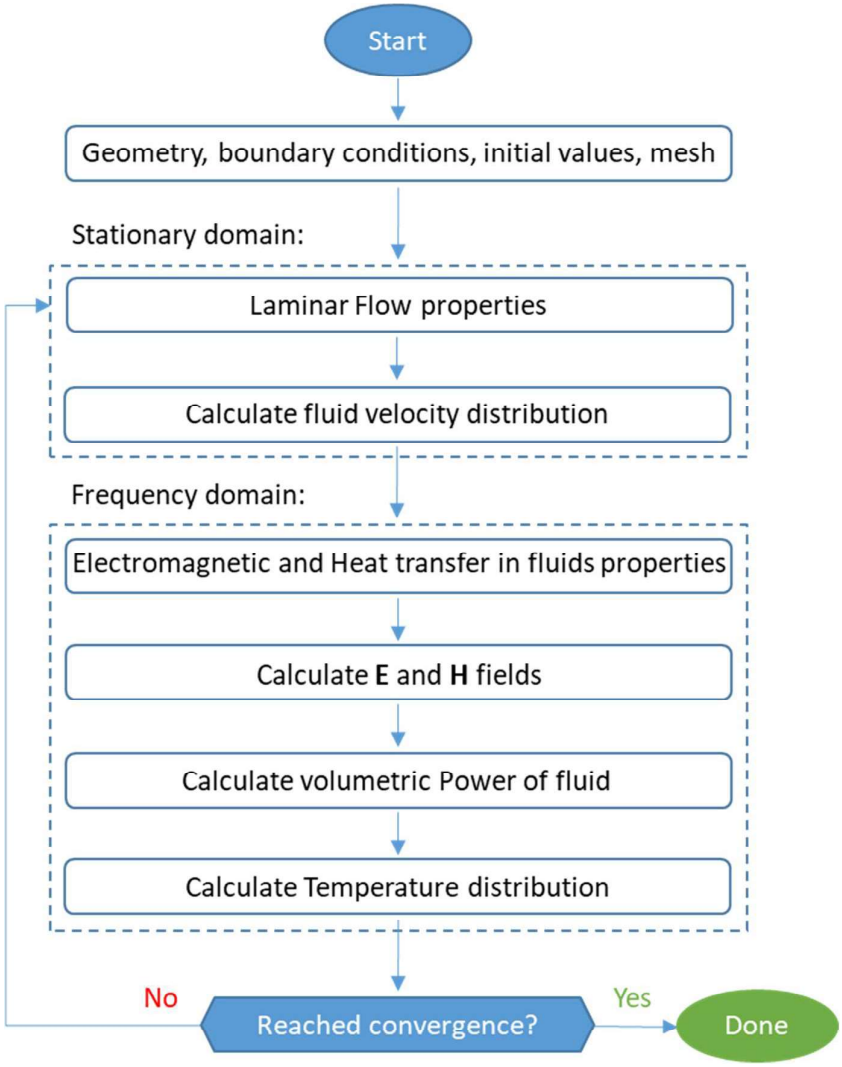

Source: Oishi, Pouzada and Gut (2022).

The model input parameters consider the materials in the microwave cavity: aluminum (metal walls), air (inside the cavity and waveguide), PTFE (applicator tube) and apple juice (in the tube). The electromagnetic properties of the materials and the temperature-dependent thermophysical properties of the apple juice are listed in Table 2.1.

Table 2.1. Material properties of the model, the dielectric, electric conductivity and thermophysical properties of apple juice were evaluated in the temperature range of 10 and 90 °C, at 2.45 GHz (a Siguemoto et al., 2016; b Bayindirli, 1992).

Property	Domain	Value	Unit
Relative dielectric permittivity (ε_r')	Air/PTFE	$\varepsilon_r' = 1$	-
	Apple juice [a]	$\varepsilon_r' = -2.00\ 10^{-4}\ T(\mathrm{K})^2 - 4.04\ 10^{-2}\ T(\mathrm{K}) + 101.09$	
Relative dielectric loss (ε_r'')	Air/PTFE	$\varepsilon_r'' = 0$	-
	Apple juice [a]	$\varepsilon_r'' = 2.00\ 10^{-3}\ T(\mathrm{K})^2 - 1.43\ T(\mathrm{K}) + 261.65$	
Electrical conductivity (σ)	Air/PTFE	$\sigma = 0$	S/m
	Apple juice [a]	$\sigma = 3.94\ 10^{-2}\ T(\mathrm{K}) - 10.31$	
Relative permeability (μ_r)	Air/PTFE	$\mu_r = 1$	-
	Apple juice	$\mu_r = 1$	
Thermal conductivity (k)	Apple juice [b]	$k = 6.82\ 10^{-2}\ e^{7.70\ 10^{-3}\ T(\mathrm{K})}$	W/(m.K)
Specific heat capacity (C_P)	Apple juice [b]	$C_P = 4185$	J/(kg.K)
Density (ρ)	Apple juice [b]	$\rho = 1060$	kg/m^3
Dynamic viscosity (μ)	Apple juice [b]	$\mu = 0.4918\ e^{-2.00\ 10^{-2}\ T(\mathrm{K})}$	Pa.s

Source: Oishi, Pouzada and Gut (2022).

2.3 EXPERIMENTAL RUNS

Siguemoto et al. (2018) pasteurized fresh apple juice (pH = 3.97 ± 0.02 and Total Soluble Solids = 12.1 ± 0.1 °Brix) in the continuous flow microwave system (Figure 2.1) at three processing temperatures (70, 80 and 90 °C) and two flow rates (0.4 and 0.8 L/min), thus a total of $2 \times 3 = 6$ conditions were tested. The residence time at the holding tube after the microwave heater was 30 s at 0.4 L/min and 15 s at 0.8 L/min and the inactivation of enzymes pectin methylesterase, peroxidase, and polyphenol oxidase was evaluated. Since the pH of the

juice is lower than 4.6 (high-acid food), the process target is enzymes rather than microorganisms (Awuah, Ramaswamy, Economides, 2007). Siguemoto et al. (2018) showed that the contribution of the microwave heater to the lethality of enzymes is minimal because of its very short residence time.

In the experimental runs, the pre-heater of the pasteurization unit was used to standardize the inlet temperature of the product to 30 °C. The temperatures were measured by Temperature Transmitters (TT) positioned at the inlet and outlet of the microwave cavity (TT2 and TT3), as shown in Figure 2.1. The food product outlet temperature was automatically controlled by adjusting the power (0 to 100%) feed to the magnetron. The temperature data measured at TT3 were used to validate the model. The processing time or flow time was considered to be the mean residence time in the applicator tube (ratio of the tube internal volume to the volumetric flow rate).

From the temperatures measured at TT2 and TT3 (Figure 2.1), it is possible to calculate the absorbed power (q, W) with the heat balance assuming steady-state operation without phase changes or heat losses:

$$P_{absorbed} = \rho\ \dot{Q}\ \ C_P\ (TT3 - TT2) \tag{2.9}$$

where ρ is the average liquid food density (kg/m^3), C_P is the average liquid food specific heat capacity (J/(kg.K)) and TT2 and TT3 are the inlet and outlet food product average recorded temperatures (K).

Based on initial simulation results, a power loss due to reflection in the microwave cavity was observed (power absorbed was lower than power supplied at port). Consequently, the supplied power used as boundary condition at the port was 18% higher than the value needed to reach the pasteurization temperature. In the experiments, the 3 stubs tuner in the wave guide was used to minimize power reflection from the cavity, but the tuner was not part of the numerical model. The model was solved and combined with the average residence time of each volumetric flow rate providing the time-temperature longitudinal distributions.

2.4 RESULTS AND DISCUSSION

2.4.1 Electric field and temperature distribution

The six combinations of processing temperatures and flow rates were successfully simulated and the electric field distribution within the microwave cavity and the temperature distribution within the applicator tube for processing at 70 °C and 0.4 L/min are show in Figure

2.5 as an example. For the applicator tube outlet, the electric field and temperature distributions are placed on the left side of the figure. Figure 2.5a illustrates the intensity of electric field halfway of the microwave cavity high ($H_c/2$, Figure 2.2b).

Figure 2.5. a) Electric field within the microwave cavity at the processing conditions of 70 °C, 0.4 L/min and 1.4 kW supplied power and b) Surface temperature distribution within the pipe and outlet cross-section.

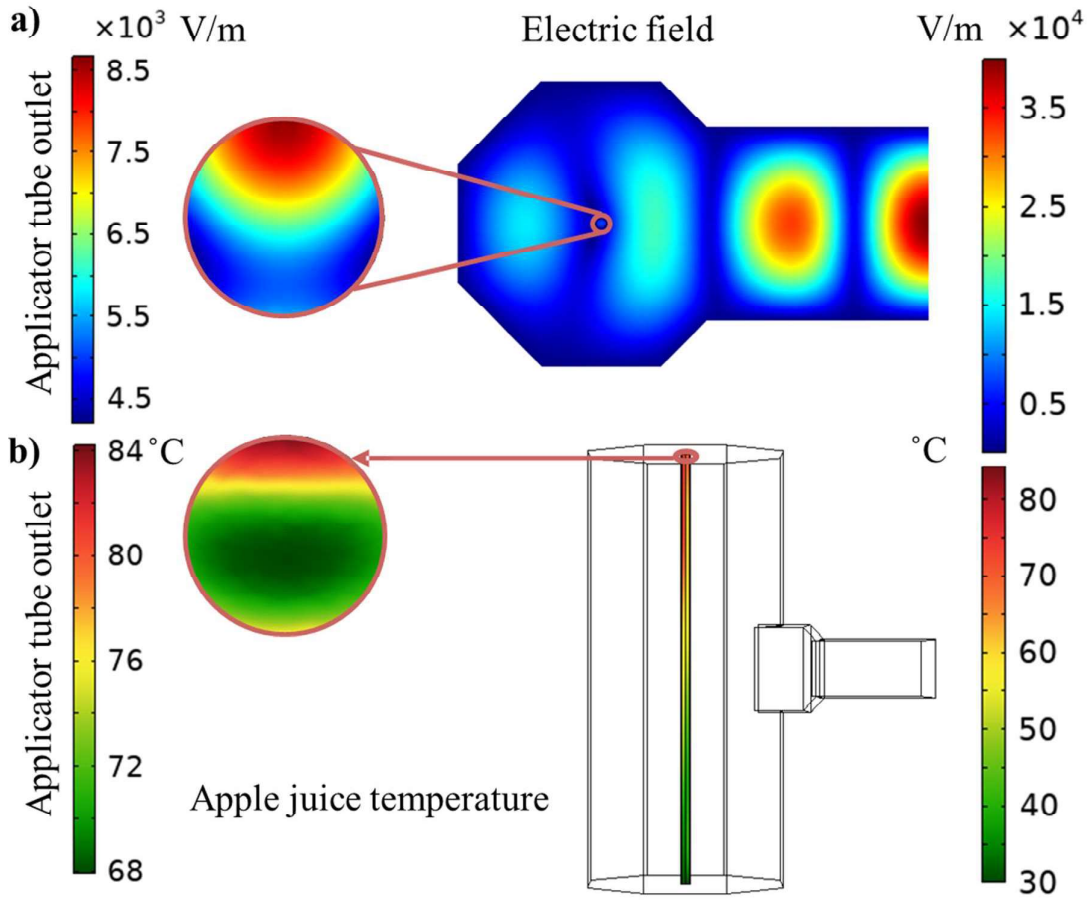

Source: Oishi, Pouzada and Gut (2022).

The surface temperature distribution along the applicator tube length is presented in Figure 2.5b. The simulation shows that the apple juice enters the tube at 30 °C and at the tube outlet the temperature reaches temperatures between 68 and 84 °C. This large temperature gradient is related to undesirable non-homogeneous electric field distribution in the applicator tube, which was also verified by Kumar et al. (2008). They processed vegetable purees with a 60 kW continuous flow microwave system and measured the temperature distribution at the end of the microwave heater. A temperature difference between the tube center and wall of 18.0

°C was observed. This non-homogeneous heating is not appropriate for food quality (nutrients, color, flavor and texture degradation of the product) and safety concerns (Kumar et al., 2007). To mitigate this problem, Kumar et al. (2008) used a static mixer after microwave heating and the temperature difference was reduced to 2.3 °C.

2.4.2 Apple juice time-temperature profile

From the experimental runs varying three microwave processing temperatures and two flow rates, Table 2.2 presents the six apple juice processing conditions with the corresponding flow rates, the power absorbed (experimental) and supplied (simulation), the TT2 and TT3 experimental temperatures and the TT3 model predictions. Based on the experimental measurement at TT3 and model prediction outlet temperatures, the average absolute prediction error was 1.6 °C. In all of the six processing conditions, the predicted temperatures were slightly higher than the actual results.

Table 2.2. Processing conditions for apple juice pasteurization with continuous microwave heating: flow rate, power absorbed and supplied and experimental and predicted temperatures after microwave heating (TT3) ([a]Siguemoto et al., 2018).

Id	Flow rate (L/min) [a]	$P_{absorbed}$ (kW)	$P_{supplied}$ (kW)	$TT2_{exp}$ (°C) [a]	$TT3_{exp}$ (°C) [a]	$TT3_{pred}$ (°C)	Error (°C)
M1	0.4	1.1	1.4	30.1	70.4	71.5	1.1
M2	0.8	2.4	2.9	29.9	70.5	73.1	2.6
M3	0.4	1.6	1.8	30.2	80.7	84.2	3.5
M4	0.8	2.9	3.4	29.9	80.5	81.0	0.5
M5	0.4	1.7	2.0	30.1	90.2	90.6	0.4
M6	0.8	3.5	4.1	30.0	90.5	92.2	1.7

Source: Oishi, Pouzada and Gut (2022).

The time-temperature histories were built based on the flow times, internal volume and mixing cup average temperature (Eq. (2.4)) in the tube. The flow time was considered as the ratio of tube internal volume (internal diameter of 6.60 mm and 0.33 m of tube length) to the volumetric flow rate. Consequently, the mean residence time in the applicator tube for the flow rates 0.4 and 0.8 L/min were 1.7 and 0.8 s, respectively.

In Figure 2.6, the continuous lines are the model simulations and the points are the measured temperatures (TT2 and TT3) from Siguemoto et al. (2018). The three temperature conditions (70, 80 and 90 °C) were evaluated and showed a good match with the experimental temperatures. The predicted temperature profiles presented some curves that might be due to the non-homogeneous heating in the applicator tube length presented in Figure 2.5b and temperature dependence on dielectric properties (Table 2.1).

Tuta and Palazoğlu (2017) heated distilled water in a continuous flow microwave cavity with a helical applicator tube and also modeled the process in COMSOL Multiphysics. They obtained temperature prediction errors of 8.3, 3.2 and 1.9 °C for flow rates of 1, 2 and 3 L/min, respectively. Authors also verified, through simulation and experiments, that the temperature at the applicator outlet is not uniform. In addition, Zhang et al. (2021) modeled microwave heating of distilled water in a cavity with a helical coil tube and obtained model prediction errors for outlet temperature of 2.6, 1.8 and 1.4% at 0.50, 0.75 and 1.00 L/min. Both works tested supplied power and outlet temperatures (< 70 °C) lower than the processing conditions in Table 2.2.

Figure 2.6. Time-temperature longitudinal mixing cup average profiles of the apple juice for processing at a) 70 °C, b) 80 °C and c) 90 °C. The lines are the model predictions and the dots are the experimental data.

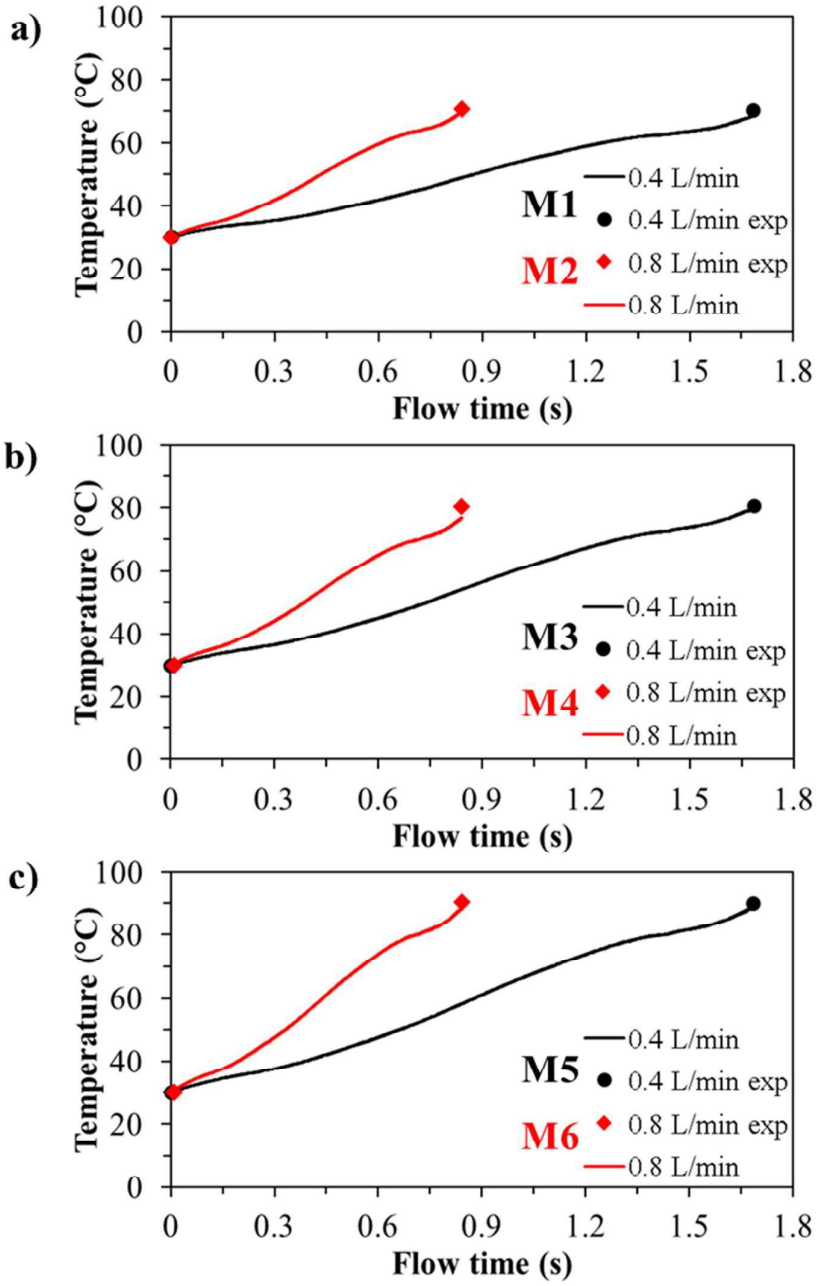

Source: Oishi, Pouzada and Gut (2022).

2.5 CONCLUSION

A continuous-flow microwave cavity for heating of apple juice was modeled in COMSOL Multiphysics software considering the governing equations of electromagnetism, heat transfer and laminar flow. The thermophysical and dielectric properties were implemented in the model as a function of temperature. Model simulations showed good temperature predictions with absolute errors below 3.5 °C. The model overestimated the heat absorption by the fluid. Simulation results showed a large temperature gradient at the outlet of the heating tube, which is undesirable concerning food safety. Temperature distribution within the tube was useful for identification of hot and cold spots. To solve this temperature gradient issue, a sanitary static mixer at the applicator tube outlet can be implemented to guarantee a uniform temperature of the liquid food at the entrance of the holding tube. This work is a valuable tool to evaluate a microwave pasteurization unit and the model can be further used to design and optimize microwave-assisted processes to guarantee food quality and safety.

2.6 REFERENCES

Abdullah SA, Lee SH, Cho IK, Li QX, Jun S, Choi W. Pasteurization of kava juice using novel continuous flow microwave heating technique. Food Sci Biotechnol 2013;22:961-966. doi: 10.1007/s10068-013-0170-1.

Awuah GB, Ramaswamy HS, Economides A. Thermal processing and quality: Principles and overview. Chemical Engineering and Processing: Process Intensification 2007;46;584-602. doi: 10.1016/j.cep.2006.08.004.

Bayindirli L. Mathematical analysis of variation of density and viscosity of apple juice with temperature and concentration. J. Food Processing Preservation 1992;16:23-25. doi: 10.1111/j.1745-4549.1992.tb00190.x.

Bird RB, Stewart WE, Lightfoot EN. Transport Phenomena, 2nd ed. New York: John Wiley & Sons 2002.

Brinley TA, Dock CN, Truong VD, Coronel P, Kumar P, Simunovic J, Sandeep KP, Cartwright GD, Swartzel KR, Jaykus LA. Feasibility of utilizing bioindicators for testing microbial inactivation in sweetpotato purees processed with a continuous-flow microwave system. J. Food Science 2007;72:E235-E242. doi: 10.1111/j.1750-3841.2007.00371.x.

COMSOL Multiphysics. Reference manual, 2022. Available in: https://doc.comsol.com/6.0/doc/com.comsol.help.comsol/COMSOL_ReferenceManual.pdf

[Accessed in 14 Apr 2022].

Coronel P, Simunovic J, Sandeep KP. Temperature profiles within milk after heating in a continuous-flow tubular microwave system operating at 915 MHz. J Food Science 2003;68. doi: 10.1111/j.1365-2621.2003.tb07004.x.

Coronel P, Truong V, Simunovic J, Sandeep KP, Cartwright GD. Aseptic processing of sweetpotato purees using a continuous flow microwave system. J. Food Science 2005;70:E531-E536. doi: 10.1111/j.1365-2621.2005.tb08315.x.

Cuccurullo G, Giordano L, Viccione G. Numerical and experimental modeling for thermal developing pipe flow with microwave heating. Int. J. Mechanics 2016;10:68-74.

Damilos S, Radhakrishnan ANP, Dimitrakis G, Tang J, Gravriilidis A. Experimental and computational investigation of heat transfer in a microwave-assisted flow system. Chem. Eng. & Processing: Process Intensification 2019;142:107537. doi: 10.1016/j.cep.2019.107537.

Dibben D. Electromagnetics: fundamental aspects and numerical modeling. In: Datta AK, Anantheswaran RC. Handbook of microwave technology for food applications. Boca Ratón: CRC Press 2001;1-31.

Erdogdu F, Karatas O, Sarghini F. A short update on heat transfer modelling for computational food processing in conventional and innovative processing. Curr Opin Food Sci 2018;23:113–9. doi: 10.1016/j.cofs.2018.10.003.

Geedipali SSR, Rakesh V, Datta AK. Modeling the heating uniformity contributed by a rotating turnable in microwave ovens. J. of Food Eng. 2007;359-368. doi: 10.1016/j.jfoodeng.2007.02.050.

Gentry TS, Roberts JS. Design and evaluation of a continuous flow microwave pasteurization system for apple cider. LWT 2005;38:227-238. doi: 10.1016/j.lwt.2004.05.016.

Gómez-Sánchez DL, Antonio-Gutiérrez O, López-Díaz AS, Palou E, López-Malo A, Ramírez-Corona N. Performance of combined technologies for the inactivation of Saccharomyces cerevisiae and Escherichia coli in pomegranate juice: The effects of a continuous-flow UV-Microwave system. Food Process Engineering 2020;43:e13565. doi: 10.1111/jfpe.13565.

Industrial Microwave Systems, 6 kW Liquid Heating Microwave System, 2450 MHz (2022). Available in: https://industrialmicrowave.com/microwave-systems-liquids-fluids-heating/6kw-microwave-system/. [Accessed in 29 Apr 2022].

Kumar P, Coronel P, Simunovic J, Sandeep KP. Feasibility of aseptic processing of a low-acid multiphase food product (salsa con queso) using a continuous flow microwave system. J. Food Science 2007;72:E121-E124. doi: 10.1111/j.1750-3841.2007.00306.x.

Kumar P, Coronel P, Truong VD, Simunovic J, Swartzel KR, Sandeep KP, Cartwright G. Overcoming issues associated with the scale-up of a continuous flow microwave system for aseptic processing of vegetable purees. Food Research Int. 2008;41:454-461. doi: 10.1016/j.foodres.2007.11.004.

Marszałek K, Mitek M, Skąpska S. Effect of continuous flow microwave and conventional heating on the bioactive compounds, color, enzymes activity, microbial and sensory quality of strawberry purée. Food Bioprocess Technol. 2015;8:1864-1876. doi: 10.1007/s11947-015-1543-7.

Muley PD, Boldor D. Multiphysics numerical modeling of the continuous flow microwave-assisted transesterification process. J. Microwave Power and Electromagnetic Energy 2012;46:139-162. doi: 10.1080/08327823.2012.11689832.

Oishi TK, Gut JAW. Modeling time-temperature history and sterilization value of mango puree under conventional and microwave assisted pasteurization. Int. J. Food Engineering 2021. doi: 10.1515/ijfe-2020-0335.

Puangsuwan K, Tongurai C, Chongcheawchamnan M. Design of microwave heating continuous belt system for palm fruit. Asia-Pacific Microwave Conference 2015. doi: 10.1109/APMC.2015.7413502.

Pitchai K, Birla SL, Subbiah J, Jones D, Thippareddi H. Coupled electromagnetic and heat transfer model for microwave heating in domestic ovens. J. Food Eng. 2012;100-111. doi: 10.1016/j.jfoodeng.2012.03.013.

Raaholt BW, Isaksson S, Hamberg L, Fhager A, Hamnerius Y. Continuous tubular microwave heating of homogeneous foods: evaluation of heating uniformity. J. Microwave Power and Electromagnetic Energy 2017;50:43-65. doi: 10.1080/08327823.2016.1157318.

Sabliov CM, Boldor D, Coronel P, Sanders TH. Continuous microwave processing of peanut beverages. J. Food Processing and Preservation 2008;32:935-945. doi: 10.1111/j.1745-4549.2008.00223.x.

Salvi D, Boldor D, Aita GM, Sabliov CM. COMSOL Multiphysics model for continuous flow microwave heating of liquids. J. Food Engineering 2011;104:422-429. doi: 10.1016/j.jfoodeng.2011.01.005.

Sierra I, Vidal-Valverde C, Olano A. The effects of continuous flow microwave treatment and conventional heating on the nutritional value of milk as shown by influence on vitamin B 1 retention. European Food Research and Technology 1999;209:352-354. doi: 10.1007/s002170050508.

Siguemoto ÉS, Gut JAW. Dielectric Properties of Cloudy Apple Juices Relevant to Microwave

Pasteurization. Food and Bioprocess Technology, 2016;9:1345-1357. doi: 10.1007/s11947-016-1723-0.

Siguemoto ÉS, Funcia ES, Pires MN, Gut JAW. Modeling of time-temperature history and enzymatic inactivation of cloudy apple juice in continuous flow microwave assisted pasteurization. Food and Bioproducts Processing 2018;111:45-53. doi: 10.1016/j.fbp.2018.06.004.

Siguemoto ÉS, Purgatto E, Hassimotto NMA, Gut JAW. Comparative Evaluation of Flavour and Nutritional Quality after Conventional and Microwave-Assisted Pasteurization of Cloudy Apple Juice. LWT 2019;111:853–60. doi: 10.1016/j.lwt.2019.05.111.

Simunovic J, Sandeep KP. Key technological advances and industrialization of continuous flow microwave processing for foods and beverages. In: Juliano P, Knoezer K, Sellahewa J, Nguyen MH, Buckow R. Food Engineering Innovations Across the Food Supply Chain. Oxford: Academic press 2021;149-162. doi: 10.1016/B978-0-12-821292-9.00012-1.

Singh RP, Heldman DR. Heat transfer in food processing. In: Singh RP, Heldman DR. Introduction to Food Engineering. Oxford: Academic press 2009;247-402.

Steed LE, Truong VD, Simunovic J, Sandeep KP, Kumar P, Cartwright GD, Swartzel KR. Continuous flow microwave-assisted processing and aseptic packaging of purple-fleshed sweetpotato purees. J. Food Science 2008;73:E455-E462. doi: 10.1111/j.1750-3841.2008.00950.x.

Stratakos AC, Delgado-Pando G, Linton M, Patterson MF, Koidis A. Industrial scale microwave processing of tomato juice using a novel continuous microwave system. Food Chemistry 2016;190:622-628. doi: 10.1016/j.foodchem.2015.06.015.

Tajchakavit S, Ramaswamy HS. Continuous-flow microwave heating of orange juice: evidence of nonthermal effects. Journal of Microwave Power and Electromagnetic Energy 1995;30:141-148. doi: 10.1080/08327823.1995.11688270.

Tajchakavit S, Ramaswamy HS, Fustier P. Enhanced destruction of spoilage microorganisms in apple juice during continuous flow microwave heating. Food R. Int. 1998;31:713-722. doi: 10.1016/S0963-9969(99)00050-2.

Teixeira AA, Dixon JR, Zahradnik JW, Zinsmeister GE. Computer optimization of nutrient retention in the thermal processing of conduction-heated foods. Food Technol 1969;23:137-42.

Tewari G. Microwave and Radio-Frequency heating. In: Tewari G, Junega V. Advances in thermal and non-thermal food preservation. Iowa: Blackwell Publishing 2007;91-98.

Topcam H, Erdogdu F. Designing system cavity geometry and optimizing process variables for

continuous flow microwave processing. Food and Bioproducts Processing 2017;127:295-308. doi: 10.1016/j.fbp.2021.03.006.

Tuta S, Palazoğlu TK. Finite element modeling of continuous-flow microwave heating of fluid foods and experimental validation. J. Food Engineering 2017;192:79-92. doi: 10.1016/j.jfoodeng.2016.08.003.

Valero E, Villamiel M, Sanz J, Martínez-Castro I. Chemical and sensorial changes in milk pasteurised by microwave and conventional systems during cold storage. Food Chemistry 2000;70:77-81. doi: 10.1016/S0308-8146(00)00074-1.

Yang H, Zhang Y, Gao W, Yan B, Zhao J, Zhang H, Chen W, Fan D. Steam replacement strategy using microwave resonance: A future system for continuous-flow heating applications. Applied Energy 2021;283:116300. doi: 10.1016/j.apenergy.2020.116300.

Zhang H, Datta AK. Microwave power absorption in single- and multiple-item foods. Trans IChemE 2003;81:257-265. doi: 10.1205/096030803322438027.

Zhang Y, Yang H, Yan B, Zhu H, Gao W, Zhao J, Zhang H, Chen W, Fan D. Continuous flow microwave system with helical tubes for liquid heating. J. Food Engineering 2021;294:110409. doi: 10.1016/j.jfoodeng.2020.110409.

Zhou J, Yang X, Ye J, Zhu H, Yuan J, Li X, Huang K. Arbitrary Lagrangian-Eulerian method for computation of rotating target during microwave heating. Int. J. of Heat and Mass Transfer 2019;134:271-285. doi: 10.1016/j.ijheatmasstransfer.2019.01.007.

Zhu H, He J, Hong T, Yang Q, Wu Y, Yang Y, Huang K. A rotary radiation structure for microwave heating uniformity improvement. Applied Thermal Engineering 2018;648-658. doi: 10.1016/j.applthermaleng.2018.05.122.

Zhu J, Kusnetsov AV, Sandeep KP. Mathematical modeling of continuous flow microwave heating of liquids (effects of dielectric properties and design parameters). Int. J. Them. Sci. 2007;46:326-341. doi: 10.1016/j.ijthermalsci.2006.06.005.

3 MULTIPHYSICS MODELING OF POLYPHENOL OXIDASE AND PEROXIDASE INACTIVATION IN CONTINUOUS-FLOW MICROWAVE THERMAL PROCESSING OF COCONUT WATER

*This chapter is based on the following paper:
Oishi TK, Cassares M, Pouzada EVS, Gut JAW. Multiphysics modeling of polyphenol oxidase and peroxidase inactivation in continuous-flow microwave thermal processing of coconut water. Brazilian Journal of Chemical Engineering 2023. DOI: 10.1007/s43153-023-00391-2

3.1 INTRODUCTION

Continuous-flow microwave-assisted processing of liquid foods is of interest to the food industry due to the rapid volumetric heating. Microwave radiation penetrates directly into the food resulting in high heat transfer rates and high energy efficiency (Zhu, Kunestov and Sandeep, 2007). Previous experiments of thermal processing in continuous flow showed a temperature profile closer to the ideal (instantaneous heating before holding) with potential to reduce the negative effects of over-processing and high temperature surfaces (Oishi and Gut, 2021; Siguemoto et al., 2018). This benefit can result in a better-quality food product due to the reduced degradation of thermosensitive components responsible for flavor and nutrition aspects (vitamins, phenolic components and antioxidant capacity) (Siguemoto et al., 2019; Sierra et al., 1999).

Green coconut water is a food product of great importance in the beverage segment due to its characteristic aroma, flavor and nutrients. Coconut water has an ideal sugar and mineral content to make a perfectly refreshing and rehydrating drink after physical activities (Prades et al., 2012). The industrialization of coconut water is necessary due to the large volume of the coconut shells, thus reducing transportation costs. However, after the extraction of coconut water, exposure to air allows the action of enzymes (that alter color and flavor) and contaminant microorganisms (Campos et al., 1996). Typically, fresh green coconut water presents a slightly acidic pH (4.7-6.4) (Porto et al., 2020; Tan and Easa, 2020). Polyphenol oxidase (PPO) and peroxidase (POD), enzymes naturally present in fresh coconut water, showed optimum activity at pH 5.5-6.0 and room temperature (Campos et al., 1996). PPO and POD are enzymes responsible for enzymatic browning and alteration of the sensorial aspects of coconut water, and they can be inactivated through thermal processing (Veitch, 2004; Mayer, 2006).

There has been some research on coconut water processing considering electric and dielectric heating technologies that can replace conventional heat exchangers, such as microwave heating (Matsui et al., 2007; Matsui et al., 2008; Franco et al., 2015; Arteza-Ríos et al., 2020) and ohmic heating (Delfiya and Thangavel, 2016; Kanjanapongkul and Baibua, 2021). These technologies offer potential for high product quality, use of electric energy obtained from sustainable sources, such as hydroelectric power, and low usage of plant space (Tang, 2015).

In experimental studies comparing conventional and microwave thermal processing, enzymes naturally present in coconut water (PPO and POD) showed lower heat resistance in microwave treatment, facilitating enzyme inactivation (Cavalcante, Funcia and Gut, 2021; Matsui et al., 2008). This higher inactivation rate under microwave heating is known as a "non-thermal effect", as electric field can cause additional changes in protein structure, affecting enzyme activity. However, the non-thermal effect of electric field on enzymes proved to be subtle and is a controversial topic in the literature (Kubo et al., 2019).

Teleken et al. (2023) modeled a continuous flow microwave heater (elliptical cavity) followed by a helical holding tube for the thermal processing of tomato pulp. The model comprised electromagnetic wave propagation, momentum transport (laminar flow), heat transport and microorganism inactivation (chemical reaction) and was numerically solved using COMSOL Multiphysics (v.5.5). The effects of the flow rate, applicator tube diameter and processing temperature were analyzed for food quality and safety concerns. The authors tested different applicator diameters (22, 30, 38 and 46 mm) and verified that microwave absorption increases with tube diameter until a certain critical value is reached, which causes a sharp decrease in absorption (46 mm in this case). Results illustrate the importance of multiphysics simulation to analyze the complexity of wave propagation in the media.

Topcam and Erdogdu (2021) developed an optimization study for a cylindrical/elliptical microwave cavity using multiphysics simulation. The objective function was to maximize the outlet temperature and the authors tested different numbers of applicator tubes going vertically through the cavity (1 to 5 tubes) and several orientations and layouts. For a cavity with two tubes and field frequency of 915 MHz, an optimized design was obtained with the tubes located symmetrically along the shortest diameter of the ellipsis, while the waveguide enters the cavity by the largest diameter.

Multiphysics modeling is an essential tool to understand the complex interaction between microwaves and the food product stream. The model can be used to further optimize the process in terms of energy efficiency, quality retention and temperature homogeneity. The

present work main steps are: 1) experimental runs with fresh coconut water in a continuous-flow microwave system, 2) multiphysics modeling of the heater and holding tube in COMSOL Multiphysics (v.6.1), 3) model validation using experimental results, verification of process temperatures, power absorption and PPO and POD residual activities.

3.2 EXPERIMENTAL RUNS

Green coconuts (*Cocos nucifera* L.) were purchased from a local market in the city of São Paulo (Brazil) in March 2021. The coconuts selected (300 units) were 7 months old and harvested 11 days before processing, without apparent damage to the fruit shell. After cleaning and sanitizing the coconut shells with a chlorine bleach solution diluted in water, the water was manually extracted using an extractor Coco Fácil (Brasil Iluminação, Brazil). The liquid extracted was filtered (0.212 mm metal mesh), homogenized and immediately processed. Samples of fresh and processed coconut water were collected in 2 mL Eppendorf and in 15 mL and 50 mL Falcon conical tubes, which were stored in a plasma freezer 349 FV (Fanen, Brazil) at -30 °C. Right before the analysis of dielectric properties and enzyme residual activity, coconut water samples were thawed by leaving the bottles in a cold-water bath at a maximum temperature of 4 °C and then gently agitated for liquid homogenization.

3.2.1 Characterization of green coconut water

Samples of fresh green coconut water were characterized based on the total soluble solids content (TSS) and pH. The TSS, expressed as °BRIX, was determined with a digital refractometer ATR-BR 46466-46496 (Schmidt-Haensch, Germany). The pH was determined with a TEC-3MP digital pH meter (Tecnal, Brazil).

The determination of the dielectric properties of green coconut water was conducted according to Kubo et al. (2021). The relative dielectric permittivity (ε_r') and loss factor (ε_r'') were measured using the high-temperature dielectric probe sensor 85070E (Agilent Technologies, Malaysia) with an electronic calibration module 85093-60008 and a network analyzer E5061B (Agilent Technologies, Malaysia). Before measurements, the system was calibrated using air (open circuit), short circuit block and deionized water. The software of the dielectric probe kit 85070E (Agilent Technologies, Malaysia) calculated the relative complex permittivity.

Green coconut water samples were placed in a jacketed capsule with the dielectric probe, and the capsule was connected to a thermostatic oil bath (TC-550, Ametek Brookfield, USA). A digital thermometer (MT455, Minipa, Brazil) was used to monitor and measure the sample temperature at the desired value. Dielectric properties were measured in a temperature range between 30 and 130 °C with intervals of 10 °C at 2.45 GHz.

The direct current (DC) electrical conductivity (σ) of coconut water was determined with a conductivity meter YSI3200 and cell YSI3252 (YSI, Ohio, USA) at temperatures from 5 to 75 °C with 5 °C intervals. For the determination, samples were immersed in the same thermostatic oil bath until the stabilization of the temperature.

The dielectric properties and electrical conductivity measurements were obtained based on triplicates for each temperature. Regression analyses of the data were performed in Excel 2019 to determine the temperature dependence (Microsoft, USA).

3.2.2 Continuous flow microwave thermal system

Fresh coconut water was microwave-assisted thermally processed with a MicroThermics pilot-scale unit (Lab25-UHT/HTST EHVH, USA) (Figure 3.1). This laboratory-scale unit has two heating steps (conventional pre-heater and microwave final heater) followed by a holding tube and a cooler. The pre-heater and the cooler steps are helical coil heat exchangers with a maximum heat load of 18 kW and 3.5 kW for hot and cold water closed circuits, respectively. The microwave heater consists of an applicator tube made of Polytetrafluoroethylene (PTFE) with a ceramic pressure sleeve material housed in a single-mode cavity connected to a waveguide and a magnetron (electromagnetic energy source) (Industrial Microwave Systems, 2022). The waveguide has a 3-stub tuner, which is used to manually keep the reflected power under 20 W (Siguemoto et al., 2018). At the beginning of the waveguide there is a 6 kW and 2.45 GHz magnetron (Industrial Microwave Systems, 2022). The microwave heater is equipped with a reflected power sensor connected to Microwave Power Meter software.

The temperature of the product and utility fluids along the microwave-assisted unit was measured by thermocouples positioned at the inlet and outlet of each section (T1, T2, T3, T4 and T5), as shown in Figure 3.1. The temperature data were recorded, after steady state processing was verified, every 10 s for 2 minutes; the average temperature recorded was used for model validation. The food product temperature after the microwave heater (T3) was

controlled automatically to reach the desired set point by adjusting the magnetron power level (0 to 100%).

The thermal treatment of the coconut water was carried out under sixteen conditions combining four different processing temperatures (80, 90, 100 and 110 °C) and four flow rates (0.5, 0.7, 0.9 and 1.1 L/min). The pre-heater was used to achieve a temperature of 50 °C at the microwave heater inlet (T2). The temperatures at the microwave heater outlet and holding tube outlet (T3 and T4) were used in the model validation.

Figure 3.1. Schematic representation of coconut water path in the MicroThermics lab unit (Raleigh, EUA).

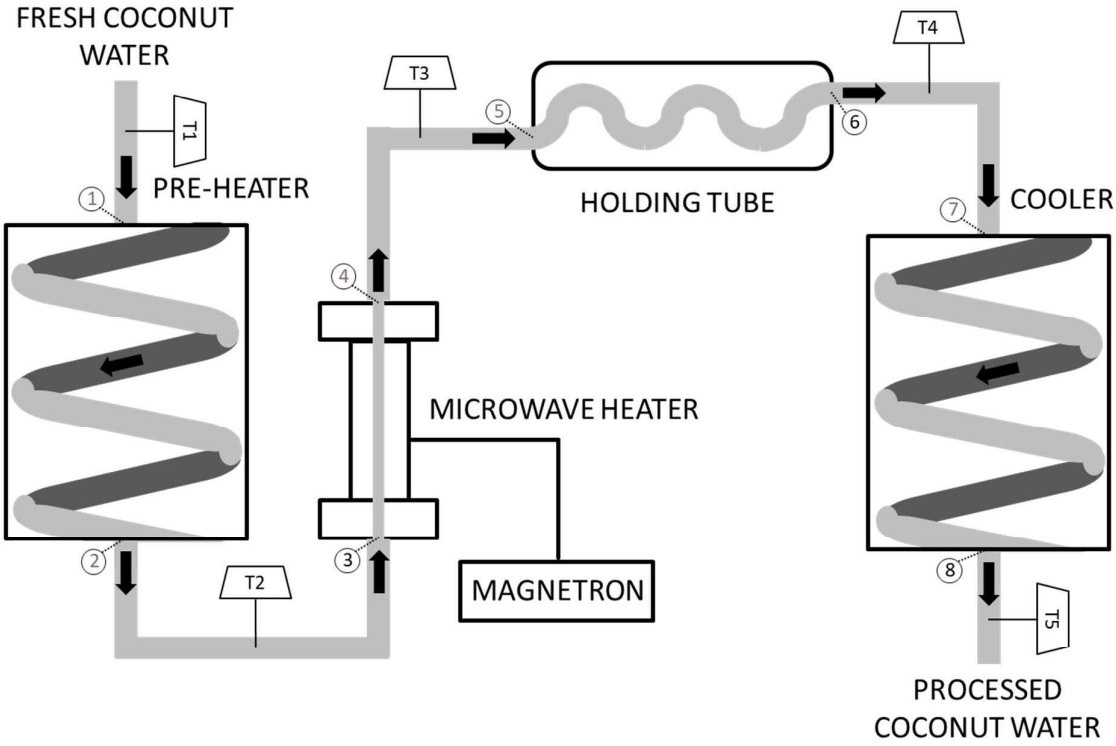

Source: Oishi et al. (2023).

The measured temperatures at thermocouples T2 and T3 were used in the following heat balance to determine the power absorbed (P_{abs}, W) by the coconut water stream:

$$P_{abs} = \rho\ Q\ C_P\ (T3 - T2) \quad (3.1)$$

where ρ is the average density (kg/m^3), Q is the volumetric flow rate (m^3/s) and C_P is the average specific heat (J/(kg.K)).

For the enzyme residual activity determination, samples of fresh and treated coconut water were analyzed to evaluate the inactivation of polyphenol oxidase (PPO) and peroxidase (POD) enzymes according to Campos et al. (1996). The enzyme activity was measured using a spectrophotometer with a microplate reader (Spectramax M2, Molecular Devices, USA). The reading for each sample was done in 8 wells of the microplate to obtain an average activity value.

The polyphenol oxidase activity was determined using Pyrocatechol (phenolic substrate for the reaction) in a phosphate buffer solution. Amounts of 138 µL 0.2 M phosphate buffer solution (pH 6.0 at 25 °C), 25 µL coconut water and 37 µL freshly prepared 0.2 M Pyrocatechol C9510-100G (Sigma-Aldrich, USA) solution were added to each well of the microplate (Cavalcante, Funcia and Gut, 2021). The changes in absorbance of the samples were monitored using a 425 nm wavelength at 26 s intervals for 30 minutes at 25 °C, stirring for 3 s between the intervals.

The peroxidase activity measurement protocol was similar to PPO; however, the phenolic substrate used was pyrogallol. Each micro-well contained 67 µL of 0.2 M phosphate buffer solution (pH 6.0 at 25 °C), 90 µL of the coconut water and 21 µL of freshly prepared 5% pyrogallol P0381-100G (Sigma-Aldrich, USA) solution in distilled water. The microplate was placed in the spectrophotometer for about 1 min at 35 °C. After the temperature stabilization, 22 µL of 73.5 mM H_2O_2 solution (Synth, Brazil) was added to start the reaction. The absorbance of the sample was read at 420 nm wavelength and 26 s intervals for 15 minutes, with 3 s stirring before readings and maintaining the temperature at 35 °C.

The residual activity results (%) for each enzyme (PPO and POD), process temperature (80, 90, 100 and 110 °C) and flow rate (0.5, 0.7, 0.9 and 1.1 L/min) were compared to the simulation results.

3.3 MODEL DEVELOPMENT

Based on the continuous flow thermal processing unit described in section 2.2, two multiphysics models were developed: microwave cavity (step 3-4 in Figure 3.1) and holding tube (step 4-7 in Figure 3.1). The 3D-geometries of both models were built using the geometry module of COMSOL Multiphysics (v.6.1) and are shown in Figure 3.2. The physics of electromagnetic waves, laminar flow, heat transfer in fluids and transport of diluted species were coupled in the finite element software COMSOL Multiphysics (v.6.1).

The microwave heater is presented in Figure 3.2 with an octagonal prism cavity geometry connected to a rectangular prism waveguide. The cavity center has a vertical applicator tube. The applicator tube in which the coconut water flows has an internal diameter of 6.60 mm and 0.33 m of tube length. In the model, the applicator tube material and the air inside the cavity were assumed to be transparent to microwave energy. A more detailed description of this microwave applicator model was previously presented by Oishi, Pouzada and Gut (2022).

Figure 3.2. COMSOL model geometry and numerical meshing for the continuous flow microwave system.

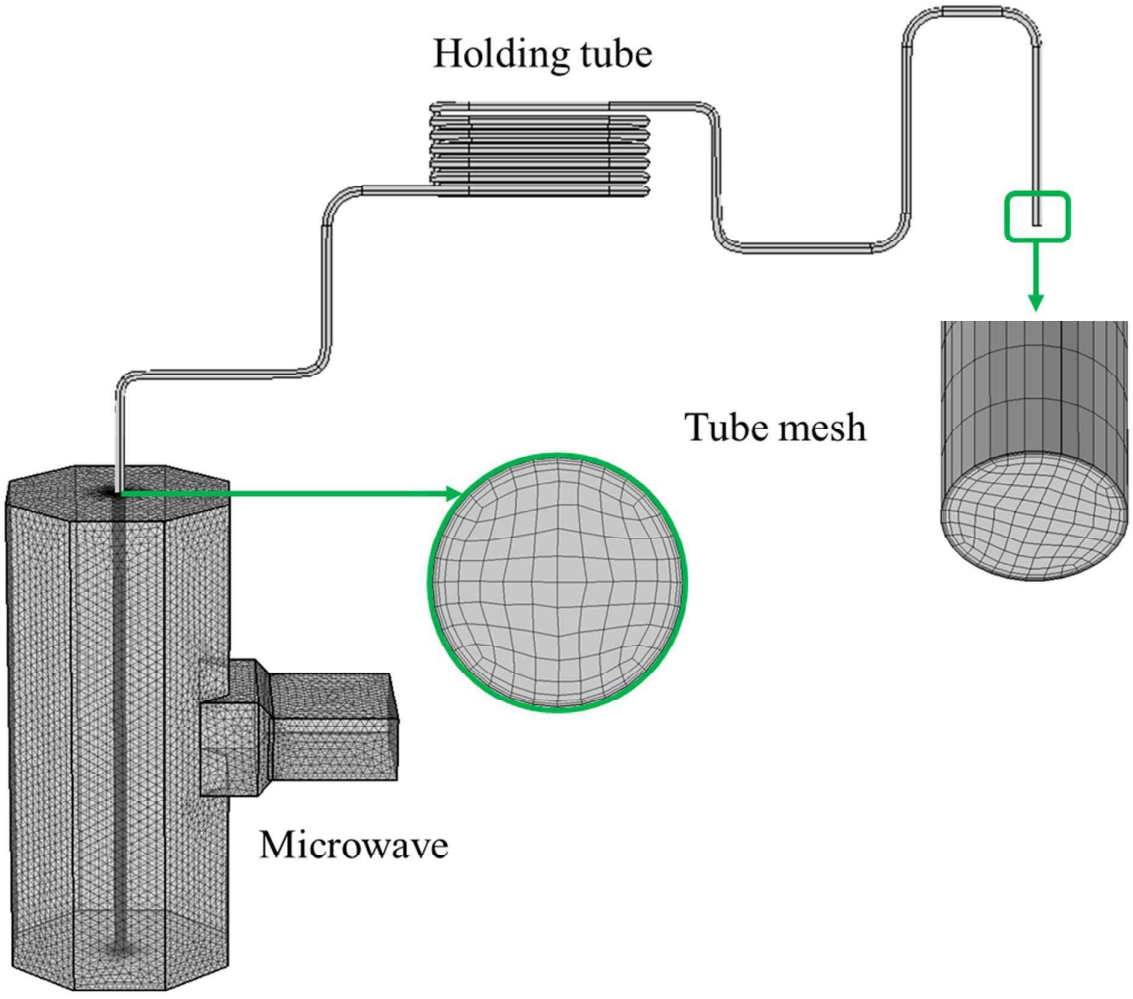

Source: Oishi et al. (2023).

For the holding tube, there was no electromagnetic energy propagation; thus, the physics of electromagnetic waves was not used. Figure 3.2 presents the holding tube model geometry

based on its assembly (MicroThermics pilot-scale unit). The food product flows through a semi-helical tube with thermal insulation (step 5-6, Figure 3.1). The holding tube has a total length of 3.12 m, internal and external diameters of 7.75 mm and 9.51 mm and a mean residence time of 18 s at the nominal flow rate of 0.5 L/min (Fortes and Gut, 2021). The tube connections (step 4-5 and 6-7, Figure 3.1) are also made of stainless steel and have the same tube diameters as the holding tube, but no thermal insulation. The tube connection length and residence time between the microwave heater and the holding tube are 56.71 cm and 2 s (step 4-5, Figure 3.1). For the connection between the holding tube and cooler, the length is 100.13 cm and the residence time is 4 s (step 6-7, Figure 3.1) at the nominal flow rate of 0.5 L/min.

3.3.1 Governing equations

Electromagnetic heating is a function of the local electric field strength. Maxwell's wave equation was solved to determine the electric field distribution (Dibben et al., 2001):

$$\nabla \times \frac{1}{\mu_r}(\nabla \times \mathbf{E}) - {k_0}^2 \left((\varepsilon_r' - i\,\varepsilon_r'') - \frac{i\,\sigma}{\omega\,\varepsilon_0} \right) \mathbf{E} = 0 \tag{3.2}$$

where μ_r is the relative permeability, $\mathbf{E}$ is the local electric field intensity (V/m), k_0 is the free space wave number (rad/m), $\omega = 2\,\pi\,f$ is the angular wave frequency (rad/s), σ is the electrical conductivity of the liquid food (S/m) and $\varepsilon_0 = 8.854 \times 10^{-2}$ is the free space permittivity (F/m).

The energy equation was solved to obtain the temperature distribution in the coconut water domain:

$$\rho\, C_p\, \mathbf{u} \cdot \nabla\, T = \nabla \cdot (k\, \nabla\, T) + P_{gen} \tag{3.3}$$

where $\mathbf{u}$ is the velocity vector (m/s), T is the temperature (K) and k is the thermal conductivity (W/(m.K)). P_{gen} is the volumetric power generation (W/m^3), which is computed using the dielectric properties of the coconut water and the electric field intensity (Geedipali et al., 2007):

$$P_{gen} = \frac{1}{2}\omega\,\varepsilon_0\,\varepsilon_r''\,|\mathbf{E}|^2 \tag{3.4}$$

The velocity profile of the food product in the tube was obtained from the momentum balance and the continuity equation for steady-state:

$$\rho\,(\mathbf{u} \cdot \nabla)\,\mathbf{u} = -\nabla\, p + \mu\,\nabla^2\,\mathbf{u} \tag{3.5a}$$

$$\rho\,\nabla \cdot (\mathbf{u}) = 0 \tag{3.5b}$$

where p is the hydrodynamic pressure (Pa) and μ is the dynamic viscosity (Pa.s).

To evaluate the enzyme residual activity along the microwave and holding tube models, a differential mass balance equation was applied to the liquid food in fully developed laminar flow and with first-order thermal inactivation kinetics:

$$\mathbf{u} \cdot \nabla A = \nabla \cdot (E_D \nabla A) - c\, A \tag{3.6a}$$

$$c = \frac{\ln (10)}{D_{T_{ref}}\, 10^{\frac{T - T_{ref}}{z}}} \tag{3.6b}$$

where E_D is the enzyme diffusivity (m^2/s), A is the local residual activity of the target enzyme, c is the first-order inactivation rate constant (1/s), $D_{T_{ref}}$ is the decimal reduction time known at a reference temperature (T_{ref}) and z is the increase in temperature required for a decimal reduction in $D_{T_{ref}}$.

For model validation, the applicator tube and holding tube mixing cup average temperature ($\bar{T}$) and residual activity ($\bar{A}$) were calculated at the outlets and compared with their respective experimental results:

$$\bar{T} = \frac{\int u\, T\, 2\, \pi\, r\, dr}{\bar{u}} \tag{3.7}$$

$$\bar{A} = \frac{\int u\, A\, 2\, \pi\, r\, dr}{\bar{u}} \tag{3.8}$$

where $\bar{u}$ is the average velocity (m/s) and r is the radial direction (m).

Bird, Stewart and Lightfoot (2002) derived the velocity profile in a straight cylindrical tube for fully-developed laminar flow, which were used in Eqs. (3.7) and (3.8) in the post-processing step:

$$u(r) = 2\, \bar{u} \left(1 - \left(\frac{r}{R}\right)^2\right) \tag{3.9a}$$

$$\bar{u} = \frac{q}{\pi\, R^2} \tag{3.9b}$$

where R is the inner radius of the applicator tube and q is the flow rate (m^3/s).

3.3.2 Boundary conditions

In the microwave heater, the boundary condition of PEC (Perfect Electric Conductor, $\mathbf{n} \times \mathbf{E} = \mathbf{0}$) was applied over the microwave cavity metallic surfaces. The TE_{10} (Transverse Electric) mode was used as the Radio Frequency (RF) source port boundary. In the previous work of Oishi, Pouzada and Gut (2022), the microwave cavity simulation showed a power loss due to reflection, i.e., the power absorbed by the food product was lower than the power

supplied by the magnetron. In the equipment, the 3-stub tuner can be used to minimize the reflected power; however, the tuner was not part of the multiphysics model. From previous simulation results, the supplied power had to be set around 15% higher than the power required to achieve the processing temperature (Eq. (3.1)). The supplied power, including 15% losses, was used in the waveguide port boundary condition in this work.

The models for heat transfer in fluids and laminar flow in the microwave cavity used inlet temperature of 50 °C and the fully developed average inlet velocity ($\bar{u}$) of 0.24, 0.34, 0.44 and 0.54 m/s for the respective volumetric flow rates 0.5, 0.7, 0.9 and 1.1 L/min.

For the enzyme inactivation model, the typical diffusivity of sucrose in water at room temperature is 10^{-9} m^2/s, and this value was used to represent the diffusion of the enzymes in the coconut water (Price, Mattsson and Murray, 2016). To compare the experimental and predicted residual activities, negligible enzyme inactivation in the pre-heater was assumed in the model due to the low temperature (T<50 °C) in the pre-heater section. Oishi and Gut (2021) analyzed POD inactivation in the MicroThermics unit; the enzyme inactivation was not significant in the cooler section due to the rapid temperature drop at the inlet. The residual activities of both enzymes (PPO and POD) were considered 100% at the microwave cavity inlet. The first-order kinetic parameters from Funcia (2020) were used for the thermal inactivation: $D_{90\,°C} = 6.0$ s and $z = 12.6$ °C for PPO and $D_{90\,°C} = 21.8$ s and $z = 16.5$ °C for POD.

The holding tube average inlet velocities were 0.18, 0.25, 0.32 and 0.39 m/s. The outlet mixing cup average residual activity ($\bar{A}$) of the microwave applicator tube was implemented as the inlet boundary condition for the holding tube model. For the inlet temperature of the holding tube, the experimental results were used as input in order not to propagate the error from the applicator simulation, since kinetics are highly dependent on temperature and, in practice, the temperature control in the equipment is reliable. In a previous study with the MicroThermics unit, heat losses to the environment at the holding tubes were observed. Therefore, the holding tube model needs to consider this heat loss. The average heat transfer coefficient obtained from Russo and Gut (2022) is 14.1 $W/(m^2.K)$ (valid for $10^3 \leq Re \leq 10^4$); this value was implemented in the model as a convective heat flux boundary condition with an average room temperature of 20 °C.

3.3.3 Mesh and solvers

The governing equations were solved in COMSOL Multiphysics using the frequency-stationary and stationary studies for the microwave heater and holding tube models, respectively. The meshing configuration for the microwave heater was set using the software predefined “free tetrahedral” with “fine” mesh element size, calibrated for fluid dynamics (Oishi, Pouzada and Gut, 2022). For both models, the “free quad” generator was applied to the tube inlet boundary; a structured mesh with hexahedral elements was thus swept for the whole tube domain. To finish, two boundary layers were added to the tube walls (adjustment factor 1.2) and the resulting meshing can be seen in Figure 3.2.

A sensitivity analysis for the number of mesh elements was conducted for both models considering a flow rate of 0.5 L/min and a processing temperature of 80 °C. The outlet temperature of the microwave applicator and the residual activity of PPO at the holding tube outlet were the most sensible variables for the mesh independence study. In Figure 3.3a, the outlet temperature of the applicator tube does not vary significantly, converging to 82.8 °C. The simulation time ranged from 47 minutes to 7 hours for 124,737 and 1,466,463 mesh elements, respectively. Since the temperature is not very sensitive to the increase in mesh element numbers, the simulation with the average mesh elements was chosen.

Figure 3.3b allows verifying how the increase in mesh element numbers affected PPO residual activity in the holding tube. The increase in the number of elements increased the simulation time from 6 minutes (33,621 elements) to 6 hours (473,438 elements). In Figure 3.3b, at the higher values of mesh elements, the residual activity of PPO did not vary significantly, converging to 28%. The criterion used to select the mesh element number was a PPO residual activity value varying less than 1% in relation to the previous value. The selected meshes have 551,224 elements with 3,629,582 equations for the microwave heater and 339,136 elements with 2,567,671 equations for the holding tube model, as presented in Figure 3.2.

Figure 3.3. Mesh independence study (0.5 L/min, 80 °C): a) Microwave applicator outlet temperature and b) Holding tube outlet PPO residual activity, both as a function of number of mesh elements.

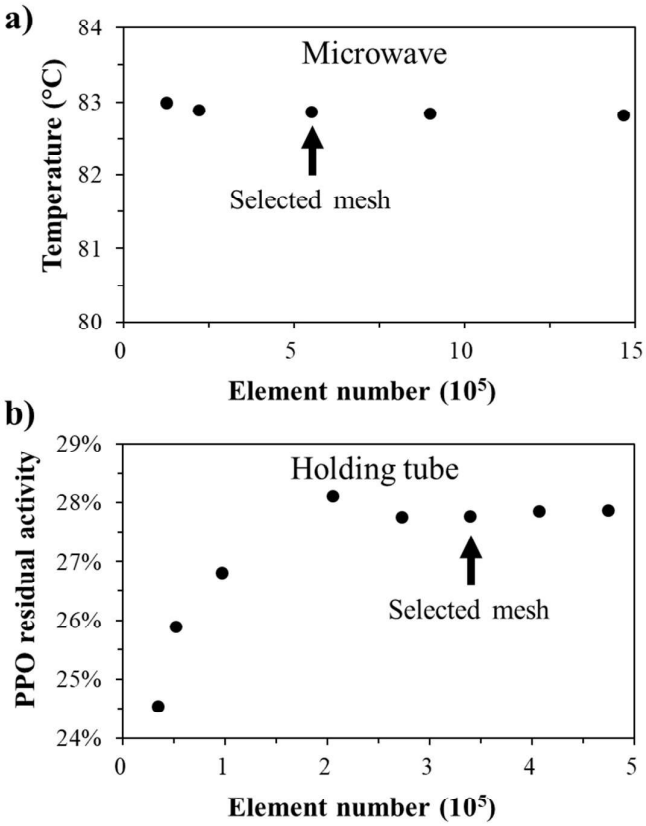

Source: Oishi et al. (2023).

The solver MUMPS (Multifrontal Massively Parallel Sparse Direct Solver) was used to solve the electromagnetic wave propagation, PARDISO (Parallel Direct Sparse Solver) was implemented for the heat transfer and fluid flow, and the transport of diluted species was solved using GMRES (Generalized Minimal Residual Method). The overall simulation time for microwave heater and holding tube were around 2 and 3 hours, respectively. The workstation used to perform the simulations was an Intel Xeon 2403 @ 1.8 GHz with 64 GB RAM.

3.4 RESULTS AND DISCUSSION

3.4.1 Physicochemical, dielectric properties and electrical conductivity determination

The green coconut water used for the continuous thermal processing was characterized based on the total soluble solids content (TSS) and pH (as described in section 2.1). The thermophysical properties (density, thermal conductivity, specific heat and viscosity) of coconut water were obtained from Fontan et al. (2009) (Table 3.1). The fresh green coconut water used in the experiments presented pH = 5.1 ± 0.2 and TSS = 5.4 ± 0.1 °BRIX.

Table 3.1. Considered thermophysical properties of green coconut water for temperatures between 5 and 80 °C ([a] Fontan et al., 2009).

Property	Domain	Value	Unit
Relative permeability (μ_r)	Coconut water [a]	1	-
Thermal conductivity (k)	Coconut water [a]	$k = 1.10\ 10^{-3}\ T(\mathrm{K}) + 0.26$	W/(kg.K)
Specific heat capacity (C_P)	Coconut water [a]	$C_p = 4.06$	kJ/(kg.K)
Density (ρ)	Coconut water [a]	$\rho = 990$	kg/m^3
Dynamic viscosity (μ)	Coconut water [a]	$\mu = 0.30\ e^{-1.90\ 10^{-2}\ T(\mathrm{K})}$	Pa.s

Source: Oishi et al. (2023).

The measured values of relative dielectric permittivity (ε_r') and dielectric loss factor (ε_r'') of fresh coconut water, at 2.45 GHz, as a function of temperature are presented in Figure 3.4a. The correlations of ε_r' and ε_r'' were adjusted for temperatures ranging from 30 to 130 °C:

$$\varepsilon_r' = -0.250\ T + 80.1 \qquad R^2 = 0.988 \qquad (3.10)$$

$$\varepsilon_r'' = 6.00\ 10^{-4}\ T^2 - 6.98\ 10^{-2}\ T + 15.5 \qquad R^2 = 0.936 \qquad (3.11)$$

Figure 3.4. a) The influence of temperature on dielectric permittivity and dielectric loss factor of fresh coconut water in the frequency of 2.45 GHz and b) Fresh coconut water electrical conductivity and temperature correlation.

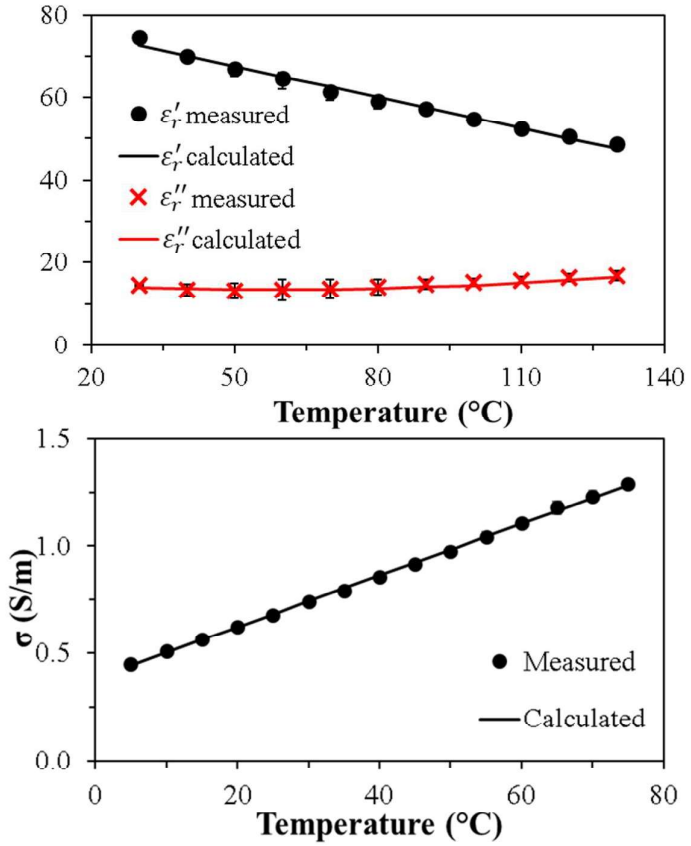

Source: Oishi et al. (2023).

At 2.45 GHz, the dielectric permittivity decreases linearly with temperature (Eq. 3.10), ranging from 74.6 to 48.6 in the 30-130 °C range. Franco et al. (2015) also observed a linear decrease in the dielectric permittivity of this product for a temperature range of 0 to 90 °C. For the dielectric loss factor, in the temperature range of 30 to 60 °C, the value dropped slightly and then raised again, resulting in the 2nd degree polynomial correlation in Eq. (3.11). This behavior is due to the balance between the two loss mechanisms: ionic loss and dipolar loss, since they are affected differently by temperature. In Figure 3.4a, the ε_r'' curve shows a subtle reduction between 30 and 50 °C (from 14.5 to 13.2) and a more pronounced rise from 70 °C to 130 °C (from 13.6 to 16.9).

The electrical conductivity (σ, S/m) of coconut water as a function of temperature is shown in Figure 3.4b. A positive linear correlation between 0.45 and 1.3 S/m was observed at

the 5-75 °C range. The adjusted linear correlation of electrical conductivity is valid for temperatures between 5 and 75 °C:

$$\sigma = 1.13\ 10^{-2}\ \mathrm{T} - 0.379 \qquad R^2 = 0.999 \qquad (3.12)$$

This positive linear correlation was also seen in Kanjanapongkul and Baibua (2021) and Franco et al. (2015) for green coconut water with similar ranges of electrical conductivity: 0.7-2.4 S/m for 25-90 °C and 0.39-1.5 S/m for 0-90 °C, respectively. Zhang and Datta (2003) also reported a positive linear dependence for various liquid foods such as beer, coffee, milk and several vegetable and fruit juices. Wang et al. (2003) reported that this linear increase in electrical conductivity is important to microwave heating because of the ionic conductivity loss mechanism at high temperatures, which causes the heating rate to be directly proportional to the electrical conductivity. Since this positive linear correlation is usual for the electrical conductivity of liquid foods, Eq. (3.12) was extrapolated for temperatures higher than 75 °C.

Due to the high concentration of electrolytes, the coconut water showed a higher electrical conductivity than in other fruit juices (0.20-0.44 S/m for apple juice, 0.06-0.17 S/m for cranberry juice, 0.08-0.23 S/m for lemonade and 0.31-0.69 S/m for orange juice between 4 and 60 °C), but it is similar to chocolate skim milk (0.53-1.09 S/m between 4 and 60 °C) (Zhang and Datta, 2003).

3.4.2 Model simulation and validation: mixing cup average temperatures

The 16 experimental runs with the MicroThermics unit are presented in Table 3.2 with the corresponding flow rates and set-point temperatures, the absorbed power calculated with Eq. (3.1) and the temperatures measured at the thermocouples T2, T3 and T4 (Figure 3.1). The temperatures at the outlet of the microwave heater and holding tube (T3 and T4) were used for the model validation.

Table 3.2. Processing conditions, absorbed power, average temperatures measurements (see Figure 3.1).

Id	Flow rate (L/min)	Set point for T3 (°C)	P_{abs} (kW)	T2 (°C)	T3 (°C)	T4 (°C)
M1	0.5	80	1.01	50.0 ± 0.1	80.0 ± 0.2	78.3 ± 0.1
M2	0.7	80	1.41	50.1 ± 0.1	80.0 ± 0.2	78.8 ± 0.1
M3	0.9	80	1.81	50.0 ± 0.1	80.0 ± 0.1	79.1 ± 0.1
M4	1.1	80	2.22	50.0 ± 0.1	80.0 ± 0.1	79.2 ± 0.2
M5	0.5	90	1.34	50.0 ± 0.1	90.0 ± 0.1	88.2 ± 0.1
M6	0.7	90	1.88	50.0 ± 0.1	90.0 ± 0.1	88.7 ± 0.1
M7	0.9	90	2.42	50.0 ± 0.1	90.0 ± 0.1	88.9 ± 0.1
M8	1.1	90	2.97	49.9 ± 0.1	90.0 ± 0.1	89.1 ± 0.1
M9	0.5	100	1.66	50.1 ± 0.1	100.0 ± 0.1	97.8 ± 0.1
M10	0.7	100	2.35	50.0 ± 0.1	100.0 ± 0.1	98.4 ± 0.1
M11	0.9	100	3.01	50.0 ± 0.1	100.1 ± 0.1	98.8 ± 0.1
M12	1.1	100	3.69	49.9 ± 0.1	100.2 ± 0.2	99.1 ± 0.1
M13	0.5	110	1.99	50.0 ± 0.1	110.1 ± 0.1	107.5 ± 0.1
M14	0.7	110	2.80	49.9 ± 0.1	110.0 ± 0.1	108.3 ± 0.1
M15	0.9	110	3.64	49.8 ± 0.1	110.2 ± 0.3	108.9 ± 0.3
M16	1.1	110	4.41	49.7 ± 0.3	110.0 ± 0.1	108.9 ± 0.1

Source: Oishi et al. (2023).

The multiphysics model for the microwave heater and holding tube was simulated for all 16 conditions. A comparison between the experimental and mixing cup simulated temperatures is shown in Figure 3.5 for the microwave heater and holding tube. For the heater, most of the predicted values were overestimated (predictions were higher than the experimental values). The condition of 0.9 L/min and 110 °C presented the largest prediction error of 6.2 °C. However, the highest flow rate (1.1 L/min) and the higher temperatures (100 and 110 °C) conditions showed good agreement with experimental results, with errors lower than 1.1 °C. The average absolute prediction error for the heater was 3.3 °C.

Figure 3.5. Average microwave and holding tube outlet temperatures, experimental and predicted from model simulation.

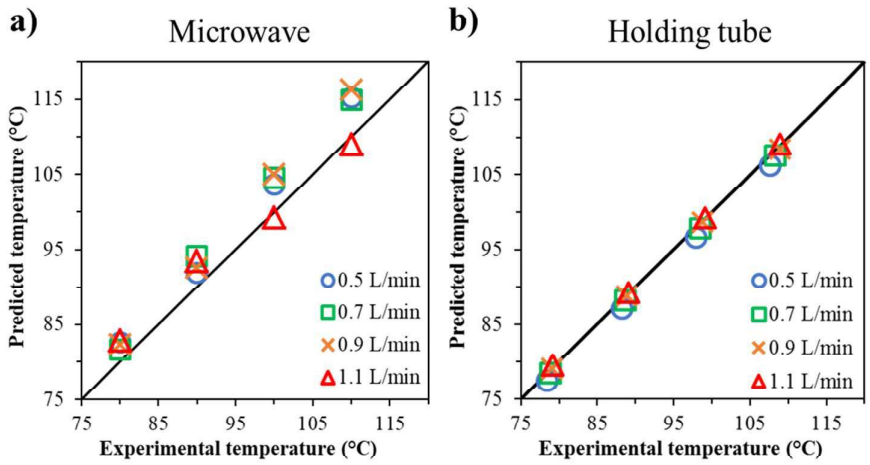

Source: Oishi et al. (2023).

Salvi et al. (2011) compared experimental and COMSOL temperature predictions for a continuous flow microwave heater (915 MHz, 4 kW). Water and a CMC 0.5% solution were microwave-assisted heated at 1 and 2 L/min, and the temperature was measured experimentally along the applicator tube. The authors observed a good agreement between experimental and predicted temperatures for the applicator tube with R^2 value higher than 0.80.

For the holding tube simulation, the multiphysics model predicted outlet temperatures by implementing the average heat transfer coefficient of 14.1 W/(m^2.K) as a convective heat flux boundary condition (Russo and Gut, 2022). The simulations showed an overall good agreement with the experimental data (Figure 3.5b). Most of the simulated temperatures were underestimated (T4 > $T_{predicted}$), except for the 1.1 L/min flow rate, which were slightly overestimated. Nevertheless, the average absolute predicted error was only 0.5 °C.

3.4.3 Model simulation and validation: enzyme residual activity

The predicted residual activities of enzymes PPO and POD at the outlet of the microwave heater were close to 99%. This low inactivation was due to the very short residence time in the microwave applicator tube, and the low inlet temperature (50 °C). The outlet residual activities at the holding tube outlet for the 16 processing conditions were calculated by the mixing cup equation (Eq. (3.8)). The model predictions were compared with the experimental

values to validate the multiphysics model regarding the residual activity of enzymes polyphenol oxidase and peroxidase.

To illustrate the simulation results for inactivation, the PPO residual activity along the holding tube and adjacent connections for processing condition M1 (1.2 kW, 0.5 L/min) is presented in Figure 3.6. At the microwave heater outlet, the residual activity of PPO was 99%, and at the exit of the holding tube connection, it was 28%. The experimental value was 29%. The connections before and after the holding tube (steps 4-5 and 6-7 in Figure 3.1) presented a significant contribution of 21% to the inactivation despite their small lengths. For the Food and Drugs Administration (FDA, 2004), the inactivation of the biological target of the thermal process is considered only to take place in the holding tube. However, in practice, inactivation also occurs in the heating step, cooling step and tube connections (Aguiar and Gut, 2014).

Figure 3.6. Simulation of the PPO residual activity along the holding tube and connections in the processing conditions of 80 °C and 0.5 L/min.

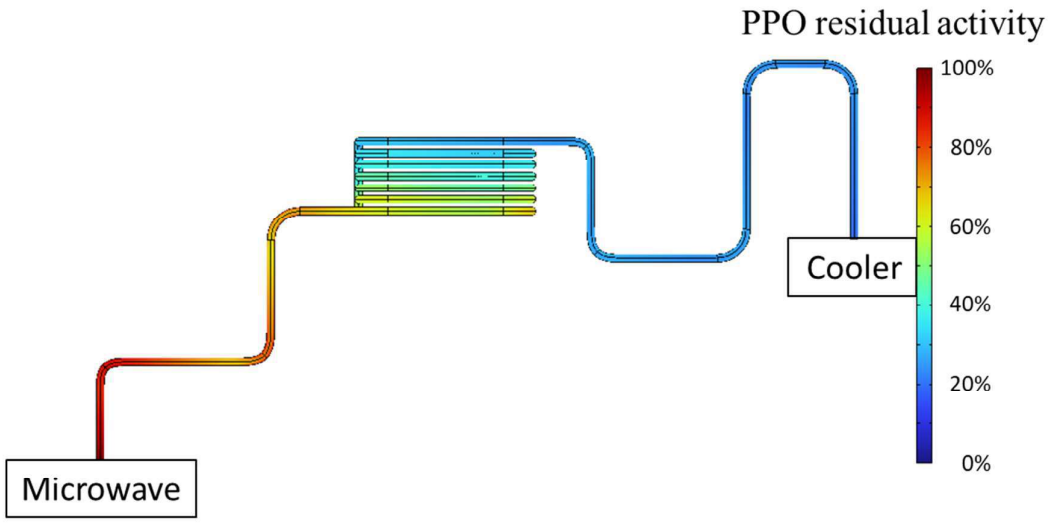

Source: Oishi et al. (2023).

In Figure 3.7, the parity plots can better present the comparison results between the model predictions and experimental data for residual activity of enzymes PPO and POD after the holding tube. The residual activity is related to the spatial temperature distribution throughout the process and the velocity field (Kubo et al., 2021). A significant residual activity of PPO was only observed when processing at 80 °C (conditions M1-M4 in Table 3.2); however, residual POD activity was observed when processing 80 and 90 °C (conditions M1-

M8 in Table 3.2), since POD has higher thermal resistance than PPO. For the other conditions, experimental or simulated activities were under 5%.

Figure 3.7. Parity plots for the residual activity of Polyphenol oxidase (PPO) and Peroxidase (POD) prediction and experimental after microwave processing. Dashed lines: ± 10%.

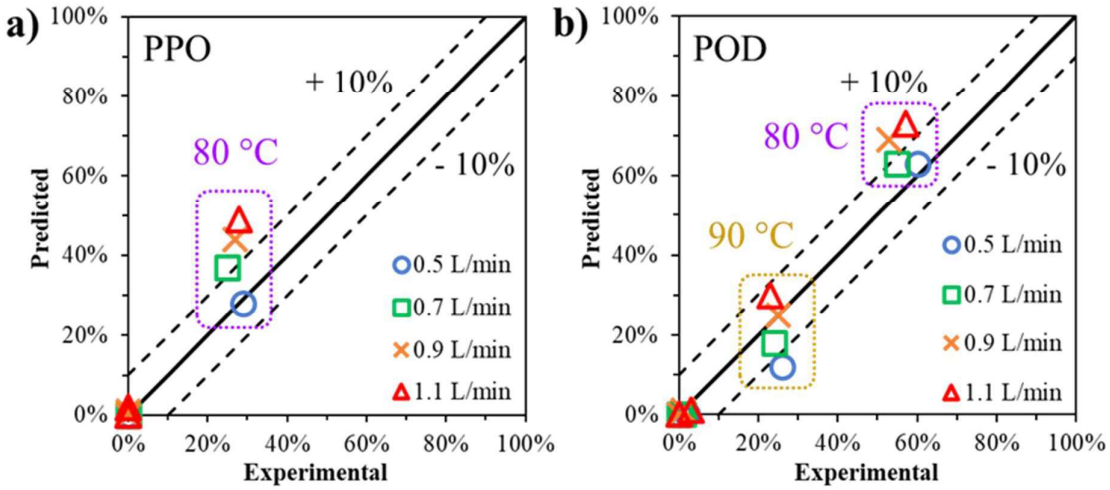

Source: Oishi et al. (2023).

The parity charts in Figure 3.7 show that most predictions for residual activity of the enzymes fall within the ± 10% dashed lines. A higher dispersion was expected in comparison to temperature predictions because of uncertainties in the assessment of biological activity and also because of the assumption that inactivation is interrupted right after the holding tube, neglecting the cooling step. Nevertheless, the model was able to provide reliable results.

3.5 CONCLUSION

The COMSOL Multiphysics software was used to simulate a continuous-flow microwave heater and a holding tube for the thermal processing of coconut water, encompassing the governing equations of electromagnetism, laminar flow, heat transfer and mass transfer with reaction. The thermophysical properties from literature and the dielectric and electric properties from measurements were implemented in the model as functions of temperature. The Polyphenol oxidase and Peroxidase first-order thermal inactivation kinetics were implemented in the model as well.

Combining four flow rates and four temperatures, coconut water was processed with a pilot-scale unit in 16 conditions and outlet temperatures and residual activities of the enzymes were measured. The multiphysics model simulated all conditions and provided reliable predictions for the outlet temperature of the heater and holding tube and residual activity of the enzymes PPO and POD after the holding tube.

Due to the complexity of combining the physics of electroactive wave propagation with fluid flow and heat transfer, a multiphysics approach is required for a reliable representation of the phenomena. The validation of this model shows that it can be further used for the analysis and design of continuous-flow microwave heaters for the thermal processing of liquid foods.

3.6 REFERENCES

Aguiar HF, Gut JAW. Continuous HTST pasteurization of liquid foods with plate heat exchangers: mathematical modeling and experimental validation using a time-temperature integrator. Journal of Food Engineering, 2014;123:78-86. https://doi.org/10.1016/j.jfoodeng.2013.09.022.

Arzeta-Ríos AJ, Guerra-Ramírez D, Reyes-Tejedo B, Ybarra-Moncada MC, Zuleta-Prada H. Microwave heating effect on total phenolics and antioxidant activity of green and mature coconut water. J. Food Eng. 2020;16:20190378. https://doi.org/10.1515/ijfe-2019-0378.

Bird B, Stewart WE, Lightfoot EN. Shell momentum balances and velocity distributions in laminar flow. In: Bird B, Stewart WE, Lightfoot EN. Transport phenomena. New York: John Wiley & Sons, 2002;40-74.B.

Campos CF, Souza PEA, Coelho JV, Glória MBA. Chemical composition, enzyme activity and effect of enzyme inactivation on flavor quality of green coconut water. J. Food Processing and Preservation 1996;20:487-500. https://doi.org/10.1111/j.1745-4549.1996.tb00761.x.

Cavalcante TABB, Funcia ES, Gut JAW. Inactivation of polyphenol oxidase by microwave and conventional heating: Investigation of thermal and non-thermal effects of focused microwaves. Food Chemistry 2021;340:127911. https://doi.org/10.1016/j.foodchem.2020.127911.

Delfiya ADS, Thangavel K. Effect of Ohmic Heating on Polyphenol Oxidase Activity, Electrical and Physicochemical Properties of Fresh Tender Coconut Water. Int. J. Food Eng 2016;12:691-700. DOI 10.1515/ijfe-2015-0329.

Dibben D. Electromagnetics: fundamental aspects and numerical modeling. In: Datta AK, Anantheswaran RC. Handbook of microwave technology for food applications. Boca Ratón: CRC Press, 2001;1-31.

FDA Food and Drug Administration - Juice, 2004, HACCP hazards and controls guidance. Available at: https://www.fda.gov/regulatory-information/search-fda-guidance-documents/guidance-industry-juice-hazard-analysis-critical-control-point-hazards-and-controls-guidance-first [Accessed 28 June 2023].

Fortes NHM, Gut JAW. Correction of residence time distribution measurements for short holding times in pasteurization processes. Int J Food Eng, 2021;17;1:11-26. https://doi.org/10.1515/ijfe-2020-0109.

Franco AP, Yamamoto LY, Tadini CC, Gut JAW. Dielectric Properties of Green Coconut Water Relevant to Microwave Processing: Effect of Temperature and Field Frequency. J. Food Eng. 2015;155:69–78. https://doi.org/10.1016/j.jfoodeng.2015.01.011.

Funcia ES. Estudo e modelagem da inativação enzimática no processamento de água de coco verde e suco de laranja por aquecimento ôhmico e dielétrico. Tese de doutorado apresentada para obtenção do título de Doutor em ciências – Escola Politécnica da Universidade de São Paulo – São Paulo, 2020.

Geedipali SSR, Rakesh V, Datta VK. Modeling the heating uniformity contributed by a rotating turnable in microwave ovens. J. of Food Eng. 2007;359-368. https://doi.org/10.1016/j.jfoodeng.2007.02.050.

Industrial Microwave Systems, 6 kW Liquid Heating Microwave System, 2450 MHz, 2022. Available in: https://industrialmicrowave.com/microwave-systems-liquids-fluids-heating/6kw-microwave-system/. [Accessed in 21 Sept 2022].

Kanjanapongkul K, Baibua V. Effects of ohmic pasteurization of coconut water on polyphenol oxidase and peroxidase inactivation and pink discoloration prevention. J. Food Eng. 2021;292:110268. https://doi.org/10.1016/j.jfoodeng.2020.110268.

Kubo MTK, Reis BHG, Sato LNI, Gut JAW. Microwave and conventional thermal processing of soymilk: Inactivation kinetics of lipoxygenase and trypsin inhibitors activity. LWT 2021;145:111275. https://doi.org/10.1016/j.lwt.2021.111275.

Kubo M, Curet S, Augusto P, Boillereaux L. Multiphysics modeling of microwave processing for enzyme inactivation in fruit juices. Journal of Food Engineering 2019;263:366-379 10.1016/j.jfoodeng.2019.07.011.

Matsui KN, Granadob LM, de-Oliveira PV, Tadini CC. Peroxidase and Polyphenol Oxidase Thermal Inactivation by Microwaves in Green Coconut Water Simulated Solutions. LWT-Food Sci. Technol. 2007;40:852-859. https://doi.org/10.1016/j.lwt.2006.03.019.

Matsui KN, Gut JAW, Granadob LM, de-Oliveira PV, Tadini CC. Inactivation Kinetics of Polyphenol Oxidase and Peroxidase in Green Coconut Water by Microwave Processing. J. Food Eng. 2008;88:169–176. doi:10.1016/j.jfoodeng.2008.02.003.

Mayer AF. Polyphenol oxidases in plants and fungi: going places? A review. Phytochemistry 2006;67:2318-2331. https://doi.org/10.1016/j.phytochem.2006.08.006.

Oishi TK, Gut JAW. Modeling time-temperature history and sterilization value of mango puree under conventional and microwave assisted pasteurization. Int. J. Food Engineering 2021. https://doi.org/10.1515/ijfe-2020-0335.

Oishi TK, Pouzada EVS, GUT JAW. Experimental validation of a multiphysics model for the microwave-assisted pasteurization of apple juice. Digital Chem Eng 2022;5:100053. https://doi.org/10.1016/j.dche.2022.100053.

Porto E, Filho EGA, Silva LMA, Fonteles TV, Nascimento RBR, Fernandes FAN, Brito ES, Rodrigues S. Ozone and plasma processing effect on green coconut water. Food Research International 2020;131:109000. https://doi.org/10.1016/j.foodres.2020.109000.

Prades A, Dornier N, Diop J, Pain P. Coconut water preservation and processing: a review. Fruits 2012;157-171. http://dx.doi.org/10.1051/fruits/2012009.

Price HC, Mattsson J, Murray B. Sucrose diffusion in aqueous solution. Phys. Chem. Chem. Phys. 2016;18:19207-19216. DOI: 10.1039/c6cp03238a.

Russo G, Gut JAW. Study of heat transfer coefficients and temperature distribution in a continuous flow pasteurizer with helical tubes using model fluids in laminar flow. Int J Food Eng 2022;18;7:559-570. https://doi.org/10.1515/ijfe-2021-0340.

Salvi D, Boldor D, Aita GM, Sabliov CM. COMSOL Multiphysics model for continuous flow microwave heating of liquids. J. Food Engineering 2011;104:422-429. https://doi.org/10.1016/j.jfoodeng.2011.01.005.

Sierra I, Vidal-Valverde C, Olano A. The effects of continuous flow microwave treatment and conventional heating on the nutritional value of milk as shown by influence on vitamin B 1 retention. European Food Research and Technology 1999;209:352–354. https://doi.org/10.1007/s002170050508.

Siguemoto ÉS, Pires MN, Funcia ES, Gut JAW. Evaluation and modeling of a microwave-assisted unit for continuous flow pasteurization of liquid foods: Residence time distribution,

time–temperature history, and integrated lethality. Journal of Food Process Engineering 2018;41(8):1-13. https://doi.org/10.1111/jfpe.12910.

Siguemoto ÉS, Funcia ES, Pires MN, Gut JAW. Modeling of time-temperature history and enzymatic inactivation of cloudy apple juice in continuous flow microwave assisted pasteurization. Food Bioproducts Processing 2018111:45-53. https://doi.org/10.1016/j.fbp.2018.06.004.

Siguemoto ÉS, Purgatto E, Hassimotto NMA, Gut, JAW. Comparative Evaluation of Flavor and Nutritional Quality after Conventional and Microwave-Assisted Pasteurization of Cloudy Apple Juice. LWT 2019;111:853–60. https://doi.org/10.1016/j.lwt.2019.05.111.

Tan TC, Easa AM. The evolution of physicochemical and microbiological properties of green and mature coconut water (*Cocos nucifera*) under different storage conditions. Food Measure 2021;15:3523–3530. https://doi.org/10.1007/s11694-021-00927-5 .

Tang J. Unlocking potentials of microwaves for food safety and quality. J Food Eng. 2015;8:E1776-E1793. https://doi.org/10.1111/1750-3841.12959.

Teleken JT, Dutra AC, Laurindo JB, Carciofi BAM. Numerical modeling of heating tomato pulp in continuous flow microwave-assisted thermal processing: Estimation of quality parameters. J Food Process Eng. 2023;4(6):e14216. https://doi.org/10.1111/jfpe.14216.

Topcam H, Erdogdu F. Designing system cavity geometry and optimizing process variables for continuous flow microwave processing. Food and Bioproducts Processing 2021;127:295-308. https://doi.org/10.1016/j.fbp.2021.03.006A.

Veitch NC. Horseradish peroxidase: a modern view of a classic enzyme. Phytochemistry 2004;65:249-259. doi:10.1016/j.phytochem.2003.10.022.

Wang Y, Wig T, Tang J, Hallberg L. Dielectric properties of food relevant to RF and microwave pasteurization and sterilization. J. Food Eng. 2003;57:257–268. http://dx.doi.org/10.1016/S0260-8774(02)00306-0.H.

Zhang, A.K. Datta, 2003, Microwave power absorption in single- and multiple-item foods. Trans IChemE 81:257-265. https://doi.org/10.1205/096030803322438027.

Zhu H, He J, Hong T, Yang Q, Wu Y, Yang Y, Huang K. A rotary radiation structure for microwave heating uniformity improvement. Applied Thermal Engineering 2018;648-658. https://doi.org/10.1016/j.applthermaleng.2018.05.122.

4 MULTIPHYSICS MODELING OF WIRE-TO-PLATE ELECTROHYDRODYNAMIC DRYING WITH AIR CROSSFLOW

4.1 INTRODUCTION

Food drying is a typical post-harvest process to remove water and prevent food losses (Iranshahi et al., 2023). Moisture in a wet solid can be presented as excess liquid on the boundaries and as a solution within the solid. Airflow and/or temperature variation can be induced in drying processes (hot air ovens, microwaves and electrohydrodynamic) to increase convective heat and mass transfer, thus increasing the drying rate (Aregawi et al., 2013).

The electrohydrodynamic (EHD) drying mechanism involves the induction of ionic winds that can increase the airflow in the space between the emitter electrode (high-voltage wire) and the ground collector surface (metallic plate with the food material) (Singh et al., 2012). The ionized particles around the wire are accelerated outwards by the Coulomb force, collide with neutral air particles and induce the ionic wind towards the ground (Defraeye and Martynenko, 2018; Iranshahi et al., 2020). This induced airflow increases convective heat and mass transfer coefficients at ambient temperature and pressure and, therefore, can be employed to accelerate the convective drying of heat-sensitive food products.

Defraeye and Martynenko (2018) developed an extensive multiphysics simulation study comparing different EHD wire-to-ground configurations (wire-to-plate, wire-to-mesh, mesh-to-mesh and wire-to-parallel plates). Different geometric configurations were tested to increase the airflow over the food surface and improve drying rate and uniformity. The wire-to-mesh with a large mesh can reduce the drying time and energy consumption due to the airflow increase at the food boundary surfaces (Iranshahi et al., 2020). Onwude et al. (2021) modeled the scale-up of an EHD dryer with wire-to-mesh geometry to dry sliced fruits. They verified that the EHD drying of multiple slices can be faster and consume less energy than in a conventional air dryer.

Zhong et al. (2019) used multiphysics modeling to simulate a multi-pin (needles as emitter electrodes) EHD drying with air crossflow of a wet tissue. The authors tested the combinations of 16 and 20 kV electric potentials and air crossflow velocities from 0.1 to 2.5 m/s. The air crossflow did not affect the ionization zone but facilitated the moisture transport from the drying region. In the simulations with air crossflow velocities higher than 0.69 m/s, the EHD air jet shifted from the inlet to the outlet, reducing EHD flow contact with the drying material (Zhong et al., 2019).

The interaction between electric field, airflow and temperature is too complex to be evaluated only through experimental assays. A multiphysics model is a useful tool to adequately investigate the effects of electric force and heat transfer on the airflow inside an EHD channel. This work aims to model and simulate an EHD wire-to-plate in combination with an air crossflow system and to assess the EHD increase in the convective heat transfer coefficient over a portion of solid food and the drying kinetics. Instead of using segregated models for the ionic wind formation (time-independent study) and for the drying (time-dependent), a fully-coupled model is proposed.

4.2 MULTIPHYSICS MODELING

The EHD wire-to-plate geometry herein was based on the laboratory-scale equipment used by Singh et al. (2016) with a rectangular prism cage made of Plexiglas with dimensions 281 x 110 x 80 mm (length x width x height). Figure 4.1 shows the EHD chamber connected to an air blower (which forced the air out of the chamber at different controlled velocities). The food samples are placed over a perforated aluminum sheet, which act as the ground (collector) electrode, with dimensions 200 x 80 mm (Figure 4.2). The temperature and relative humidity sensors and mass scale in Figure 4.1 are connected to a data logger; the food mass, air temperature and relative humidity data are recorded every minute during drying (Singh et al., 2016). The EHD chamber has seven high voltage (HV) copper wires (emitting electrodes), with 0.5 mm diameter and 25 mm spacing between each wire (Figure 4.2). The emitting electrodes are stimulated by a direct current (DC) power HV supply unit with a maximum voltage of 30 kV. The gap between the wires and the ground is 15 mm.

Herein, a multiphysics model was developed based on the assembly configuration in Figure 4.1. Each rectangular food slice is aligned under a wire, so an air-jet can be created directly above each slice (Onwude et al., 2021). This set-up allows the two-dimensional modeling of one food slice under one wire (wire-to-plate configuration), as shown in Figure 4.1 as “COMSOL domain”, to analyze the effect of the ionic wind on the drying. The horizontal changes in air temperature and humidity were neglected because of the low drying rate, thus allowing the simulation of a single slice. The 2-D geometry was modeled with the geometry node of COMSOL Multiphysics (v.6.1). The control volume of the EHD system has one high-voltage wire (electrode radius = 250 μm), the ground sheet was placed at the bottom (15 mm gap), and a wall was placed at the top (40 mm height). A food slice (10 mm width x 5 mm height) was placed over the ground surface.

Figure 4.1. Schematic representation of the EHD dryer (side view, not to scale).

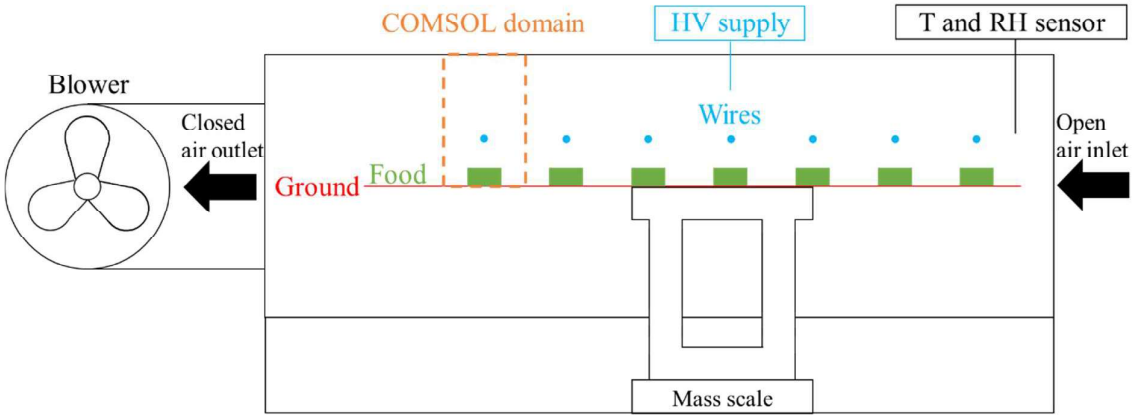

Source: The author (2023).

Figure 4.2. Picture of the EHD experimental setup with no food (top view).

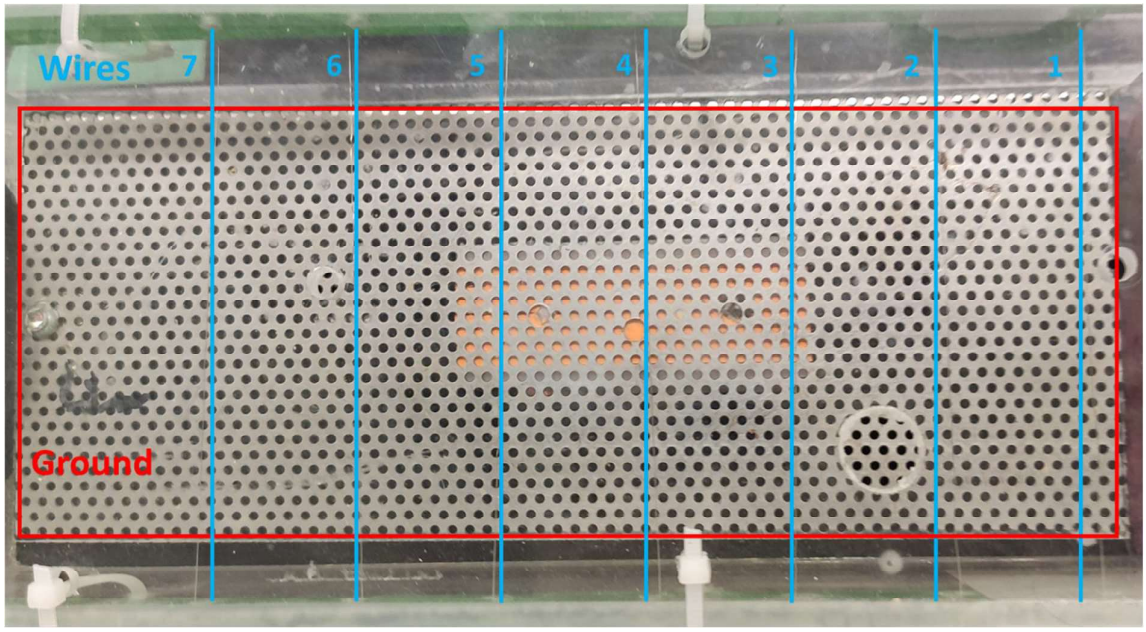

Source: The author (2023).

This model was developed by considering the modeling studies of Defraeye and Martynenko (2018) and Onwude et al. (2021). The authors segregated the COMSOL multiphysics model into two studies: (1) time-independent EHD airflow: electrostatics, turbulent flow and heat transfer in fluids and (2) time-dependent drying of the food slice: two partial differential equations (PDE) physics (moisture and energy transport). The first study was used to simulate the ionic wind and airflow to determine the convective coefficients over the

food slice, while the simulation of the drying process required a time-dependent model that used the coefficients from the first model.

In this work, the multiphysics model was solved into one fully-coupled time-dependent study with the physics of electrostatics, turbulent flow, heat transfer in fluids and two partial differential equations (PDE) related to moisture and energy transport. The EHD drying model was developed considering the following assumptions: (1) ionization zone as the external wire surface (ionization zone radius = wire radius), (2) constant thermophysical and dielectric properties of air, food and wire, (3) incompressible air and (4) evaporation only occurs at the food surface.

4.2.1 Governing equations

ELECTROSTATIC MODEL:

Maxwell's equations were used to describe the electrostatic physics and to determine the electric field strength (**E**, V/m), electric potential (V, V) and space charge density (q, C/m^3) in the control volume (Defraeye and Martynenko, 2018). **E**, V and q are related by the following equations:

$$\nabla \cdot \varepsilon_0 \, \varepsilon_r \, \mathbf{E} = q \tag{4.1}$$

$$\mathbf{E} = -\nabla V \tag{4.2}$$

where ε_0 is the dielectric permittivity of vacuum (8.854 10^{-12} F/m) and ε_r is the relative dielectric permittivity of the material (air or food).

The continuity equation for the electric current density (**J**, A/m^2) in the drift air zone (Ohm's law) was considered as follows (Jewell-Larsen et al., 2008):

$$\nabla \cdot \mathbf{J} = 0 \tag{4.3}$$

The current density in the drift zone (air) can be calculated from the sum of the equation terms: ion mobility (from wire to ground), charge convection and diffusion of electric charges (Saadatmand, Goharkhah and Nejad, 2022). However, for the EHD driven-flow case, the second and third terms are smaller than the first one (Jewell-Larsen et al., 2008). Consequently, **J** can be reduced to the following equation:

$$\mathbf{J} = q \, b \, \mathbf{E} \tag{4.4}$$

where b is the ion mobility (m^2/(V.s)).

To couple the electrostatics and airflow models in COMSOL, the electric force ($\mathbf{f_E}$, N/m^3) was expressed through the Coulomb (electrophoresis) force equation (Landau and Lifshitz, 1963):

$$\mathbf{f_E} = q\,\mathbf{E} \tag{4.5}$$

TURBULENT FLOW MODEL:

The fluid flow of air was modeled considering turbulent flow behavior of a single-phase Newtonian incompressible fluid using the CFD module and the Turbulent Flow k-ε interface of the software. The Navier-Stokes equation was solved by applying the k-ε interface, which is the Reynolds-averaged Navier-Stokes (RANS) equation for conservation of momentum and the continuity equation (COMSOL, 2023). The velocity profile of the fluid domain was described by the momentum conservation equation with $\mathbf{f_E}$ as the external force term:

$$\rho_{air}\frac{d\mathbf{u}}{dt} + \rho_{air}\,\mathbf{u}\cdot\nabla\,\mathbf{u} = -\nabla\,p + \mu_{air}\,\nabla^2\,\mathbf{u} + \mathbf{f_E} \tag{4.6}$$

where ρ_{air} is the air density (1.2 kg/m^3 at 20 °C), $\mathbf{u}$ is the air velocity (m/s), t is time (s), p is the air pressure (Pa) and μ_{air} is the air viscosity ($1.8 \cdot 10^{-5}$ kg/(m.s) at 20 °C) (Iranshahi et al., 2020).

HEAT TRANSFER IN FLUIDS MODEL:

The heat transfer in fluids was coupled with turbulent flow physics to determine the heat transfer of the air over the food surface using the energy equation:

$$\rho_{air}\,C_{Pair}\left(\frac{\partial T_{air}}{\partial t} + \mathbf{u}\,\nabla\,T_{air}\right) = k_{air}(\nabla^2\,T_{air}) \tag{4.7}$$

where C_{Pair} is the air specific heat capacity (4182 J/(kg.K) at 20 °C), T_{air} is the air temperature (K) and k_{air} is the thermal conductivity of the air (0.026 W/(m.K) at 20 °C).

MOISTURE TRANSFER MODEL:

The moisture transfer is attributed to convection via EHD generated airflow (ionic wind) and air crossflow. The moisture conservation equation was modeled as:

$$\frac{\partial w_m}{\partial t} + \nabla\cdot(-D_m\,\nabla\,w_m) = 0 \tag{4.8}$$

where w_m is the moisture content of food (kg/m^3), t is time (s) and D_m is the effective moisture diffusivity in the food (m^2/s).

The relation of water potential (ψ, Pa) with water activity (a_w) is required to determine the moisture capacity (Aregawi et al., 2013; Defraeye and Verboven, 2017):

$$\psi = \rho_l \, R_v \, T \ln(a_w) \tag{4.9}$$

$$K_m = D_m \, C_m = D_m \, \frac{\partial w_m}{\partial \psi} \tag{4.10}$$

where ρ_l is the density of liquid water (1000 kg/m^3 at 20 °C), K_m is the moisture permeability of food (s) and C_m is the moisture capacity (s^2/m^2).

ENERGY TRANSFER MODEL:

The energy conservation equation was modeled as follows (Datta, 2008):

$$(C_{Ps} \, w_s + C_{Pl} \, w_m) \frac{\partial T}{\partial t} + \nabla \cdot (-k_{food} \, \nabla \mathrm{T}) = 0 \tag{4.11}$$

where C_{Ps} is the specific heat capacity of the dry matter (J/(kg.K)), w_s is the dry matter density (kg/m^3), C_{Pl} is the specific heat capacity of liquid water (4182 J/(kg.K) at 20 °C) and k_{food} is the thermal conductivity of food (W/(m.K)).

4.2.2 Boundary conditions and initial values

ELECTROSTATIC MODEL:

For the boundary conditions of the model, the initial values of the electric potential and the space charge density of the ground and food were set to zero. The relative permittivity of the air and food were set to constant values: 1 and ε_{food}, respectively. Different wire electric potential values were studied $V_w = 0$, 10, 15 and 20 kV.

TURBULENT FLOW MODEL:

A zero static pressure at the air inlet boundary was implemented. For the air crossflow, the fully developed average air velocity was $u_{cross} = 0$, 1 and 2 m/s at the outlet boundary. The wire, ground and food boundaries were considered as walls with no slip condition.

HEAT TRANSFER IN FLUIDS MODEL:

The ground surface and the top wall surfaces were set to adiabatic. In this physics, the boundary condition heat flux was used to calculate the spatial distribution of convective heat transfer coefficient (h_T, W/(m^2.K)) over the air-food interface (Ayuttaya et al., 2013). The predefined COMSOL multiphysics coupling "nonisothermal flow" conjugates the physics of turbulent flow and heat transfer in fluids.

$$-\mathbf{n} \cdot (-k_{air} \nabla T_{air}) = h_T (T_{food} - T_{air}) \tag{4.12}$$

It's possible to estimate the convective mass transfer coefficient (h_M, s/m^2) distribution over the food surface by the adapted Chilton-Colburn analogy factor (AF) for convective heat and mass transfer coefficient valid at temperatures below 100 °C (Defraeye, Blocken and Carmeliet, 2012):

$$AF = \frac{h_M}{h_T} = \left(\frac{\delta}{k_{air}}\right)^{\frac{2}{3}} \frac{1}{(R_v \; T_{air} \; \rho_{air} \; C_{Pair})^{\frac{1}{3}}} \tag{4.13}$$

where δ is the water vapor diffusion coefficient, R_v is the specific gas constant for water vapor (461.52 J/(kg.K)). The typical value of AF for moist air is $7.0 \cdot 10^{-9}$ at ambient conditions (Defraeye, Blocken and Carmeliet, 2012).

MOISTURE TRANSFER MODEL:

On the bottom surface of the control volume, where the ground electrode is placed, there is no moisture diffusion. On the air-food surface, the boundary condition for mass transfer states that the moisture loss equals the convective vapor loss (Defraeye and Verboven, 2017). The boundary condition for the air-food surface interface (continuity flux) of the moisture balance PDE in Eq. (4.8) used the convective mass transfer coefficient in Eq. (4.13) to calculate the moisture content:

$$\mathbf{n} \cdot (-D_m \nabla w_m) = h_M (p_{vw} - p_{v,ref}) \tag{4.14}$$

The vapor pressure at the air-food interface (p_{vw}, Pa) and in the air ($p_{v,air}$, Pa) were determined as a function of water activity and air relative humidity (RH_{air}) (Defraeye, Blocken and Carmeliet, 2012):

$$p_{vw} = a_w \, p_{v,sat} \, (T_w(\mathrm{K})) \tag{4.15}$$

$$p_{v,air} = RH_{air} \, p_{v,sat} \, (T_{air} \, (\mathrm{K})) \tag{4.16}$$

$$p_{v,sat}(T(\mathrm{K})) = \exp\left(65.8094 - \frac{7066.27}{T(\mathrm{K})} - 5.976 \ln(T(\mathrm{K}))\right) \tag{4.17}$$

where $p_{v,sat}$ is the saturated vapor pressure (Pa).

ENERGY TRANSFER MODEL:

A zero-energy flux was set on the bottom surface of the control volume, where the ground electrode is placed. The heat loss at the air-food interface by the conduction and by the liquid water removal is equal to the convective heat transfer with the air and water vapor loss (evaporation) (Defraeye and Verboven, 2017). The boundary condition for the air-food surface interface (continuity flux) of the energy transfer PDE in Eq. (4.11) used the convective heat transfer coefficient in Eq. (4.12) to calculate the energy transport:

$$\mathbf{n} \cdot \left(-k_{food} \nabla T\right) = h_T\left(T_{food} - T_{air}\right) - h_v \left[h_M\left(p_{vw} - p_{v,ref}\right)\right] \quad (4.18)$$

where h_v is the water vapor enthalpy (J/kg).

The enthalpies of liquid water (h_l, J/kg) and water vapor (h_v, J/kg) were considered as:

$$h_l = C_{Pl}\,(T - 273.15) \quad (4.19)$$

$$h_v = C_{Pv}\,(T - 273.15) + L_v \quad (4.20)$$

where L_v is the latent or vaporization heat ($2.5 \cdot 10^6$ J/kg at 20 °C) and C_{Pv} is the specific heat capacity of water vapor (1880 J/(kg.K) at 20 °C) (Iranshahi et al., 2020).

4.2.3 Study Case: EHD drying of sliced apple

The EHD wire-to-plate with air crossflow was used to simulate the drying process of sliced apple (cv. *Braeburn*). The apple slice was assumed to be initially fresh cut (10 mm width x 5 mm height) with uniform moisture content $w_{m\_initial} = 780$ kg/m^3 and uniform temperature of 20 °C (Onwude et al., 2021). The relative dielectric permittivity of apple was set to 54 (Marra, et al., 2010). Although the relative dielectric permittivity of the apple changes during drying (decreases with moisture reduction), the large ε_r of the apple compared to the air ($\varepsilon_{air} = 1$) makes the resulting average electric potential on the apple surface relatively low: 72 V for the applied wire potential of 15 kV. A constant relative permittivity was used in this study, due to the lack of more detailed data.

The apple thermal conductivity was $k_{food} = 0.42$ W/(m.K) and the moisture permeability was $K_m = 8 \cdot 10^{-16}$ s (Defraeye and Radu, 2017). After severe dehydration, the apple dry matter moisture content and heat capacity are $w_s = 130$ kg/m^3 and $C_{Ps} = 1634$ J/(kg.K) (Defraeye and Radu, 2017). The ambient air was assumed to be at constant temperature of 20 °C and relative humidity of 30%.

Aregawi et al. (2013) determined the sorption isotherms of an apple drying by hygrometric instrument method (HIM) data fitted with the Ferrero Fontan model at 25 °C (Fontan et al., 1982):

$$w_m(a_w) = w_s \left(\frac{0.15926}{\ln\left(\frac{1.0177}{a_w}\right)} \right)^{\frac{1}{0.97014}} \tag{4.21}$$

The main objective of the food drying process is to decrease the water activity (a_w) to increase the shelf-life of perishable goods inhibiting micro-organisms growth and/or undesired enzyme activity (Bonazzi and Dumoulin, 2014). The enzyme activity in most foods is inhibited at $a_w \leq 0.75$, and for suppressing the micro-organisms growth an $a_w \leq 0.6$ is necessary (Bonazzi and Dumoulin, 2014). Therefore, the drying time (t_{crit}, h) was considered as the time required for the food slice to reach the average safe moisture content (w_{safe}, kg/m^3) corresponding to $a_w = 0.6$.

4.2.4 Mesh and solvers

For reliable numerical results, good meshing is essential. A small number of mesh elements may not describe the system correctly, but a large number can lead to an unfeasible computational time. The EHD drying model involves complex multiphysics problems of electrostatics, fluid flow, heat transfer in fluids and moisture and energy transport. Mesh independence study is an important step in a Computational Fluid Dynamics (CFD) problem (Sangare et al., 2020). When the model solution does not change, for a given precision, with the increasing mesh element number, the calculation can be considered independent of the mesh (Gyurik et al., 2019).

The meshing was built using the COMSOL predefined “free tetrahedral” with a “extremely fine” mesh element size, calibrated for fluid dynamics. Eight boundary layers were added to the external surface of the food and wire (adjustment factor 1.2). The workstation used to perform the simulations was an Intel Xeon 291 2403 @ 1.8 GHz with 64 GB RAM.

A sensitivity analysis for the number of mesh elements was conducted considering an electric potential of 15 kV and no air crossflow. The average convective heat transfer coefficient (h_T in Eq. (4.12)) of the three exposed food boundaries (sides and top) was the most sensitive variable for the mesh independence study. Figure 4.3 allows verifying how the increase in mesh element number affected the convective heat transfer coefficient. The increase in the number of elements increased the simulation time from 6 minutes (1,784 elements) to 218 minutes (103,533 elements). In Figure 4.3, for the higher values of mesh elements, h_T did not vary significantly, converging to 39.4 W/(m^2.K). The selected mesh had 103,533 elements with 534,765 equations with a simulation time of 218 minutes, as presented in Figure 4.4.

Figure 4.3. Mesh independence study for the electric potential of 15 kV: food surface average convective heat transfer coefficient as a function of mesh elements.

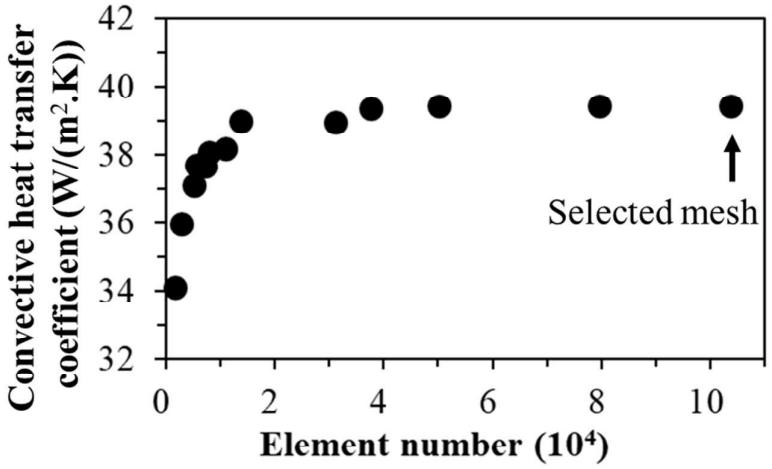

Source: The author (2023).

Figure 4.4. COMSOL model geometry and numerical meshing for the wire-to-plate EHD drying.

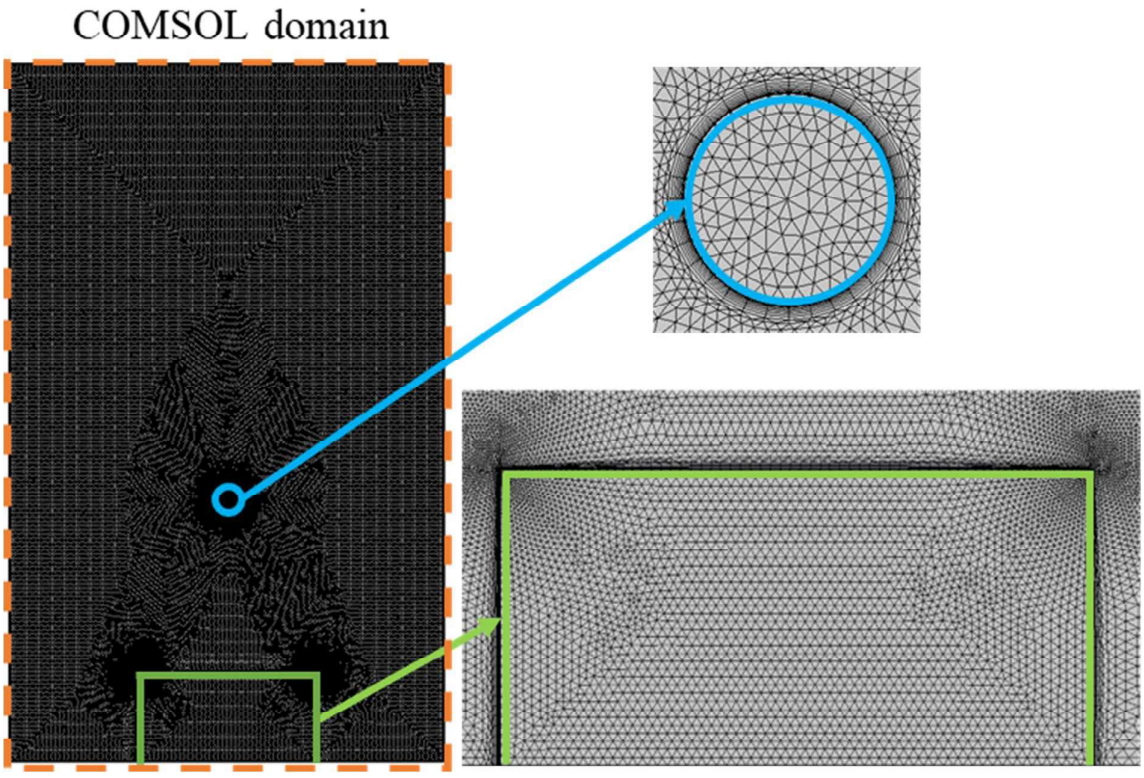

Source: The author (2023).

The simulation procedure flow chart of the EHD airflow drying is summarized in Figure 4.5. The model was solved taking into consideration the physics of electrostatics (where the V_w was applied and the resulting **E**, q and V were calculated), turbulent flow (where the **E** was used to calculate the $\mathbf{f_E}$ which was then used to calculate **u**), heat transfer in fluids (where the **u** was used to calculate the temperature distribution and the convective coefficients h_T and h_M), moisture transport (where the h_M was set as a boundary condition to calculate w_m) and energy transport (where the h_T was set as a boundary condition to calculate the heat loss) (Figure 4.5).

The fully-coupled direct solver MUMPS (Multifrontal Massively Parallel Sparse Direct Solver) was implemented for all the models on the time-dependent study.

Figure 4.5. Simulation procedure flow chart for the time-dependent electrostatics, turbulent flow, heat transfer in fluids and moisture and energy transport physics.

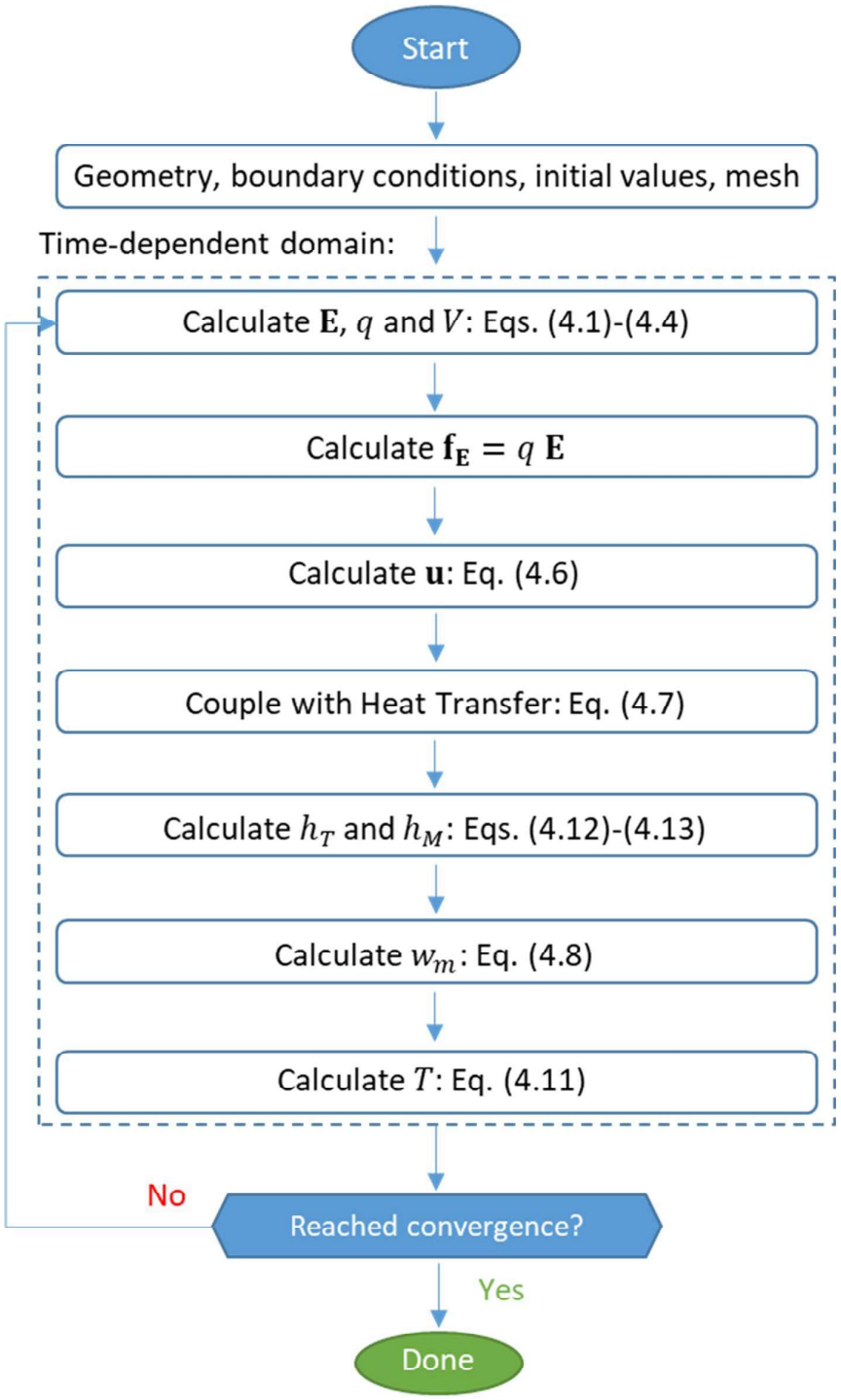

Source: The author (2023).

4.3 RESULTS AND DISCUSSION

4.3.1 EHD wire-to-plate airflow

The simulation results of wire-to-plate electric potential and electric field are presented in Figure 4.6, considering the electric potential of 15 kV at the wire and no air crossflow. A slightly higher electric field is found in the space between the wire and food surface due to the higher electric permittivity of the apple and lower the distance between the wire and the apple. This results in a stronger electric field and higher air speed (Defraeye and Martynenko, 2018). The complex spatial distribution of electric potential and electric field around the wire and food indicates that they depend on the geometrical configuration (Defraeye and Martynenko, 2018). Therefore, a change in wire radius or gap between the wire and ground can fully change the spatial distribution of potential and electric field.

Figure 4.6. EHD wire-to-plate COMSOL simulation results: electric potential, electric field strength for the electric potential of 15 kV with no forced convection.

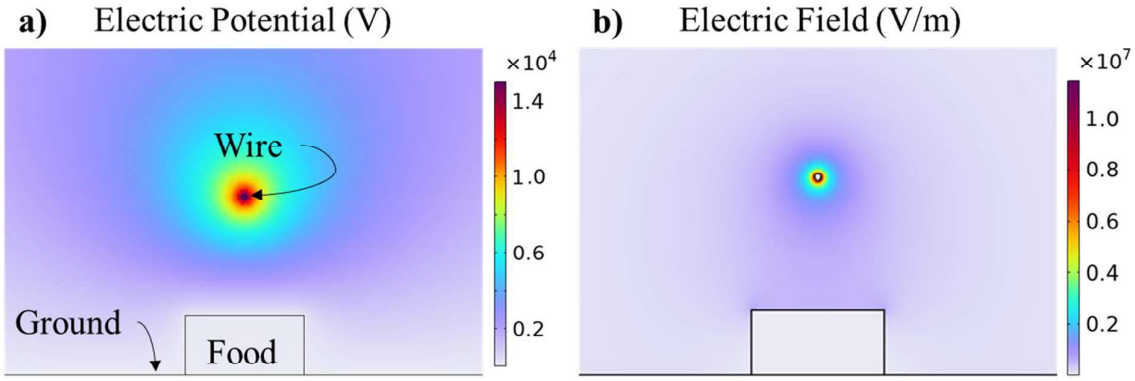

Source: The author (2023).

The comparison of the air velocity simulation results: a) only electric potential of 15 kV, b) only air crossflow velocity of 1 m/s and c) a combination of 15 kV and 1 m/s are presented in Figure 4.7. In Figure 4.7a, the EHD air jet concentrates the air velocity around the wire and the flow to the ground electrode (impinging flow). In this case, the spatial velocity distribution on the food surface is not uniform, the velocity at the lateral surfaces is zero and the average velocity is only 0.04 m/s.

Figure 4.7. EHD wire-to-plate COMSOL simulation results: air velocity for a) the electric potential of 15 kV, b) air crossflow velocity of 1 m/s and c) the combination of 15 kV electric potential and 1 m/s air crossflow velocity.

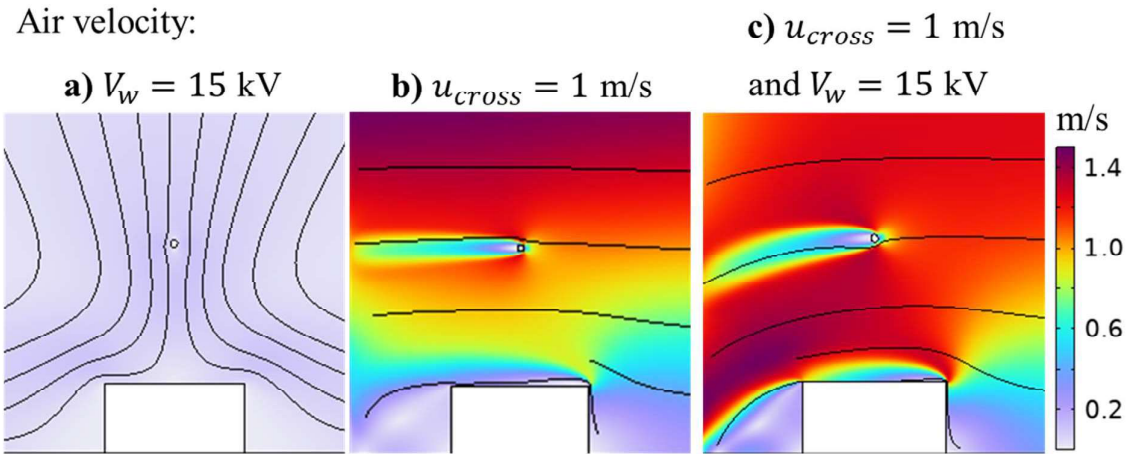

Source: The author (2023).

Defraeye and Martynenko (2018) simulated different EHD wire-to-ground configurations (wire-to-plate, wire-to-mesh, mesh-to-mesh and wire-to-parallel plates). The wire-to-plate configuration results showed a disadvantage due to the low airflow in the side boundaries of the food; thus, reducing the drying rate on these surfaces. Moreover, combining EHD and air crossflow can increase the turbulence over the lateral surfaces and improve drying efficiency (Singh et al., 2016).

The simulation of air crossflow velocity of 1 m/s (Figure 4.7b) presented a few air jets on the side boundaries, and the average air velocity on the food surface of 0.06 m/s is still low for efficient convective drying. Zhong et al. (2019) noted that fluid flow was affected by both air crossflow and EHD impinging flow in simulation results of 20 kV and $u_{cross} = 0.2$ m/s. EHD impinges the food drying surface and the air crossflow removes the air jets to the channel flow.

In Figure 4.7c, the combination of EHD and air crossflow improved the turbulence at the lateral surfaces of the food slice and the spatial distribution of air velocity increased on the space between the wire and the food surface. Also, the average air velocity on the food surface was 0.19 m/s, so the convection can be improved by combining EHD and u_{cross}.

4.3.2 Impact of air crossflow on EHD drying parameters

The multiphysics model for the EHD air flow was simulated for 11 conditions varying crossflow air velocity and wire potential (Table 4.1). The impact of EHD drying parameters (wire potential and air crossflow velocity) on the food surface (apple top and sides) average convective heat transfer coefficient (h_T) and surface air velocity (u_{fs}) can be seen in Figure 4.8.

Table 4.1. Drying conditions of air crossflow velocity and wire electric potential.

Code	Crossflow air velocity (u_{cross})	Wire potential (V_w)
A010	0 m/s	10 kV
A015	0 m/s	15 kV
A020	0 m/s	20 kV
A100	1 m/s	0 kV
A110	1 m/s	10 kV
A115	1 m/s	15 kV
A120	1 m/s	20 kV
A200	2 m/s	0 kV
A210	2 m/s	10 kV
A215	2 m/s	15 kV
A220	2 m/s	20 kV

Source: The author (2023).

The average h_T and u_{fs} show similar trends: the values increase with higher electric potentials, resulting in 2nd degree polynomial behavior. This 2nd degree behavior was also found in the previous study of Defraeye and Martynenko (2018). Since the applied electric potential increases the airflow over the food surface, the h_T distribution is also dependent on V_w (Defraeye and Martynenko, 2018).

Figure 4.8. Average food surface of a) convective heat transfer coefficient and b) air velocity as a function of the wire potential and forced air crossflow velocity (0, 1 and 2 m/s).

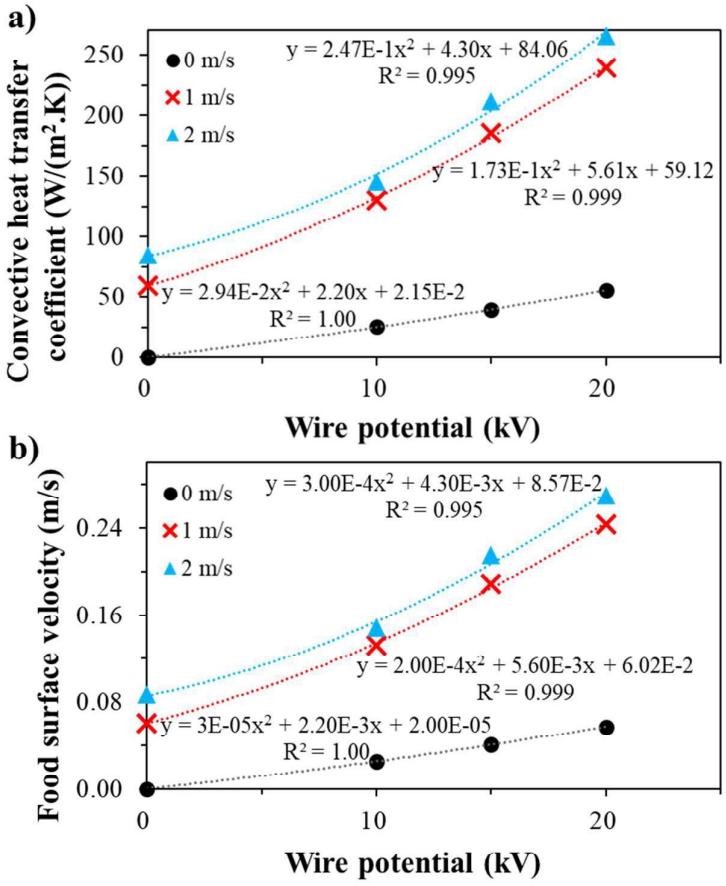

Source: The author (2023).

The combination of high-voltage wire potential and air crossflow velocity highly affected the processing parameters more than the increase in V_w or in u_{cross} alone. The conditions A100 (only 1 m/s) and A020 (only 20 kV) presented similar value of h_T = 57 W/(m^2.K). Combining 1 m/s and 20 kV (A120) can increase the convective heat transfer coefficient to 240 W/(m^2.K). However, the EHD processing conditions A120 and A220 (increase in air crossflow velocity from 1 to 2 m/s at the same 20 kV) only increased the h_T value from 240 to 266 W/(m^2.K). The increase in V_w for A110 and A120 conditions (from 10 to 20 kV at the same u_{cross} = 1 m/s) can raise the convective coefficient from 130 to 240 W/(m^2.K).

4.3.3 Results for EHD drying with air crossflow

The safe moisture content of the apple (w_{safe}, kg/m^3) was calculated from Eq. (4.21) and was considered as 37.8 kg/m^3. The drying curves of the apple slice (moisture content over time) are shown in Figure 4.9 for different air crossflow velocities and wire potentials.

Figure 4.9. Food surface average moisture content over time for different wire potentials and air crossflow velocity a) 0 m/s, b) 1 m/s and c) 2 m/s.

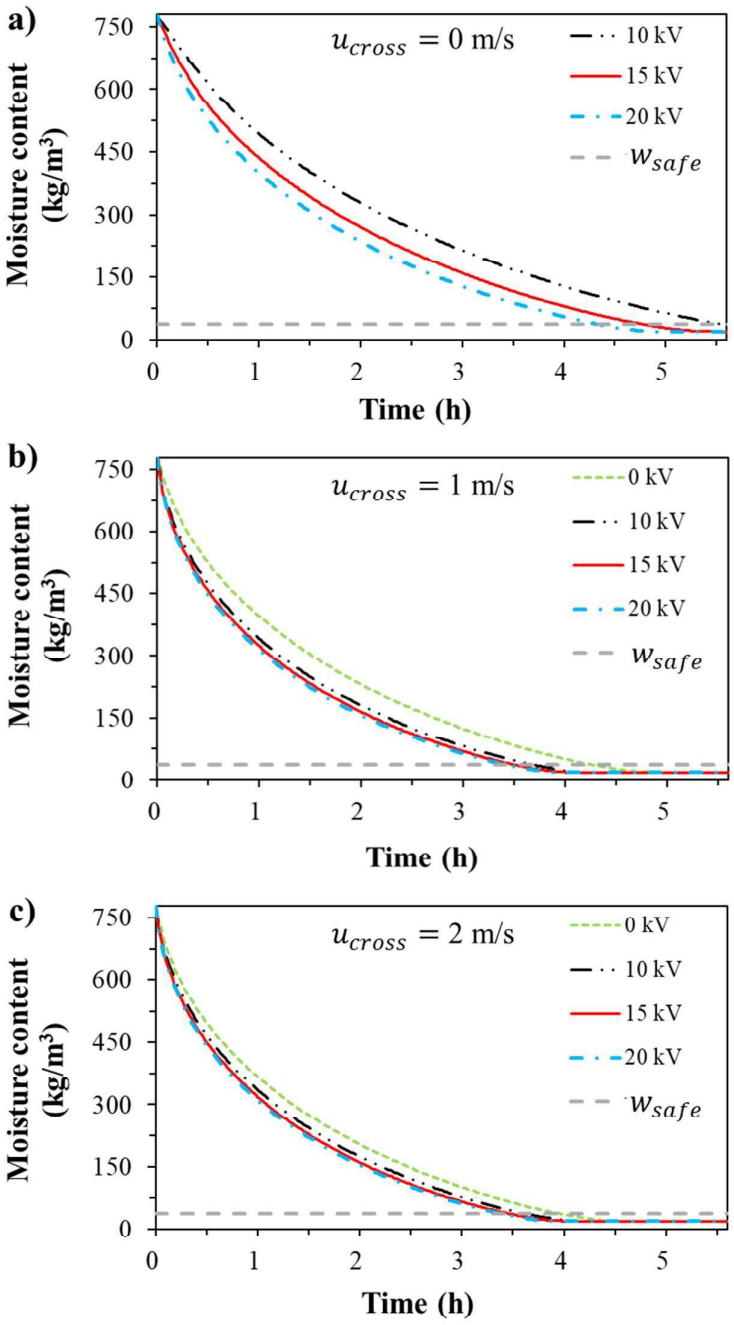

Source: The author (2023).

In Figure 9, the apple drying curves simulation results show a higher moisture removal at the beginning of the drying process, and, over time, the moisture decreases until achieve equilibrium (drying stops) (Mirzaei-Baktash et al., 2022). Golestani, Raisi and Aroujalian (2013) hot-air dried apple slices (60 x 5 mm) and the falling drying period was the dominant mechanism for moisture removal. This result shows that the loss of free water at apple surface was not significant, and the internal diffusion was the principal mechanism for moisture loss during the apple drying process (Onwude et al., 2016).

From Figure 4.9a, it can be observed that the increase in electric potential by itself increases the drying rate. In the previous study of Defraeye and Martynenko (2018), for the distance between wire to ground of 2.0 cm, the increase in V_w from 12 to 20 kV increased the drying rate, but values over 20 kV had a low effect on drying.

In Figure 4.9b and c, the combination with air crossflow further increased the drying rate, but the change in wire potential had a low impact on the drying speed. For high convective heat and mass transfer coefficients, the moisture transfer resistance on the boundary layer is much smaller than the internal moisture transport resistance of the apple (Defraeye and Martynenko, 2018). Therefore, the internal moisture transport resistance dominates the drying kinetics at high convective heat and mass transfer coefficients.

Figure 4.10 shows that the drying time decreases in a 2^{nd} degree polynomial correlation with increasing wire potential. The drying processing conditions without air crossflow presented higher drying time, but the increase in wire potential from 10 to 20 kV decreased the drying time from 5.5 to 4.3 h. The condition A020 (only 20 kV) and A100 (only 1 m/s air crossflow) presented similar drying times of 4.3 h. Combining 20 kV and 1 m/s (condition A120) can decrease the drying time to 3.4 h. This result is similar to the previous experimental study of apple hot air drying at 60 °C and 0.6 m/s conditions (Golestani, Raisi and Aroujalian, 2013).

Singh et al. (2015) investigated the electrohydrodynamic drying of wheat flour combined with 1.0, 1.5 and 2.0 m/s air crossflow velocities. The experiment with the highest drying rate was obtained with the highest wire potential and air crossflow (15 kV and 2.0 m/s) tested. However, a similar drying time was observed for the experiment with lower wire potential and air crossflow velocity (12.5 kV and 1.0 m/s) (Singh et al., 2015). Herein, the drying time difference between the combinations of 1 and 2 m/s with 10, 15 and 20 kV was less than 19 minutes. The combination of high voltage and air crossflow drying showed better results than only one of the drying factors, but the increase in wire potential or air crossflow velocity has a low impact on drying time.

Figure 4.10. Drying time as a function of the wire potential and air crossflow velocity (0, 1 and 2 m/s).

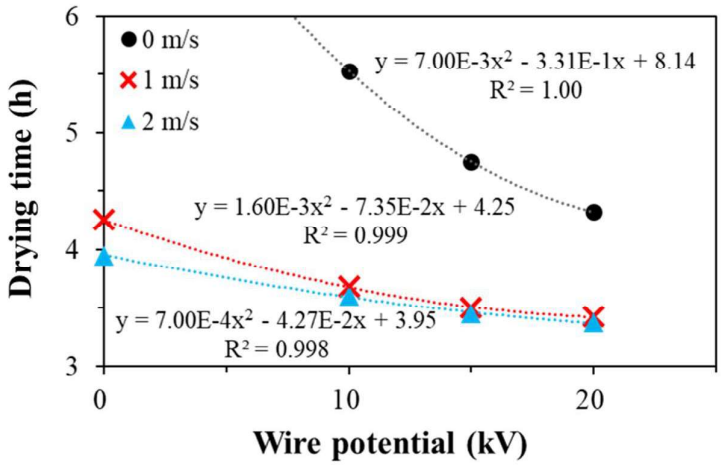

Source: The author (2023).

4.4 CONCLUSION

The COMSOL Multiphysics software was used to simulate a wire-to-plate electrohydrodynamic drying with air crossflow of apple slices. In this work, the EHD-driven airflow model (electrostatics, turbulent flow and heat transfer in fluids) was fully-coupled with the food drying model (moisture and energy transport) by the convective heat and mass transfer coefficients. The EHD phenomenon was successfully investigated through the wire-to-plate configuration. The COMSOL Multiphysics software could well represent the EHD-driven airflow from wire to ground combined with air crossflow.

Four wire potentials and three air crossflow velocities were combined and simulated for the apple slice drying. The resulting convective heat transfer coefficient, air velocity on the food surface, moisture content and drying time were presented for each of the 11 drying conditions. The combination of high voltage and air crossflow impacted the EHD processing parameters; however, the increase in one of the drying factors had a low effect on drying time. The developed fully coupled EHD drying model was useful to evaluate the impact of the convective heat transfer coefficient on the drying kinetics. This model will be useful to simulate and validate the lab-scale EHD dryer with air crossflow system and 7 wires to further study food quality retention, energy efficiency and optimization.

4.5 REFERENCES

Aregawi W, Defraeye T, Saneinejad S, Vontobel P, Lehmann E, Carmeliet J, Derome D, Verboven P, Nicolai B. Dehydration of apple tissue: Intercomparison of neutron tomography with numerical modelling. Int J Heat Mass Transfer 2013;67:173-182. https://doi.org/10.1016/j.ijheatmasstransfer.2013.08.017

Ayuttaya SSN, Chaktranond C, Rattanadecho P. Numerical analysis of electric force influence on heat transfer in a channel flow (theory based on saturated porous medium approach). Int J Heat Mass Transfer 2013;64:361-374. http://dx.doi.org/10.1016/j.ijheatmasstransfer.2013.04.010

Bonazzi C, Dumoulin E. Quality changes in food materials as influenced by drying processes. Modern Drying Technology 2014;3(4):1–20. https://doi.org/10.1002/9783527631728.ch14.

COMSOL Multiphysics. Reference manual, 2023. Available in: https://doc.comsol.com/6.1/doc/com.comsol.help.comsol/COMSOL_ReferenceManual.pdf [Accessed in 25 Aug 2023].

Datta AK. Status of Physics-Based Models in the Design of Food Products, Processes, and Equipment. Comprehensive Reviews Food Sci Food Safety 2008;7:121-129. https://doi.org/10.1111/j.1541-4337.2007.00030.x.

Defraeye T, Blocken B, Carmeliet J. Analysis of convective heat and mass transfer coefficients for convective drying of a porous flat plate by conjugate modelling. Int J Heat Mass Transfer 2012;55:112-124. https://doi.org/10.1016/j.ijheatmasstransfer.2011.08.047.

Defraeye T, Martynenko A. Electrohydrodynamic drying of food: New insights from conjugate modeling. J Cleaner Production 2018;198:269-284.

Defraeye T, Radu A. Convective drying of fruit: A deeper look at the air-material interface by conjugate modeling. Int J Heat Mass Transfer 2017;108:1610-1622. https://doi.org/10.1016/j.ijheatmasstransfer.2017.01.002.

Defraeye T, Verboven P, Convective drying of fruit: Role and impact of moisture transport properties in modelling. J F Eng 2017;193:95-107. http://dx.doi.org/10.1016/j.jfoodeng.2016.08.013

Fontan CF, Chirife J, Sancho E, Iglesias HA. Analysis of a Model for Water Sorption Phenomena in Foods. J Food Science 1982;47:1590-1594. https://doi.org/10.1111/j.1365-2621.1982.tb04989.x

Golestani R, Raisi A, Aroujalian A. Mathematical Modeling on Air Drying of Apples Considering Shrinkage and Variable Diffusion Coefficient. Drying Tech. 2013;31:40-51. DOI: 10.1080/07373937.2012.714826.

Gyurik L, Egedy A, Zou J, Miskolczi N, Ulbert Z, Yang H. Hydrodynamic modelling of a two-stage biomass gasification reactor. J Energy Inst 2019;92(3):403e12. https://doi.org/10.1016/j.joei.2018.05.007

Iranshahi K, Rubinetti D, Onwude DI, Psarianos M, Schlüter OK, Defraeye T. Electrohydrodynamic drying versus conventional drying methods: A comparison of key performance indicators. Energy Conversion and Management 2023;279116661. https://doi.org/10.1016/j.enconman.2023.116661.

Iranshahi K, Martynenko A, Defraeye T. Cutting-down the energy consumption of electrohydrodynamic. Energy 2020;208:118168.

Jewell-Larsen NE, Karpov SV, Krichtafovitch IA, Jayanty V, Hsu C, Mamishev AV. Modeling of corona-induced electrohydrodynamic flow with COMSOL multiphysics. Proc. ESA Annual Meeting on Electrostatics 2008;E1.

Landau LD, Lifshitz EM. Electrohydrodynamic of Continuous Media. New York: Pergamon, 1963.

Marra F, De Bonis MV, Ruocco G. Combined microwaves and convection heating: a conjugate approach. J. Food Eng. 2010;97:31e39.

Mirzaei-Baktash H, Hamdami N, Torabi P, Fallah-Joshaqani S, Dalvi-Isfahan M. Impact of different pretreatments on drying kinetics and quality of button mushroom slices dried by hot-air or electrohydrodynamic drying. LWT 2022;15:112894. https://doi.org/10.1016/j.lwt.2021.112894.

Mujumdar AS. Principles, Classification, and Selection of Dryers. In: Mujumdar AS. Handbook of Industrial Drying. Boca Ratón: CRC Press 2006;4-31.

Onwude DI, Hashim N, Janius RB, Nawi NM, Abdan K. Modeling the Thin-Layer Drying of Fruits and Vegetables: A Review. Comprehensive Reviews Food Sci Food Safety 2016;15:599-618. doi: 10.1111/1541-4337.12196.

Onwude DI, Iranshahi K, Rubinetti D, Martynenko A, Defraeye T. Scaling-up electrohydrodynamic drying for energy-efficient food drying via physics-based simulations. J. Cleaner Production 2021;329:129690.

Saadatmand A, Goharkhah M, Nejad AM. Heat transfer enhancement in mini channel heat sinks utilizing corona wind: A numerical study. Int. J. Heat Mass Transfer 2022;182:121970. https://doi.org/10.1016/j.ijheatmasstransfer.2021.121970

Sangare D, Bostyn S, Moscosa-Santillan M, Gokalp I. Hydrodynamics, heat transfer and kinetics reaction of CFD modeling of a batch stirred reactor under hydrothermal carbonization conditions. Energy 2021;219:119635. https://doi.org/10.1016/j.energy.2020.119635

Singh A, Orsat V, Raghavan V. A Comprehensive Review on Electrohydrodynamic Drying and High-Voltage Electric Field in the Context of Food and Bioprocessing. Drying Tech.: An Int. J. 2012;30:1812-1820.

Singh A, Vanga SKK, Nair GR, Gariepy Y, Orsat V, Raghavan V. Electrohydrodynamic drying (EHD) of wheat and its effect on wheat protein conformation. LWT 2015;64:750-758. http://dx.doi.org/10.1016/j.lwt.2015.06.051

Singh A, Vanga SKK, Nair GR, Gariepy Y, Orsat V, Raghavan V. Electrohydrodynamic Drying of Sand. Drying Tech: An Int. J. 2016;35:312-322.

Zhong C, Martynenko A, Wells P, Adamiak K. Numerical investigation of the multi-pin electrohydrodynamic dryer: Effect of cross-flow air stream. Drying Technology 2019;37(13):1665-1677. DOI: 10.1080/07373937.2018.1531291.

5 GENERAL CONCLUSIONS

The general purpose of this PhD work was to develop and evaluate multiphysics models for the microwave-assisted thermal process in fruit juices (apple juice and coconut water) and the electrohydrodynamic (EHD) drying with air crossflow in a solid sliced fruit (apple). These electro-technologies are on the verge of industrial implementation, with some pilot-scale systems and a few studies of energy efficiency and quality retention available. A multiphysics model can couple first-principle equations (transport phenomena and electric field force) to simulate complex interactions between fluid, solid and high-voltage electrode, reducing experimental runs, time and costs. To better understand the effects of electric fields on the continuous-flow thermal processing of liquid foods and the convective drying of solid foods, the COMSOL Multiphysics software was used to simulate these food processes.

To obtain a broad understanding of the heating mechanism of the continuous flow microwave heater, a microwave cavity was modeled in COMSOL Multiphysics and validated with previous apple juice pasteurization experiments. Model simulations of electric field and temperature presented a non-homogeneous electric field distribution in the microwave applicator tube. Temperature distribution was useful for identifying undesired hot and cold spots for food quality and safety concerns.

Regarding FDA (Food and Drug Administration) recommendations for industries of fruit-based beverages, the inactivation of the biological target of the thermal process is considered only to take place in the holding tube. However, in practice, inactivation also occurs in the heating step, cooling step and tube connections. From this, the COMSOL Multiphysics software was used to simulate the continuous flow microwave heater and a holding tube for the thermal processing of coconut water. Based on literature data, the Polyphenol oxidase (PPO) and Peroxidase (POD) first-order thermal inactivation kinetics were implemented in the model as the biological target of the microwave-assisted thermal process. The connections before and after the holding tube presented a significant contribution of 21% out of 71% in total enzyme inactivation. The model simulations for the residual activity of both enzymes provided reliable predictions with deviations under 10%. This computational model can adequately simulate the microwave cavity and the holding tube for the continuous flow processing of coconut, showing it can be further used for process analysis and design.

To better investigate the electrohydrodynamic airflow through a EHD channel, a wire-to-plate electrohydrodynamic drying with air crossflow of apple slices was simulated in a fully-coupled time-dependent COMSOL Multiphysics model. The COMSOL Multiphysics software

could well represent the EHD-driven airflow from wire to ground combined with air crossflow. The resulting convective heat transfer coefficient, air velocity on the food surface, moisture content and drying time were presented for each of the 11 drying conditions. The combination of high voltage and air crossflow impacted the EHD processing parameters; however, the increase in one of the drying factors had a low effect on drying time. This model will be useful to simulate and validate the lab-scale EHD dryer with air crossflow system and 7 wires to further study food quality retention, energy efficiency and optimization.

5.1 FUTURE OUTLOOK

Considering the results obtained in this thesis, the transmission of microwaves makes it difficult to understand the energy input-absorption, resulting in inefficient heating. The relationship between incident wave and absorbed energy is essential to determine the wave reflection and the energy conversion rate. Also, a better understanding of heat transfer and uniformity (microwave penetration depth, tube diameter size and mixing effects) can improve heating efficiency and avoid unwanted over-processing.

The microwave heater and holding tube multiphysics model can be improved by including the following considerations may be proposed to better investigate the continuous-flow microwave energy efficiency and process optimization:

- Further investigation on the waveguide 3-stub tuner used to reduce the reflection loss;
- Design improvements of applicator tube diameter and geometry to contemplate mixing effects;
- Test modeling with Finite Element Method (FEM).

The evaluation of quality changes during storage of apple juice and coconut water after microwave thermal is essential to attend consumer demands for high-quality food products. Another further investigation of this PhD is to explore the effects on the molecular structure and inactivation mechanisms of PPO and POD enzymes during microwave-assisted heat treatment through molecular dynamics (MD) simulations. The MD simulations can be used to explore the molecular changes of PPO and POD during electric field processing.

Electrohydrodynamic drying is an emerging alternative non-thermal technology with potential to retain color and nutritional qualities of fruits and vegetables better than conventional dryers. However, the ionic discharges present a low drying surface due to the formation of small plasma volume. This plasma can generate ozone and free radicals that can initiate the oxidation of lipids and flavonoids of dried fruits and vegetables. Additional studies

evaluating the effects of EHD drying on antioxidant activity and phenolic compounds through experimental procedures and MD simulations can be conducted.

The fully-coupled time-dependent COMSOL Multiphysics model of a wire-to-plate electrohydrodynamic drying with air crossflow could well represent the EHD-driven airflow from wire to ground combined with air crossflow. The drying model can be improved by including the following considerations:

- Dielectric properties of the food material varying with the moisture content;
- Development of experimental studies to understand the food deformation during drying, some studies consider the volume loss of the food to be equal to the volume of moisture evaporated (iso-volume) and the same volume loss in all directions (isotropic shrinkage);
- Evaporation accounted for increase moisture of air crossflow stream outside the boundary layer;
- Model geometry from 2D to 3D and simulate the entire EHD dryer with 7 wires and 7 pieces of food (Figure 4.1).

These considerations can help contemplate the whole EHD drying process of any fresh heat-sensible food product. Moreover, the increase in scale and improvements in the drying model are essential steps for validation, energy efficiency and quality retention studies.